Université Paris – Sud XI

École doctorale : Physique de la région parisienne

Laboratoire de Physique des Solides

Discipline : Physique Théorique

Thèse de doctorat

par **Yi LIU**

devant être soutenue le 30 septembre 2013

Dynamics, Synchronization and Spin Squeezing in a Two-Spin Model

Composition du jury :

Franck LALOË	Président de jury
Kurt GIBBLE	Rapporteur
Anna MINGUZZI	Rapporteur
Peter ROSENBUSCH	Examinateur
Jean-Noël FUCHS	Directeur de thèse
Frédéric PIECHON	Co-directeur de thèse

Contents

1 Introduction 1
- 1.1 Synchronization transition on atomic chips 1
- 1.2 Interpretations of the experimental results 5
- 1.3 Proposition of the simplified two-spin model 7

2 Classical dynamics and sync 11
- 2.1 Description of the model and solution 11
  - 2.1.1 Model 11
  - 2.1.2 Dynamics 14
- 2.2 Phase transition 17
- 2.3 Characteristic time scales 19
- 2.4 Phase portrait 20
  - 2.4.1 x-axis symmetry 22
  - 2.4.2 Fixed points and stability analysis 24
  - 2.4.3 Qualitative picture from the phase portrait 28
- 2.5 Relation to the BH dimmer and the LMG model 30
- 2.6 Summary 32

3 Quantum dynamics and no sync 35
- 3.1 Spin One Half 37
- 3.2 Large spins: numerics 41
- 3.3 Effective models for the dynamics 46
  - 3.3.1 Effective model in the dephased regime 46
  - 3.3.2 Effective model in the synchronized regime 51
  - 3.3.3 Improved method in the synchronized regime 55
- 3.4 Cumulant expansion method 59
  - 3.4.1 Direct expansion 59
  - 3.4.2 Improved cumulant expansion 62

3.4.3 Comments on the cumulant expansion 65
3.5 Phase-space method 66
3.5.1 Remarks on the phase-space method 74
3.6 Summary 75
3.7 Appedix: Effective models detail 76
3.7.1 Dephased regime ($J \ll \delta/2$): $\{|m_1, m_2\rangle\}$ basis 76
3.7.2 Synchronized regime ($J \gg \delta/2$): $\{|S_t, m_t\rangle\}$ basis . . . 78
3.7.3 Improved method in the synchronized regime ($J \gg \delta/2$) 80
3.8 Appendix: Coherent states 83
3.8.1 D algebra of coherent state 83
3.8.2 The equation of motion for Husimi function 85
3.8.3 Change of variables to canonical variables 87

4 Squeezing and Entanglement 89
4.1 Introduction to spin squeezing 89
4.1.1 Spin squeezing parameter of Kitagawa and Ueda . . . 90
4.1.2 Spin squeezing parameter of Wineland et al 91
4.2 Numerical results 92
4.3 Effective models 93
4.3.1 Weak interaction regime $J \ll \delta$ 94
4.3.2 Strong interaction regime $J \gg \delta$ 96
4.3.3 Husimi function of the effective model 97
4.4 Summary and discussion 99
4.5 Appendix 99
4.5.1 Weak interaction regime ($J \ll \delta/2$) 99
4.5.2 Strong interaction regime ($J \gg \delta/2$) 100

5 Conclusion and outlook 101

6 Appendix: Dynamics on a spin chain 105
6.1 Statement of the problem 105
6.2 A possible direction 106
6.3 Summary and discussion 107

Bibliography 109

Acknowledgements

This thesis would not have taken its present form without the help and support of many people. Some of these are scientific discussions, some are moral support, and some are unconditional love. It is not possible to list all of the people who deserve recognition in such a brief acknowledgement. I can only try my best.

First I would like to thank my thesis advisor Jean-Noël Fuchs, who is both an excellent physicist and wonderful advisor who can convey the underlying physics in a clear and transparent manner. His clear mind has always helped me to go in the right direction, and to save a lot of time that would otherwise be wasted in vain. Many of the ideas in this thesis originate from discussion with him. Doing a thesis under his guidance is a great experience for me.

I would also like to express my gratitude to Frédéric Piéchon my co-advisor, whose availability for scientific discussions and wide knowledge of a variety domains of physics have made a huge difference in this thesis. He gives me the deep impression that the physics is unified in a beautiful and astonishing manner.

The discussions with various researchers have benefited me greatly. Thanks to the group of Peter Rosenbusch. Through the valuable discussions and collaboration, I have been able to appreciate the physics of cold atoms. And I am grateful to Franck Laloë, whose physical insight demonstrates the right way of doing physics for me.

Thanks to the members of theory group at Laboratoire de Physique des Solides, who made the three years of working and studying there an unforgettable memory. Thanks to Marc Goerbig, the biggest smuggler of caffeine of LPS. Though he has not successfully converted me into a big consumer, Mark's supplies have made the café chat a warm and cozy occasion. I am grateful to Marcello Civelli whose good temper makes him a nice companion for a PhD student. I am fortunate to have met the numerous PhD students

and postdocs who have been here during the last three years. Jean-Réné Souquet shares the same room with me and is a mathematical dictionary when I can not solve an integral or a differential equation. I hope being in the same room with me is not boring for him. The little bottle of Ricard with the signature of Dennis Chevallier is a nice souvenir. And thanks to Lih-King Lim, Albert Mathias, François Crépin, Doru Sticlet, Raphaël de Gail, Emilio Winograd, Clément Dutreix, and Nicolas Thiébaut, whose company fills the three years with laugh and joy.

I am deeply indebted to my familly, whose unconditional support and love make my journey possible. Thanks to my parents who always support me in the difficult times of life. And to Zhen, my wife, who lightens the world up during the gloomy days.

Chapter 1

Introduction

Spin waves are the elementary excitations of coupled spin systems with finite magnetization or staggered magnetization. Long before the advent of cold atoms, the physics of spin waves has been an active field of research, and was found in a large variety of systems. It has been studied in ferromagnets and antiferromagnets[1], in paramagnetic systems[2, 3, 4, 5], and in dilute gases such as spin-polarized ^{3}He gas and solution of ^{3}He in ^{4}He[6, 7, 8, 9, 10, 11]. After the first realization of Bose-Einstein condensation (BEC)[12, 13, 14, 15], the study of spin waves in quantum atomic gases[16, 17, 18, 19, 20, 21, 22, 23] has renewed the area by making possible both the study of spin waves far from equilibrium and the direct observation of dynamical behaviors. In this thesis, we study a model based on the experimental observations of spin waves in cold atomic gases.

1.1 Synchronization transition on atomic chips

The motivation of this thesis originates from a series of experiments on sn atomic chip performed in 2010[24]. The atomic chip works as follows. First, a magnetic potential is set up which traps two internal states of rubidium atoms (denoted as $|0\rangle$ and $|1\rangle$). The magnetic trapping potential takes the form of an elongated cigar-shape harmonic potential, usually with an axial-frequency much lower than the radial-frequencies, and can be considered as a quasi one-dimensional harmonic potential if we average out the radial movement. The temperature of the system is typically close to but above the BEC temperature so that the system is weakly degenerate. The time between two collisions for an atom is usually large compared to the period of its orbital movement in the harmonic potential. Thus the system is in the

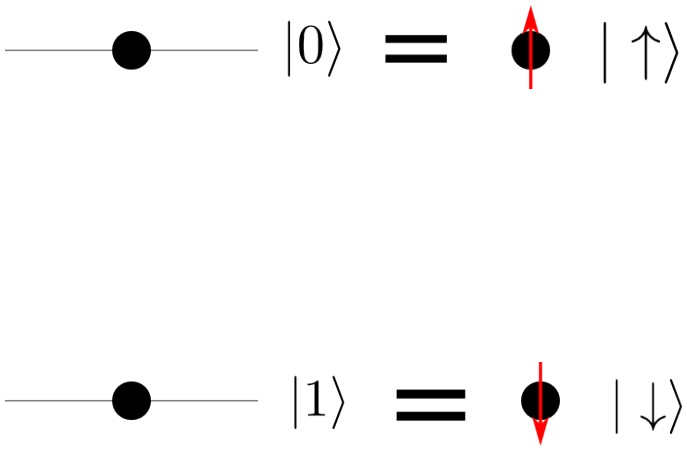

Figure 1.1: Schematic illustration of the map between the two level system and the spin $1/2$ system.

Knudsen (collisionless) regime. Each rubidium atom can be considered as a pseudo-spin $1/2$ particle[25], with (see Fig. 1.1)

$$\begin{aligned} |0\rangle &\rightarrow |\uparrow\rangle, \\ |1\rangle &\rightarrow |\downarrow\rangle. \end{aligned} \tag{1.1}$$

Hereafter, we use the spin language to denote the internal states of rubidium atoms in describing the Ramsey contrast experiment (see Fig. 1.2). Initially, all the atoms are prepared in the $|\uparrow\rangle$ state. Then a radio-frequency pulse of $\pi/2$ around the y-axis rotates the atom into the state

$$\frac{1}{\sqrt{2}}\left(|\uparrow\rangle + |\downarrow\rangle\right), \tag{1.2}$$

which is the coherent state pointing in the x-direction. The transition matrix of this radio-frequency pulse takes the form

$$R_y(\pi/2) = \frac{1}{\sqrt{2}}\left(|\uparrow\rangle\langle\uparrow| - |\uparrow\rangle\langle\downarrow| + |\downarrow\rangle\langle\uparrow| + |\downarrow\rangle\langle\downarrow|\right). \tag{1.3}$$

The atoms are left to evolve freely in the harmonic trapping potential. During this evolution, the atoms experience an external magnetic field and interact with each other through collisions. After a delay of T_R, the Ramsey time,

another $\pi/2$ pulse around the y-axis is applied to the atoms and the population of atoms in the two states (N_0 and N_1 for the population in the state $|0\rangle$ and $|1\rangle$) are measured. The probability to find the atom in the $|1\rangle$ state is

$$\mathrm{P}_1 \equiv \frac{N_1}{N_0 + N_1} \tag{1.4}$$

If an atom at the end of the free evolution is in the state

$$|\psi(t)\rangle = \frac{1}{\sqrt{2}}\left(e^{-i\phi/2}|\uparrow\rangle + e^{i\phi/2}|\downarrow\rangle\right), \tag{1.5}$$

which is the coherent state pointing in the direction $(\cos\phi, \sin\phi, 0)^T$, then after the second pulse, it will be in the state

$$|\psi\rangle_f = R_y(\pi/2)|\psi(t)\rangle = -i\sin(\phi/2)|\uparrow\rangle + \cos(\phi/2)|\downarrow\rangle. \tag{1.6}$$

If the system consists of N atoms in the same state, then the populations of the two states are

$$\begin{aligned} N_0 &= N|\langle\uparrow|\psi\rangle_f|^2 = N\sin^2(\phi/2), \\ N_1 &= N|\langle\downarrow|\psi\rangle_f|^2 = N\cos^2(\phi/2). \end{aligned} \tag{1.7}$$

From the above expression, we can deduce that

$$\mathrm{P}_1 = \frac{N_1}{N_0 + N_1} = \frac{1}{2}(1 + \cos\phi). \tag{1.8}$$

This probability is thus related to the relative angle ϕ of the atoms in the xy-plane gained in the free evolution process. We can extract the information of the spin configuration $z = e^{i\phi}$ in the xy-plane from this relation. However, in the above argument, we have assumed that all atoms are in the same state, and thus coherent. In real experiments, this coherence can be broken down due to the inhomogeneity of the magnetic field and collisions during the free evolution, which is called inhomogeneous broadening. We can define the Ramsey fringe contrast to describe this decoherence. The Ramsey fringe contrast is defined as

$$\mathrm{C}_{Ramsey} \equiv \left|\frac{z(t)}{z(0)}\right| = \frac{|z(t)|}{N}, \tag{1.9}$$

where

$$z = \sum_i z_i \tag{1.10}$$

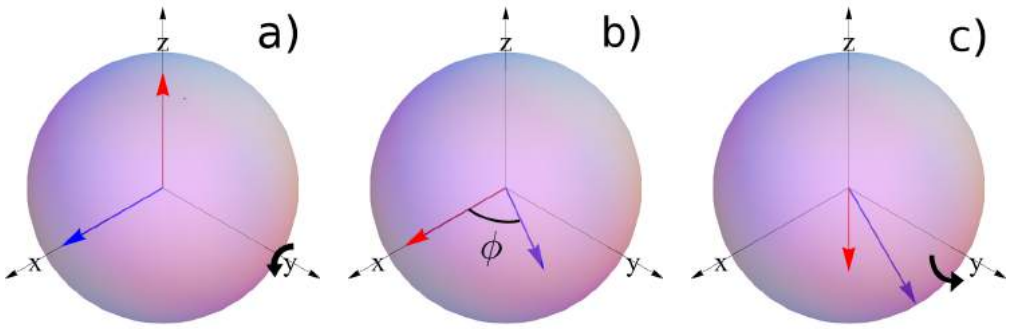

Figure 1.2: Schematic illustration of the Ramsey procedure. a) A first $\pi/2$ pulse is applied to rotate the spin from $(0,0,1)^T$ to $(1,0,0)^T$. b) Free evolution period, where the spin gains a phase ϕ in the xy-plane. c) The second $\pi/2$ pulse is applied. The spin is rotated from $(\cos\phi, \sin\phi, 0)^T$ to $(0, \sin\phi, -\cos\phi)^T$. The red arrows are the initial positions of the spin and the blue arrows the end positions in each process.

is the total spin configuration. Let us consider an inhomogeneous broadening uniformly distributed between $[0, \Delta_0]$ for all atoms, where Δ_0 is the characteristic inhomogeneity. Then after a free evolution of t, each atom obtains a spin configuration $z_i = e^{i\Delta_i t}$. The Ramsey contrast is

$$\mathrm{C}_{Ramsey} = \left| \frac{1}{\Delta_0} \int_0^{\Delta_0} e^{i\Delta t} d\Delta \right| = \frac{2}{\Delta_0 t} |\sin(\frac{\Delta_0 t}{2})|. \tag{1.11}$$

The contrast vanishes at $t = \pi/\Delta_0$ and then oscillates with small amplitude close to zero.

In 2010, this kind of experiment was performed with $N \approx 10^4$ ^{87}Rb atoms. In this system, each atom experiences an external inhomogeneous magnetic field in the z-direction which tends to dephase the atoms. The atoms also interact with each other through collisions. The contributions of collisions can be categorized into three groups. The first group is the density mean-field which acts as an additional inhomogeneous field due to the inhomogeneous density profile. The second is the spin mean-field which gives rise to the exchange interaction with a rate $\omega_{ex} \propto an$, where n is the local density and a the s-wave scattering length. This effect is called identical spin rotation effect(ISRE). These two groups originate from the forward/backward scattering. The third one is the lateral collision which randomizes the system, and brings the atoms into local equilibrium with a rate $\gamma_c \propto an^2$. The effective inhomogeneity Δ_0 is the sum of the external field and the density mean-field

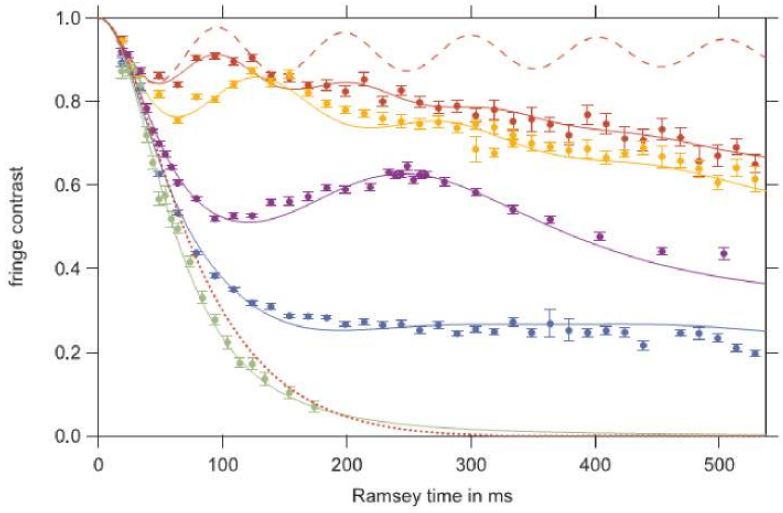

Figure 1.3: Experimental results of the Ramsey contrast as a function of time. From bottom to top, the symbols with different colors represent experimental results for increasing interaction strengths. The solid lines are numerical simulations of the kinetic equation. The top dashed line shows that a strong interaction can lead to an almost complete synchronization. This figure is taken from [24].

term which acts as an inhomogeneous magnetic field. In the experiment, the time scales are such that

$$\frac{2\pi}{\omega_{x,y,z}}(t) \ll \frac{2\pi}{\Delta_0} \sim \frac{2\pi}{\omega_{ex}} (\text{or } \frac{2\pi}{\Delta_0} \ll \frac{2\pi}{\omega_{ex}}) \ll \frac{1}{\gamma_c}, \tag{1.12}$$

where $\omega_{x,y,z}$ is the frequency of the harmonic potential.

The experimental results show that if the interaction is superior to a critical value, the Ramsey contrast stops decaying and even shows revivals (see the dashed line in 1.3), indicating that the spins of the atoms are synchronized. For certain experimental conditions, the coherence time is larger by an order of magnitude than the previous prediction which has not taken into the ISRE effect[26].

1.2 Interpretations of the experimental results

The surprising result of the experiment was explained with the kinetic theory of spin waves, where the distribution in energy space was employed since the system is in the Knudsen regime. This idea originates from previous work

on fermionic systems[22, 23], which are naturally in the collisionless regime at low temperature due to Pauli blocking. The equation of motion for the spin density reads[24]

$$\begin{aligned}&\partial_t \vec{S}(E,t) + \gamma_C[\vec{S}(E,t) - \bar{\vec{S}}(t)] \\ &\approx \left[\Delta(E)\hat{e}_z + \omega_{ex}\int_0^\infty dE' \frac{E'^2}{2} e^{-E'} K(E,E')\vec{S}(E',t)\right] \times \vec{S}(E,t),\end{aligned} \tag{1.13}$$

where $\Delta(E) = \Delta_0 E$, $\bar{\vec{S}}(t)$ is the average spin, $E^2/2$ the density of states, and $K(E,E')$ the interaction kernel. The above equation has been brought to a dimensionless form where the energy is measured in units of $k_B T$. In this equation, the interacting kernel is a point-wise contact term in real space. In the energy space, as we average over many orbital movements in the harmonic potential, which is justified because of the condition in Eq. 1.12, the interacting term becomes long ranged. Thus the above equation describes the collective dynamics of the spins.

In the above equation, we have used

$$\vec{S}(E,t) = \langle \hat{\vec{S}}(E,t)\rangle, \tag{1.14}$$

where $\hat{\vec{S}}$ is quantum operator of spin and $\langle \hat{\vec{S}}(E,t)\rangle$ the quantum expectation value. When writing the interaction term in Eq. 1.13, we have assumed that

$$\langle \vec{S}(E',t) \times \vec{S}(E,t)\rangle \approx \langle \vec{S}(E',t)\rangle \times \langle \vec{S}(E,t)\rangle. \tag{1.15}$$

Therefore the quantum correlations between two spins are neglected and the spins are treated as classical objects.

A different point of view is to consider just two quantum spins $1/2$[27] (see Fig. 1.4). The Hamiltonian takes the form

$$H = B_0 S_1^z + (B_0 + D) S_2^z + \omega_{ex} \vec{S}_1 \cdot \vec{S}_2. \tag{1.16}$$

In this Hamiltonian, the two spins experience an inhomogeneous magnetic field with the inhomogeneity D (equivalent to Δ_0 used in demonstrating the Ramsey fringe contrast), and they interact with each other through an exchange term of strength ω_{ex}. Initially, the two spins point in the x-direction, i.e. $|\psi(0)\rangle = (1/\sqrt{2})(|\uparrow\downarrow\rangle + |\downarrow\uparrow\rangle)$. Using the singlet-triplet basis defined as

$$\begin{aligned}|u\rangle &= |\uparrow\uparrow\rangle, \\ |d\rangle &= |\downarrow\downarrow\rangle, \\ |t\rangle &= \frac{1}{\sqrt{2}}(|\uparrow\downarrow\rangle + |\downarrow\uparrow\rangle), \\ |d\rangle &= \frac{1}{\sqrt{2}}(|\uparrow\downarrow\rangle + |\downarrow\uparrow\rangle),\end{aligned} \tag{1.17}$$

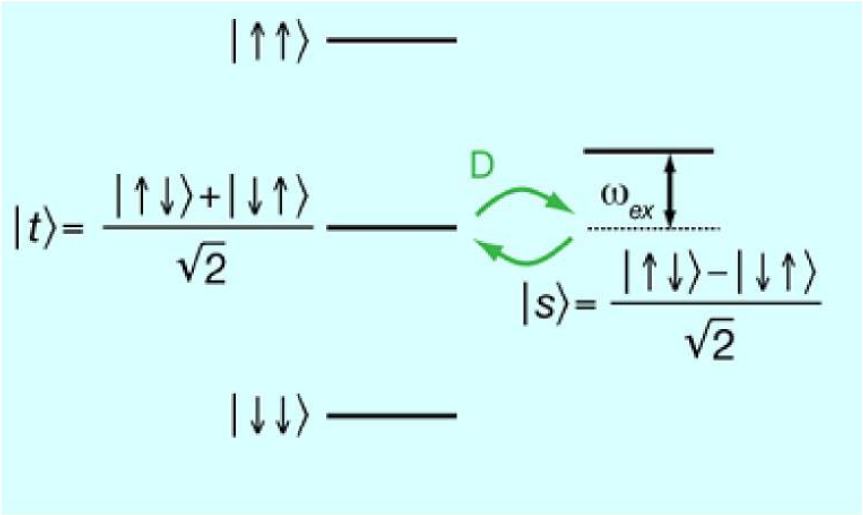

Figure 1.4: Qualitative picture with the singlet-triplet basis (taken from [27]). The dephasing is the transition between $|t\rangle$ and $|s\rangle$ caused by the inhomogeneous torque D. The interaction creates a gap of ω_{ex} between the two states. If the interaction is large, the transition between the two states is difficult and the two spins are kept synchronized for a long time.

the Hamiltonian reads

$$H = \begin{pmatrix} \frac{1}{2}(2B_0 + D) + \frac{\omega_{ex}}{4} & 0 & 0 & 0 \\ 0 & -\frac{1}{2}(2B_0 + D) + \frac{\omega_{ex}}{4} & 0 & 0 \\ 0 & 0 & \frac{\omega_{ex}}{4} & -\frac{D}{2} \\ 0 & 0 & -\frac{D}{2} & -\frac{3\omega_{ex}}{4} \end{pmatrix}. \quad (1.18)$$

From the structure of the Hamiltonian, it is clear that the two states $|t\rangle$ and $|s\rangle$ are coupled (see the 2×2 block of the right bottom). The dephasing is due to the transition between $|t\rangle$ and $|s\rangle$ with a transition element proportional to D. The two states are separated by an energy gap ω_{ex}. If this gap is very large, then it is difficult for the transition to happen. However, the coherence time is only pushed far away but not to infinity by the large interaction.

1.3 Proposition of the simplified two-spin model

The kinetic theory has taken into account the collective nature of the dynamics but has neglected the quantum correlations between pairs of spins. The two spins $1/2$ picture has considered the quantum correlations but has neglected the collective behavior. Therefore, we want to consider a model

which treats the quantum correlations and the collective behavior. An intuitive choice would be to consider a system of N quantum spins $1/2$. But the dimension of the Hilbert space is too large ($= 2^N$). Simplification is necessary. A simplified picture is to split the N atoms into two classes, each consisting of $N/2$ atoms, based on their orbital energies[22] (see Fig.1.5). Each class can be considered as a quantum macro-spin of size $S = N/4$. Since the atoms in each class have different trajectories in the harmonic trapping potential, they experience a different mean magnetic field which has a dephasing effect on the two macro-spins. The ISRE, on the other hand, tries to synchronize them. Besides, since we are in the Knudsen regime, the energy-changing lateral collisions are rare. The atoms in the two groups remain in their groups for a long time. This justifies the separation of atoms into two stable groups. Thus we consider a strongly simplified Hamiltonian for this picture which reads

$$H = \frac{\delta_S}{2}(S_1^z - S_2^z) + J_S \vec{S}_1 \cdot \vec{S}_2. \tag{1.19}$$

In the above Hamiltonian, the inhomogeneity of the mean magnetic field on the two spins is denoted by δ_S (This is equivalent to $2\Delta_S$ in [28]). The interaction between the two macro-spins is taken to be a Heisenberg exchange interaction with the strength J_S. In writing the above Hamiltonian, we have used the rotating reference frame with the same angular velocity as that of the mean precession of the two macro-spins. The ration J_S/δ_S can be fixed by equating it to ω_{ex}/Δ_0 in the experiments. Initially, the two spins are in the x-direction. The quantity of interest is the total spin defined as

$$\vec{S}_t \equiv \vec{S}_1 + \vec{S}_2. \tag{1.20}$$

The contrast of this toy model is defined as

$$\mathrm{C}(t) \equiv \left| \frac{\langle \vec{S}_t(t) \rangle}{\langle \vec{S}_t(0) \rangle} \right|. \tag{1.21}$$

The definition of synchronization in this two-spin model is that the contrast should never reach zero, i. e. the norm of the total spin is always finite. There are other definitions of synchronization. Our model can also be applied to other domains, such as two interacting quantum dots[29, 30], two nanodisks with large magnetic moments[31], and two coupled molecular magnets[32].

In this thesis, we want to answer the following questions. Is there a synchronization transition in the model of two spins? What is the effect of quantum correlations neglected in the kinetic theory? The latter question

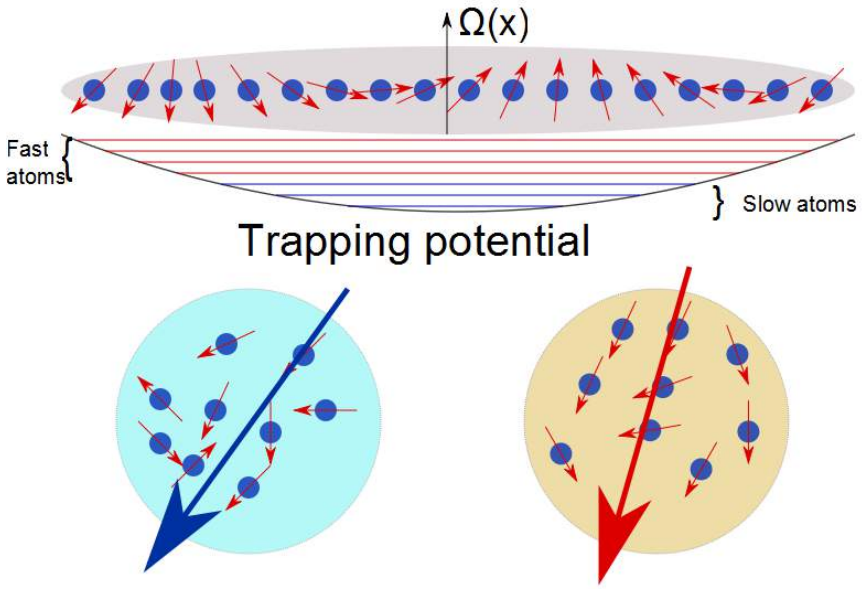

Figure 1.5: Schematic illustration of the toy model. In the upper part, the cloud of atoms are shown. Each atom is represented by a blue ball with a red arrow indicating the spin state. The inhomogeneous magnetic field in the z-direction is labeled by $\Omega(x)$, where x is the direction along the axis of the cigar-shaped cloud. In the middle part, the orbitals are split into two groups. The red ones signify the fast moving atoms, and the blue ones the slow moving atoms. In the lower part, we consider each of the two groups of atoms as a macro-spin of size $S = N/4$. The blue arrow denotes the slow atoms and the red arrow the fast atoms.

is equivalent to: what is the difference between the classical dynamics and quantum dynamics of two spins? Finally, what is the effect of the spin size S on the synchronization?

The thesis is organized as follows. In chapter 2, we study the classical dynamics of the two-spin model to see if there is a synchronization. Then in chapter 3 the quantum dynamics of the two-spin model is studied, with the goal of finding out the influence of the quantum correlations on the dynamics. We also study systems with different spin sizes to understand how the classical limit emerges. In chapter 4, we study spin squeezing in the two-spin model. We conclude in chapter 5 and outline some perspectives. In chapter 6, an appendix is presented on preliminary results on the related model of a finite one-dimensional spin 1/2 chain.

Chapter 2

Classical dynamics and Synchronization

In this chapter, we consider the classical dynamics of the two-spin sytem. We consider the following question: under what condition would our system with the specific initial state be synchronized?

2.1 Description of the model and solution

2.1.1 Model

The model consists of two spins initially lying parallel in the transverse plane of an inhomogeneous magnetic field, interacting with each other through an exchange interaction (see Fig. 2.1). Initially, the system is in the state

$$\begin{cases} S_i^x = S, \\ S_i^y = 0, \\ S_i^z = 0. \end{cases} \qquad i = 1, 2 \tag{2.1}$$

The Hamiltonian of the system takes the form

$$H = \frac{\delta_S}{2}(S_1^z - S_2^z) + J_S \vec{S}_1 \cdot \vec{S}_2 \tag{2.2}$$

The first term describes the inhomogeneity of the magnetic field, and the second term is the usual $SU(2)$ invariant Heisenberg exchange interaction between the two spins. When J_S is positive, the interaction is anti-ferromagnetic. When J_S is negative, the interaction is ferromagnetic. Although the two cases seem a huge difference, the dynamics is not altered much by changing

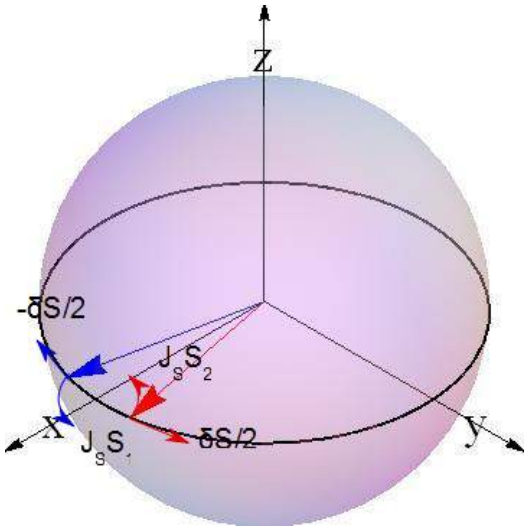

Figure 2.1: Schematic illustration of the model. The two spins are represented by blue and red arrow respectively. The effective magnetic field is the combination of the external magnetic field ($\pm\delta_S/2$) and the exchange coupling to the other spin ($J_S\vec{S}_{2,1}$).

the sign of interaction. When changing J_S to $-J_S$, we find $S_i^y(t) \to -S_i^y(t)$ and $S_i^z(t) \to -S_i^z(t)$, while $S_i^x(t)$ invariant. This is related to the specific initial state that we have chosen. Another property of the system's dynamics related to the initial state is that during the temporal evolution, we always have $S_1^x(t) = S_2^x(t)$, $S_1^y(t) = -S_2^y(t)$, and $S_1^z(t) = -S_2^z(t)$.

The equations of motion for this system can be obtained by the usual Hamiltonian mechanical methods, using the Poisson bracket. For the spins, the Hamiltonian is a bit different in the sense that $S^{x,y,z}$ are not canonical variables. But still the equations of motion for the two spins can be obtained as:

$$\begin{aligned} \frac{d}{dt}\vec{S}_1 &= \frac{\delta_S}{2}\hat{e}_z \times \vec{S}_1 + J_S\vec{S}_2 \times \vec{S}_1, \\ \frac{d}{dt}\vec{S}_2 &= -\frac{\delta_S}{2}\hat{e}_z \times \vec{S}_2 + J_S\vec{S}_1 \times \vec{S}_2. \end{aligned} \tag{2.3}$$

In the above equations, the first terms on the right hand side are the usual term describing the motions caused by the inhomogeneous magnetic field. The second terms on the right hand side reflect the exchange interaction between the two spins. The nonlinearity of the dynamics can be readily seen from the second terms. Without this interaction term, the dynamics is simply two independent spins moving in the magnetic field of their own, and is easy to solve. The initial conditions are given in Eq. 2.1.

The subindex S of δ_S and J_S is used to indicate the dependence on the size of the spin. Now we want to rescale the parameters of the system so that the spin-dependence can be canceled out. To do this, we consider systems of different spin sizes, but with same total energy. Incorporating the spin dependence of the spin observable into the parameters of the Hamiltonian, we rescale the spin operators by a factor of $1/S$, the inhomogeneity of the magnetic by a factor of S and the interaction strength by S^2:

$$\begin{aligned} \vec{n}_{1,2} &\equiv \vec{S}_{1,2}/S, \\ \delta &\equiv S\delta_S, \\ J &\equiv S^2 J_S. \end{aligned} \tag{2.4}$$

After this rescaling, the Hamiltonian reads:

$$H = \frac{\delta}{2}(n_1^z - n_2^z) + J\vec{n}_1 \cdot \vec{n}_2, \tag{2.5}$$

and the equations of motion are:

$$\begin{aligned} S\frac{d}{dt}\vec{n}_1 &= \frac{\delta}{2}\hat{e}_z \times \vec{n}_1 + J\vec{n}_2 \times \vec{n}_1, \\ S\frac{d}{dt}\vec{n}_2 &= -\frac{\delta}{2}\hat{e}_z \times \vec{n}_2 + J\vec{n}_1 \times \vec{n}_2. \end{aligned} \tag{2.6}$$

Now the only spin size dependence is on the left hand side of the above equations of motion using rescaled parameters. This dependence can be eliminated from our analysis by rescaling the time, i.e., $\tilde{t} \equiv t/S$. After this novel rescaling, the equations of motion take the final form:

$$\begin{aligned} \frac{d}{d\tilde{t}}\vec{n}_1 &= \frac{\delta}{2}\hat{e}_z \times \vec{n}_1 + J\vec{n}_2 \times \vec{n}_1, \\ \frac{d}{d\tilde{t}}\vec{n}_2 &= -\frac{\delta}{2}\hat{e}_z \times \vec{n}_2 + J\vec{n}_1 \times \vec{n}_2, \end{aligned} \tag{2.7}$$

with the initial conditions:

$$\begin{aligned} \vec{n}_1(0) &= \hat{e}_x, \\ \vec{n}_2(0) &= \hat{e}_x. \end{aligned} \tag{2.8}$$

To obtain the final form of the equations of motion, three rescalings are employed. The first rescaling is the one of the inhomogeneity of the external field, which is physically transparent. The second one is the one of the exchange interaction by a factor of S^2. An additional S is the consequence of the nonlinear nature of the interaction term, analogous to the rescaling of

$1/N$ of the interaction term in the infinite range Ising model, where N is the total number of spins of the system. The last one is the rescaling of time, which seems less intuitive. In summary, we have used the rescaling

$$\begin{aligned}\tilde{t} =&\frac{t}{\Lambda_S},\\ \delta =&\Lambda_S \delta_S,\\ J =&\Lambda_S^2 J_S,\\ \vec{n}_i =&\frac{\vec{S}_i}{\Lambda_S},\end{aligned} \tag{2.9}$$

with $\Lambda_S = S$ being the rescaling constant.

2.1.2 Dynamics

To solve the equations of motion Eq. (2.7) and to shed light on the nature of the dynamics, it is advantageous to change the variables from the single spin variables to the total spin and spin difference:

$$\begin{aligned}\vec{n}_t \equiv&\vec{n}_1 + \vec{n}_2,\\ \vec{n}_d \equiv&\vec{n}_1 - \vec{n}_2.\end{aligned} \tag{2.10}$$

Then the equations of motion for these two variables read:

$$\begin{aligned}\frac{d}{d\tilde{t}}\vec{n}_t =&\frac{\delta}{2}\hat{e}_z \times \vec{n}_d(\tilde{t}),\\ \frac{d}{d\tilde{t}}\vec{n}_d =&\frac{\delta}{2}\hat{e}_z \times \vec{n}_t(\tilde{t}) + J\vec{n}_t(\tilde{t}) \times \vec{n}_d(\tilde{t}).\end{aligned} \tag{2.11}$$

The initial conditions are:

$$\begin{aligned}\vec{n}_t(0) =&2\hat{e}_x,\\ \vec{n}_d(0) =&0.\end{aligned} \tag{2.12}$$

There are some constants of motion which will help to solve the problem. First, note that $\vec{n}_1 \cdot \frac{d\vec{n}_1}{dt} = 0$ and $\vec{n}_2 \cdot \frac{d\vec{n}_2}{dt} = 0$, indicating that the norms of $\vec{n}_1$ and $\vec{n}_2$ are conserved. Using this fact, it can be shown that $\vec{n}_t$ and $\vec{n}_d$ are always perpendicular to each other because $\vec{n}_t \cdot \vec{n}_d = (\vec{n}_1 + \vec{n}_2) \cdot (\vec{n}_1 - \vec{n}_2) = \vec{n}_1^2 - \vec{n}_2^2 = 0$. In addition, the rotational symmetry of the whole system around the z-axis leads to the observation that $n_t^z(t) = n_t^z(0) = 0$. Although the norms of $\vec{n}_t$ and $\vec{n}_d$ are not constants of motion, their sum is:

$$\vec{n}_t^2 + \vec{n}_d^2 = (\vec{n}_1 + \vec{n}_2)^2 + (\vec{n}_1 - \vec{n}_2)^2 = 2(\vec{n}_1^2 + \vec{n}_2^2) = 4.$$

The facts that $n_t^z \equiv 0$ and $\vec{n}_t \cdot \vec{n}_d \equiv 0$ suggest that $\vec{n}_t$ rotates always in the xy-plane, while $\vec{n}_d$ is orthogonal to it. This motivates the utilization of a reference frame rotating with the total spin $\vec{n}_t$:

$$\begin{cases} \hat{e}_\parallel &\equiv \cos\phi\hat{e}_x + \sin\phi\hat{e}_y, \\ \hat{e}_\perp &\equiv -\sin\phi\hat{e}_x + \cos\phi\hat{e}_y, \\ \hat{e}_z &\equiv \hat{e}_z, \end{cases} \tag{2.13}$$

such that

$$\begin{aligned} \vec{n}_t =& n_\parallel \hat{e}_\parallel, \\ \vec{n}_d =& n_\perp \hat{e}_\perp + n_z \hat{e}_z. \end{aligned} \tag{2.14}$$

In the above definition of the reference frame basis, the angle ϕ is a function of time with the initial condition $\phi(0) = 0$. And the time derivative of the basis are:

$$\begin{cases} \frac{d\hat{e}_\parallel}{d\tilde{t}} &= \dot{\phi}\hat{e}_\perp, \\ \frac{d\hat{e}_\perp}{d\tilde{t}} &= -\dot{\phi}\hat{e}_\parallel, \\ \frac{d\hat{e}_z}{d\tilde{t}} &= 0, \end{cases} \tag{2.15}$$

where the dot means derivative with respect to the rescaled time. In this rotating reference frame, the equations of motion for $\vec{n}_t$ and $\vec{n}_d$ can be written explicitly as:

$$\begin{aligned} \dot{n}_\parallel \hat{e}_\parallel + n_\parallel \dot{\phi}\hat{e}_\perp =& -\frac{\delta}{2} n_\perp \hat{e}_\parallel, \\ \dot{n}_\perp \hat{e}_\perp - n_\perp \dot{\phi}\hat{e}_\parallel + \dot{n}_z \hat{e}_z =& (\frac{\delta}{2} n_\parallel - J n_\parallel n_z)\hat{e}_\perp + J n_\parallel n_\perp \hat{e}_z. \end{aligned} \tag{2.16}$$

Equating components, we get:

$$\begin{aligned} \dot{\phi} =& 0, \\ \dot{n}_\parallel =& -\frac{\delta}{2} n_\perp, \\ \dot{n}_\perp =& \frac{\delta}{2} n_\parallel - J n_\parallel n_z, \\ \dot{n}_z =& J n_\parallel n_\perp. \end{aligned} \tag{2.17}$$

The first equation in the above equation shows that $\hat{e}_\parallel$ and $\hat{e}_\perp$ do not rotate in time and that $\vec{n}_t$ is always along the x-axis, while $\vec{n}_d$ in the yz-plane. Now we can identify $\hat{e}_\parallel = \hat{e}_x$ and $\hat{e}_\perp = \hat{e}_y$. Then the ansatz $\vec{n}_t = 2\cos\theta(\tilde{t})\hat{e}_x$, with

the initial condition $\theta(0) = 0$, yields

$$\begin{aligned} n_\perp =& \frac{4}{\delta} \sin\theta\dot{\theta}, \\ n_z =& \frac{4J}{\delta} \sin^2\theta. \end{aligned} \tag{2.18}$$

Using the remaining constant of motion $\vec{n}_t^2 + \vec{n}_d^2 = 4$, we have

$$n_\perp^2 = 4 - n_\parallel^2 - n_z^2 = 4\sin^2\theta(1 - \frac{4J^2}{\delta^2}\sin^2\theta). \tag{2.19}$$

But from Eq (2.18), we also have $n_\perp^2 = \frac{16}{\delta^2}\sin^2\theta(\dot{\theta})^2$. Consequently, we obtain the differential equations governing the temporal evolution of θ

$$\frac{16}{\delta^2}\sin^2\theta(\dot{\theta})^2 = 4\sin^2\theta(1 - \frac{4J^2}{\delta^2}\sin^2\theta), \tag{2.20}$$

or simply:

$$(\dot{\theta})^2 = (\frac{\delta}{2})^2(1 - (\frac{2J}{\delta})^2\sin^2\theta) \tag{2.21}$$

Assuming $\dot{\theta} > 0$, we get

$$\frac{d\theta}{\sqrt{1 - \frac{4J^2}{\delta^2}\sin^2\theta}} = \frac{\delta}{2}d\tilde{t}. \tag{2.22}$$

The left hand side of the above equation takes the form of an elliptic integral. The implicit solution for θ is

$$F(\sin\theta, \frac{2J}{\delta}) = \frac{\delta}{2}\tilde{t}, \tag{2.23}$$

where the function $F(\sin\theta, \frac{2J}{\delta})$ is the elliptic integral of the first kind. The contrast defined as $|\vec{n}_t(\tilde{t})|/|\vec{n}_t(0)|$ takes the form

$$\mathrm{C}(\tilde{t}) = \left| cn[\frac{\delta}{2}\tilde{t}, \frac{2J}{\delta}] \right|, \tag{2.24}$$

where we have used the Jacobi elliptic function cn. Then the solution for the single spin components is:

$$\begin{aligned} n_1^x &= \cos\theta = n_2^x, \\ n_1^y &= \sin\theta\sqrt{1 - (\frac{2J}{\delta})^2\sin^2\theta} = -n_2^y, \\ n_1^z &= \frac{2J}{\delta}\sin^2\theta = -n_2^z, \end{aligned} \tag{2.25}$$

where θ is the solution obtained in Eq. 2.23.

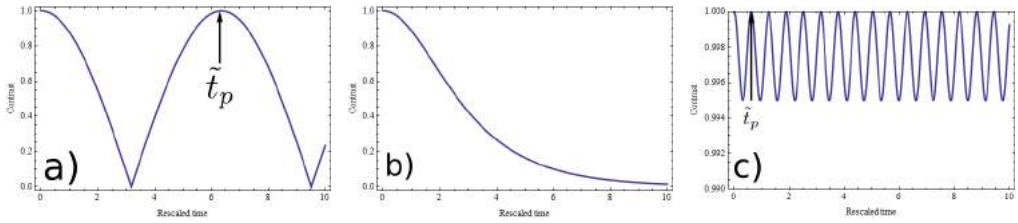

Figure 2.2: The contrast as a function of time. The unit of time is taken to be $1/\delta$. a) Dephased regime $J = 0.1\delta$, b) critical point $J = 0.5\delta$, and c) synchronized regime $J = 5\delta$. In the dephased and synchronized regime, the oscillation period $\tilde{t}_p$ is indicated by an arrow.

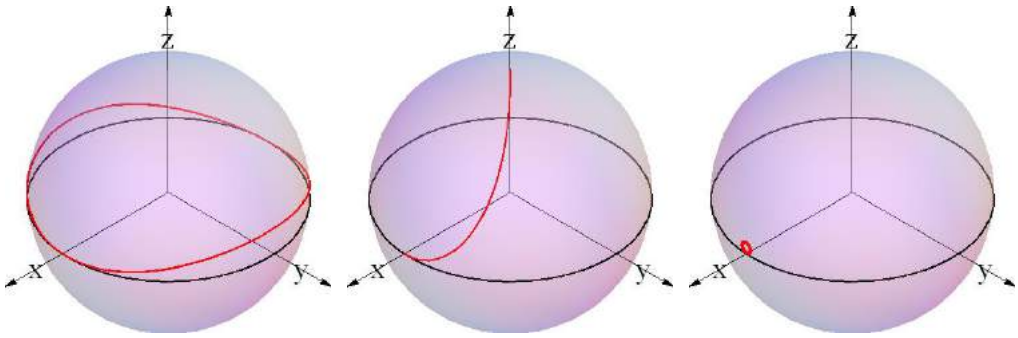

Figure 2.3: The trajectory of spin number 1 on the Bloch sphere. The initial position is $(1, 0, 0)^T$, from the x-axis. The thick black line is the equator. The red lines are the trajectories of the spin number 1.

2.2 Phase transition

After solving the equations of motion, we find that there are two regimes in which the system behaves differently (see Fig. (2.2)). In the small interaction ($J < \delta/2$) or dephased regime, the contrast reaches periodically zero and then goes back, signifying total dephasing. In the opposite large interaction ($J > \delta/2$) or synchronized regime, the contrast never goes to zero, and there is thus spin synchronization. At the critical point ($J = \delta/2$), it takes an infinitely long time for the contrast to reach zero. We can also plot the trajectory of spin number 1 (see Fig(2.3)). We see that in the dephased regime, the spin rotates mainly around the z-axis as expected, considering the fact that magnetic field is much stronger than the exchange interaction. The exchange interaction causes the spin to deviate a little bit from the transverse plane. In the synchronized regime, the spin rotates instead around the x-axis, the direction of total spin, because in this regime the interaction plays a dominant role in the dynamics.

In order to capture the physics of the two-spin model, a mapping onto the nonlinear pendulum proves helpful. To see this, we differentiate Eq. 2.21 again with respect to time

$$2\dot{\theta}\ddot{\theta} = -2J^2 \sin\theta\cos\theta\dot{\theta}, \tag{2.26}$$

or, eliminating $\dot{\theta}$ on both sides

$$\ddot{\theta} = -\frac{J^2}{2}\sin(2\theta). \tag{2.27}$$

Making a change of variable $\Theta = 2\theta$, we obtain

$$\ddot{\Theta} + J^2 \sin\Theta = 0, \tag{2.28}$$

the initial conditions being $\Theta(0) = 0$ and $\dot{\Theta}(0) = \delta$. This equation is just the usual equation of motion for a nonlinear pendulum of angle Θ initially at its stable fixed point, $\Theta(0) = 0$, and with an initial angular velocity $\dot{\Theta}(0) = \delta$. For our model, the oscillation frequency is J while for a real pendulum, this frequency is determined by $\sqrt{g/l}$ with l the length of the pendulum and g the acceleration of gravity. In this language, Contrast $= |\cos(\Theta/2)|$. In the dephased regime, the pendulum has enough energy to go through the highest point, the unstable fixed point, and to continue to the stable fixed point underneath and move on periodically. At the critical point, there is just enough energy for the pendulum to go to the unstable fixed point asymptotically. In the synchronized regime, the pendulum has not enough energy to go to unstable fixed point. It is confined in a small region near the initial position, where it oscillates periodically. In this regime, we can approximate the equation by a linear pendulum whose equation reads

$$\ddot{\Theta} + J^2\Theta = 0, \tag{2.29}$$

with the initial condition

$$\begin{aligned} \Theta(0) &= 0, \\ \dot{\Theta}(0) &= \delta. \end{aligned} \tag{2.30}$$

The solution is $\Theta(\tilde{t}) = (\delta/J)\sin(J\tilde{t})$. The period of the contrast can be readily obtained as $\tilde{t}_p \approx \pi/J$. For $J \gg \delta/2$, the contrast can be approximated as

$$\mathrm{C}(\tilde{t}) \approx 1 - \frac{\delta^2}{8J^2}\sin^2(J\tilde{t}). \tag{2.31}$$

Before going further into more detailed and more quantitative studies, it is necessary to emphasize that the image of a rigid nonlinear pendulum is just one way to understand the underlying physics. As we will see later in this chapter, our model can be also related to a non-rigid and nonlinear pedulum.

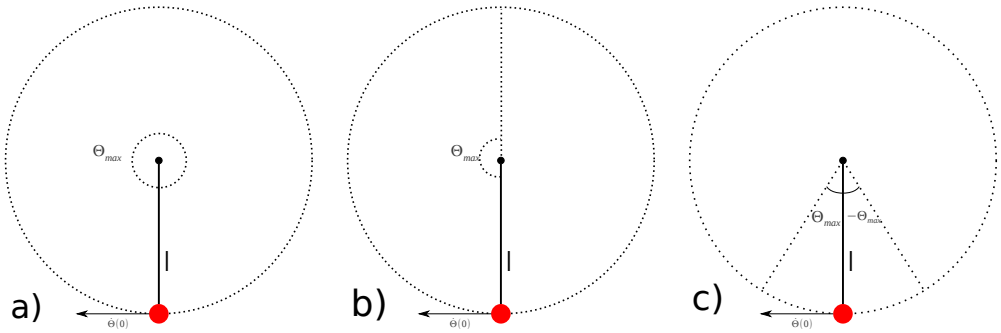

Figure 2.4: Analogy with a pendulum. a) Dephased regime ($J < \delta/2$): the pendulum can move along the whole circle and thus dephase completely. The corresponding movement of the spin is also dephased around the z-axis. b) Critical point ($J = \delta/2$): the pendulum goes to the unstable fixed point and stays there. The spin movement is similar in that the individual spins go to the poles of their Bloch sphere and stay there. c) Synchronized regime ($J > \delta/2$): the pendulum is confined to move in a small region $[-\Theta_{max}, \Theta_{max}]$ near the initial position. The spins in this regime move around their initial directions.

2.3 Characteristic time scales

The dynamics of the classical system can be characterized by some time scales expressed in the rescaled quantities. In our system of two spins, there are two characteristic time scales. The first one captures the initial decay, i.e., $\mathrm{C}(\tilde{t}) = 1 - (\tilde{t}/\tilde{t}_i)^2$ for short times. Expanding the solution for the contrast in Eq. 2.24 to leading order, we obtain

$$\mathrm{C}(\tilde{t}) \approx 1 - \frac{\delta^2 \tilde{t}^2}{8} \tag{2.32}$$

Fitting this with the aforementioned expression, we get

$$\tilde{t}_i = 2\sqrt{2}/\delta. \tag{2.33}$$

It is worth noting that this initial decay is independent of J, and thus does not depend on the regime. The reason for this observation is that the initial decay time describes the short time behavior of the two spins. During this period, the two spins are well aligned together such that the exchange interaction between them does not come into play. Consequently, the only factor having influence on the dynamics is the magnetic field. Besides, as plotted in Fig. 2.5, the fit is less satisfying in the synchronized regime. This is related to the fact that in this regime, the interaction is large and has a greater impact on

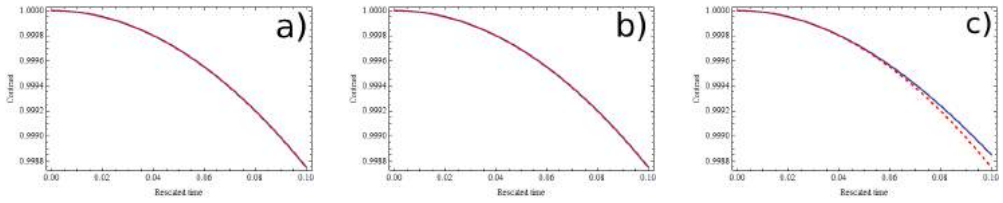

Figure 2.5: The initial decay of contrast fitted with the expression $\text{Contrast}(\tilde{t}) = 1 - (\tilde{t}/\tilde{t}_i)^2$ with $\tilde{t}_i = 2\sqrt{2}/\delta$. a) Dephased regime ($J = 0.1\delta$). b) Critical point ($J = 0.5\delta$). c) Synchronized regime ($J = 5\delta$). The blue line is the contrast and the dotted red line the fit.

the initial temporal evolution of the system, causing the dynamics deviating earlier from the simple independent rotation around the external magnetic field.

The other time scale is the oscillation period of the contrast. Note that in the dephased regime the period of the contrast is not equivalent to the period of the system dynamics, but only half of it, because the contrast is defined to be positive by a modulus. In the dephased regime ($J < \delta/2$), this time scale takes the form

$$\tilde{t}_p = 2\frac{\delta}{2}\int_0^1 \frac{dx}{\sqrt{(1-\frac{4J^2}{\delta^2}x^2)(1-x^2)}} = \frac{4}{\delta}K(\frac{2J}{\delta}), \tag{2.34}$$

where the function $K(\frac{2J}{\delta})$ is the complete elliptic integral of the first kind. If $J \ll \delta$, the period can be approximated in the following way. In this limit, the angle Θ (see Eq. 2.28) varies almost linearly with time as $\Theta \approx \delta\tilde{t}$ because the kinetic energy of pendulum is so large that during the whole period, the change due to the gravity potential is negligible compared to it. Then the period is $\tilde{t}_p \approx \frac{2\pi}{\delta}$. When $J > \delta/2$, the period of the dynamics is

$$\tilde{t}_p = 2\frac{2}{\delta}\int_0^1 \frac{\delta/(2J)dy}{\sqrt{(1-y^2)(1-\frac{\delta^2}{4J^2}y^2)}} = \frac{2}{J}K(\frac{\delta}{2J}), \tag{2.35}$$

where a change of variable is performed $y \equiv (2J/\delta)\sin\theta$. In Table. 2.1, a summary of the characteristic time scales in the classical model are listed.

2.4 Phase portrait

In the preceding sections, we have sticked to one specific initial condition $\vec{n}_1 = \vec{n}_2 = (1,0,0)^T$. In the following, we will loosen this constraint by

	Initial decay ($\tilde{t}_i$)	Period ($\tilde{t}_p$)
Dephased regime ($J < \delta/2$)	$2\sqrt{2}/\delta$	$\frac{4K(2J/\delta)}{\delta} \approx \frac{2\pi}{\delta}$
Critical point ($J = \delta/2$)	$2\sqrt{2}/\delta$	$\frac{2}{\delta} \ln \frac{\delta/2}{\lvert\delta/2 - J\rvert} \to \infty$
Synchronized regime ($J > \delta/2$)	$2\sqrt{2}/\delta$	$\frac{2K(\delta/2J)}{J} \approx \frac{\pi}{J}$

Table 2.1: Characteristic time scales in the classical two-spin model.

considering different initial conditions and look at the global behavior of the system under a special symmetry. The content of this symmetry, the x-axis symmetry, states that if we start with an initial condition satisfying

$$\begin{aligned} n_1^x(0) =& n_2^x(0), \\ n_1^y(0) =& -n_2^y(0), \\ n_1^z(0) =& -n_2^z(0), \end{aligned} \tag{2.36}$$

then in the following dynamics, this symmetry ise conserved. In the following subsection, we give a heuristic proof of this statement.

In classical mechanics, phase portrait is a powerful tool to study the qualitative aspects of the system under consideration. Usually, the phase portraits are done by plotting the intersection of the equi-energy surfaces with the phase space. For our system, since there is no dissipation, the energy of the system is determined uniquely by the initial condition

$$E = \frac{\delta}{2}(n_1^z(0) - n_2^z(0)) + J\left[n_1^x(0)n_2^x(0) + n_1^y(0)n_2^y(0) + n_1^z(0)n_2^z(0)\right]. \tag{2.37}$$

In phase portraits, the important geometrical properties of the systems can be deduced from typical trajectories in the phase space, such as the nature of fixed points, the limit circles and the separatrices. However, it is not easy to visualize the phase portraits for more than one degree of freedom. So we concentrate mainly on a single spin, say the spin number 1, with the phase space coordinates $(\phi_1, \cos\theta_1)$. Then we are obliged to confine ourselves to certain subspace of the whole phase space because we need to eliminate the influence of the other spin by considering regions in the phase space with some specific symmetric properties. Since the previously considered initial state and the following temporal evolution of the system always have the symmetry $n_1^x(\tilde{t}) = n_2^x(\tilde{t})$, $n_1^y(\tilde{t}) = -n_2^y(\tilde{t})$, and $n_1^z(\tilde{t}) = -n_2^z(\tilde{t})$, we plot typical trajectories starting in phase space with this symmetry. With this symmetry, the energy of the system is given by

$$E = \delta n_1^z(0) + J\left[(n_1^x(0))^2 - (n_1^y(0))^2 - (n_1^z(0))^2\right]. \tag{2.38}$$

2.4.1 x-axis symmetry

Before making the phase portrait, it is necessary to check whether this symmetry in the initial state will be conserved during the succeeding temporal evolution. The origin of this symmetry should come as a surprise if we only consider the Hamiltonian, which does not have this symmetry. Yet one can check numerically that this symmetry is not broken in the dynamics. As shown in the first column in Fig. 2.6, this x-axis symmetry is conserved for initial conditions starting in the xy-plane (see Fig. 2.6.a), xz-plane (see Fig. 2.6.b), and somewhere else (see Fig. 2.6.c) when the dynamics is dephased ($J = 0.1\delta$). In the synchronized regime ($J = 5\delta$), this symmetry still exists (see the second row of Fig. 2.6).

From an analytical point of view, this x-axis symmetry is related to the special initial condition, and can be obtained as follows. First, note that n_t^z is always conserved, because of the invariance under the rotation of the whole system around z-axis. So if for initial condition we have $n_1^z(0) = -n_2^z(0)$, then for all the dynamics $n_t^z(\tilde{t}) \equiv 0$ is guaranteed. The total spin can only move in the xy-plane and $n_1^z(\tilde{t}) = -n_2^z(\tilde{t})$ is true in the following temporal evolution of the system. Eqs. 2.13 and 2.14 should hold. As a result Eq. 2.16 follows and we get $\dot{\phi} \equiv 0$, indicating that $n_t^y(\tilde{t}) \equiv 0$. So we have the two following relations

$$\begin{aligned} n_1^z(\tilde{t}) &= -\, n_1^z(\tilde{t}), \\ n_1^y(\tilde{t}) &= -\, n_1^y(\tilde{t}). \end{aligned}$$

We need to still prove that $n_1^x(\tilde{t}) = n_2^x(\tilde{t})$. To this end, we need to show $n_d^x(\tilde{t}) = 0$. From Eq. 2.11, we get for the component n_d^x

$$\frac{d}{d\tilde{t}} n_d^x = \frac{\delta}{2} n_t^y + J(\vec{n}_t \times \vec{n}_d)^x. \tag{2.39}$$

The first term on the right hand side of the above equation is identically zero since $n_1^y(\tilde{t}) = -n_2^y(\tilde{t})$. The second term is a vector product and thus perpendicular to the two vectors $\vec{n}_t(\tilde{t})$ and $\vec{n}_d(\tilde{t})$. Because of the fact that $n_1^y(\tilde{t}) = -n_2^y(\tilde{t})$ and $n_1^z(\tilde{t}) = -n_2^z(\tilde{t})$, $\vec{n}_t(\tilde{t})$ has only x-component. Then the x-component of $\vec{n}_t \times \vec{n}_d$ is zero. Consequently

$$\frac{d}{d\tilde{t}} n_d^x(\tilde{t}) \equiv 0. \tag{2.40}$$

With the initial condition $\vec{n}_d^x(0) = 0$, we have $\vec{n}_d^x(\tilde{t}) \equiv 0$. Therefore, it is proven that the x-axis symmetry is preserved during the dynamics.

Interaction	Initial conditions $\vec{n}_1(0) = (0.6, 0.8, 0)$	$\vec{n}_1(0) = (0.6, 0, 0.8)$	$\vec{n}_1(0) = (0.6, 0.48, 0.64)$
$J = 0.1\delta$	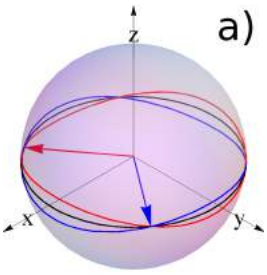	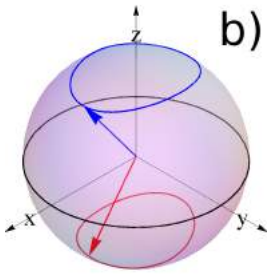	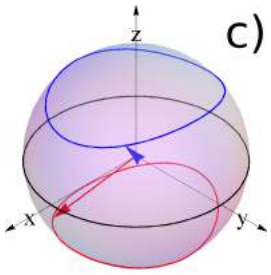
$J = 5\delta$	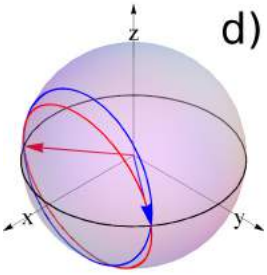	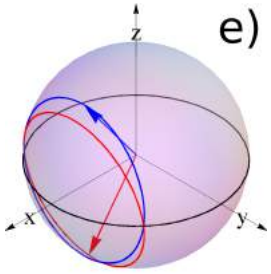	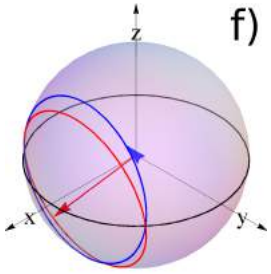

Figure 2.6: Trajectories of spin 1 (blue line) and spin 2 (red line) with different interaction strength and different initial conditions. In the first row the trajectories in the dephased regime ($J = 0.1\delta$) are presented. The second row has the same initial condition but in the synchronized regime ($J = 5\delta$). In the first column the initial condition is: $n_1^x(0) = n_2^x(0) = 0.6$, $n_1^y(0) = -n_2^y(0) = 0.8$, and $n_1^z(0) = -n_2^z(0) = 0$ (starting from the equator plane). In the second column the initial condition is: $n_1^x(0) = n_2^x(0) = 0.6$, $n_1^y(0) = -n_2^y(0) = 0$, and $n_1^z(0) = -n_2^z(0) = 0.8$ (starting from the xz-plane). In the third column the initial condition is: $n_1^x(0) = n_2^x(0) = 0.6$, $n_1^y(0) = -n_2^y(0) = 0.48$, and $n_1^z(0) = -n_2^z(0) = 0.64$. The blue and red arrow denotes the initial conditions of spin number 1 and 2 respectively.

2.4.2 Fixed points and stability analysis

For the sake of simplicity, we restrict ourselves to considering the phase portrait for the single spin number 1 with the x-axis symmetry constraint mentioned above. The Hamiltonian expressed in the canonical variables $(\phi_i, \cos\theta_i)$, $i = 1, 2$ is

$$H = \frac{\delta}{2}(\cos\theta_1 - \cos\theta_2) + J[\sin\theta_1 \sin\theta_2 \cos(\phi_1 - \phi_2) + \cos\theta_1 \cos\theta_2], \quad (2.41)$$

where we have used:

$$\begin{aligned} n_i^x &= \sin\theta_i \cos\phi_i, \\ n_i^y &= \sin\theta_i \sin\phi_i, \\ n_i^z &= \cos\theta_i. \end{aligned} \quad (2.42)$$

The Hamiltonian equations for the canonical variables $(\phi_1, \cos\theta_1)$ read:

$$\begin{aligned} \frac{d}{d\tilde{t}}\phi_1 &= \frac{\partial H}{\partial \cos\theta_1} = \frac{\delta}{2} + J\left[\cos\theta_2 - \sin\theta_2 \cos(\phi_1 - \phi_2)\frac{\cos\theta_1}{\sin\theta_1}\right], \\ \frac{d}{d\tilde{t}}\cos\theta_1 &= -\frac{\partial H}{\partial \phi_1} = J \sin\theta_1 \sin\theta_2 \sin(\phi_1 - \phi_2). \end{aligned} \quad (2.43)$$

Using the symmetry $n_1^x = n_2^x$, $n_1^y = -n_2^y$, or equivalently in the canonical variables' language $\theta_1 = \pi - \theta_2$, and $\phi_1 = -\phi_2$, the above equations transform into

$$\begin{aligned} \frac{d}{d\tilde{t}}\phi_1 &= \frac{\delta}{2} - J(\cos\theta_1 + \cos\theta_1 \cos(2\phi_1)), \\ \frac{d}{d\tilde{t}}\cos\theta_1 &= J \sin^2\theta_1 \sin(2\phi_1). \end{aligned} \quad (2.44)$$

To get a qualitative understanding of the dynamical system and plot the phase portrait, it is desirable to start by finding the fixed points of the system. Solving the equations $d\phi_1/d\tilde{t} \equiv 0$ and $d\cos\theta_1/d\tilde{t} \equiv 0$, we get the fixed points

$$\begin{aligned} \theta_1 &= 0, \pi, \\ \phi_1 &\quad \text{arbitrary}. \end{aligned} \quad (2.45)$$

When $J > \delta/4$, there are two additional fixed points

$$\begin{aligned} \theta_1 &= \arccos\left(\frac{\delta}{4J}\right), \\ \phi_1 &= 0, \pi. \end{aligned} \quad (2.46)$$

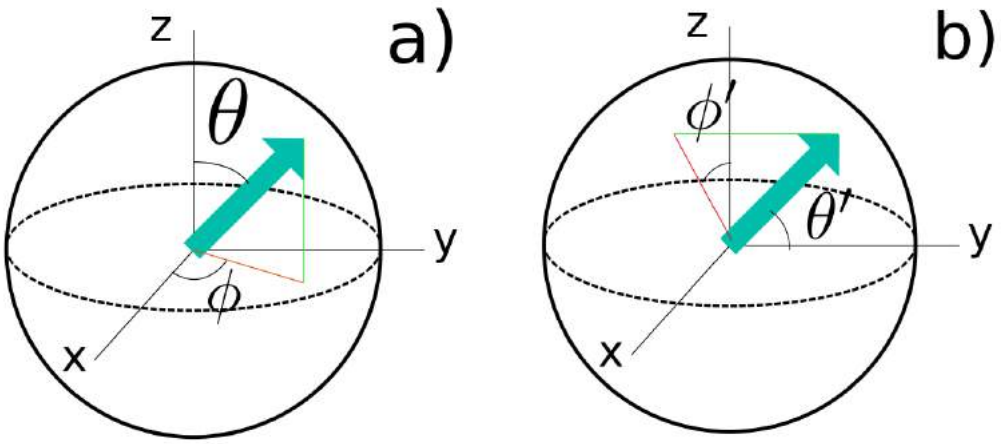

Figure 2.7: The two definition of angles in the stability analysis. a) Definition of θ and ϕ with $\theta \in [0, \pi]$ and $\phi \in [0, 2\pi)$. b) Definition of θ' and ϕ' with $\theta' \in [0, \pi]$ and $\phi' \in [0, 2\pi)$.

We then study the stability of these fixed points using linear approximation around them. The expansion around the fixed points ($\theta = 0, \phi$) need special attention because the coordinate we used is singular at these two points. So we change the definition of the angles (see Fig. 2.7) and use the Hamiltonian of the form

$$\begin{aligned} H =& \frac{\delta}{2}(\sin\theta_1' \cos\phi_1' - \sin\theta_2' \cos\phi_2') + J[\sin\theta_1' \sin\theta_2' \cos(\phi_1' - \phi_2') \\ &+ \cos\theta_1' \cos\theta_2'], \end{aligned} \tag{2.47}$$

with the new definitions of spin variables

$$\begin{aligned} n_i^x &= \sin\theta_i' \sin\phi_i', \\ n_i^y &= \cos\theta_i', \\ n_i^z &= \sin\theta_i' \cos\phi_i'. \end{aligned} \tag{2.48}$$

The x-axis symmetry now reads

$$\begin{aligned} \theta_1' &= \pi - \theta_2', \\ \phi_1' &= \pi - \phi_2'. \end{aligned} \tag{2.49}$$

Then the equations of motion read

$$\begin{aligned} \frac{d}{d\tilde{t}}\phi_1' &= -\frac{\delta}{2}\cos\phi_1' \cot\theta_1' + J\cos\theta_1'[\cos(2\phi_1') - 1], \\ \frac{d}{d\tilde{t}}\cos\theta_1' &= \frac{\delta}{2}\sin\theta_1' \sin\phi_1' - J\sin^2\theta_1' \sin(2\phi_1'). \end{aligned} \tag{2.50}$$

For computational convenience, we use the differential equations on (ϕ_1', θ_1') instead of on $(\phi_1', \cos\theta_1')$. The equations of motion for these variables read

$$\begin{aligned}\frac{d}{d\tilde{t}}\phi_1' =& -\frac{\delta}{2}\cos\phi_1'\cot\theta_1' + J\cos\theta_1'[\cos(2\phi_1') - 1],\\ \frac{d}{d\tilde{t}}\theta_1' =& -\frac{\delta}{2}\sin\phi_1' + J\sin\theta_1'\sin(2\phi_1').\end{aligned} \tag{2.51}$$

The original fixed points are transformed to $(\theta_1' = \pi/2, \phi_1' = 0)$. Around this fixed point, a linear expansion yields

$$\begin{aligned}\frac{d}{d\tilde{t}}\delta\phi_1' =& \frac{\delta}{2}\delta\theta_1',\\ \frac{d}{d\tilde{t}}\delta\theta_1' =& (2J - \frac{\delta}{2})\delta\phi_1'.\end{aligned} \tag{2.52}$$

In order to find the stability property of this fixed point, we assume that the solution of the linearized equations takes the form

$$\begin{pmatrix}\delta\phi_1'\\ \delta\theta_1'\end{pmatrix} = c_1\vec{D}_1 e^{\lambda_1\tilde{t}} + c_2\vec{D}_2 e^{\lambda_2\tilde{t}}, \tag{2.53}$$

where the two eigenvalues of the system are denoted as λ_1, and λ_2, and the two eigenvectors as $\vec{D}_1$, and $\vec{D}_2$. The eigenvalues are determined by the equation

$$\begin{vmatrix}-\lambda & \frac{\delta}{2}\\ 2J - \frac{\delta}{2} & -\lambda\end{vmatrix} = 0, \tag{2.54}$$

or equivalently $\lambda^2 - \delta/2(2J - \delta/2) = 0$. From this equation it is clear that when $J < \delta/4$, the fixed point $(\theta_1 = 0, \phi)$ is an elliptic point because the two eigenvalues of the linear expansion equations are purely imaginary $(\lambda = \pm i\sqrt{\delta/2(\delta/2 - 2J)})$, while this fixed point is a saddle point when the interaction strength is strong $J > \delta/4$ because the two eigenvalues $\lambda_1 = -\sqrt{\delta/2(2J - \delta/2)}$, and $\lambda_2 = \sqrt{\delta/2(2J - \delta/2)}$ satisfy $\lambda_1 < 0 < \lambda_2$. Note that at the transition point $(J = \delta/4)$, the fixed point changes its nature between the two regimes. For the transition point $(J = \delta/4)$, the linearized equations read

$$\begin{aligned}\frac{d}{d\tilde{t}}\delta\phi_1' =& \frac{\delta}{2}\delta\theta_1',\\ \frac{d}{d\tilde{t}}\delta\theta_1' =& 0.\end{aligned} \tag{2.55}$$

Then it is easily seen that $\lambda_1 = \lambda_2 = 0$, indicating a degenerate solution. We assume that the general solution of the above equation takes the form

$$\begin{aligned} \delta\phi_1' =& c_1 + c_2\tilde{t}, \\ \delta\theta_1' =& \delta\theta_1'(0). \end{aligned} \tag{2.56}$$

Then $c_2 = (\delta/2)\delta\theta_1'(0)$. This transition point is special with regard to the fact that when passing the transition $J = \delta/4$ from below, two additional fixed points ($\cos\theta_1 = \delta/(4J), \phi_1 = 0, \pi$) emerge from the north pole ($\theta_1 = \pi, \phi$). This is the non-isolated fixed point in the linear analysis language and signifies a bifurcation transition.

The same analysis can be implemented for the fixed point $(\theta_1 = \pi, \phi_1)$ using the transformed axes. In the new axes defined in Eq. 2.48, this fixed point is transformed to $(\theta_1' = \pi/2, \phi_1' = \pi)$. We obtain the same equations of motion as obtained in Eq. 2.51, but a linear expansion results in different equations. The linearized equations are

$$\begin{aligned} \frac{d}{d\tilde{t}}\delta\phi_1' =& -\frac{\delta}{2}\delta\theta_1', \\ \frac{d}{d\tilde{t}}\delta\theta_1' =& (2J + \frac{\delta}{2})\delta\phi_1'. \end{aligned} \tag{2.57}$$

Using the same approach as in Eq. 2.53, the equation for the eigenvalues reads

$$\begin{vmatrix} -\lambda & -\frac{\delta}{2} \\ 2J + \frac{\delta}{2} & -\lambda \end{vmatrix} = 0. \tag{2.58}$$

For this fixed point, the eigenvalues are $\lambda_1 = i\sqrt{\delta/2(2J + \delta/2)}$ and $\lambda_2 = -i\sqrt{\delta/2(2J + \delta/2)}$. Then the fixed point $(\theta_1 = \pi, \phi)$ is always an elliptic fixed point no matter how the interaction strength changes.

When $J > \delta/4$, there are two additional fixed points at $(\cos\theta_1 = \delta/(4J), \phi_1 = 0, \pi)$. We use the original definitions of spin variables (see Eq. 2.42) since this fixed point is not singular. Then the equations of motion for (θ_1, ϕ_1) read

$$\begin{aligned} \frac{d}{d\tilde{t}}\delta\phi_1 =& 2J\sqrt{1 - \frac{\delta^2}{16J^2}}\delta\theta_1, \\ \frac{d}{d\tilde{t}}\delta\theta_1 =& -2J\sqrt{1 - \frac{\delta^2}{16J^2}}\delta\phi_1. \end{aligned} \tag{2.59}$$

Then the eigenvalues satisfy the equation

$$\lambda^2 + 4J^2(1 - \frac{\delta^2}{16J^2}) = 0 \tag{2.60}$$

	$J < \delta/4$	$J > \delta/4$
$(\theta_1 = 0, \phi_1)$	Elliptic	Saddle
$(\theta_1 = \pi, \phi_1)$	Elliptic	Elliptic
$(\theta_1 = \arccos(\delta/(4J)), \phi_1 = 0, \pi)$	non-existing	Elliptic

Table 2.2: Stability of fixed points in different regimes.

with the solution $\lambda_1 = -2iJ\sqrt{1 - \frac{\delta^2}{16J^2}}$ and $\lambda_2 = 2iJ\sqrt{1 - \frac{\delta^2}{16J^2}}$. This suggests that the fixed point $(\cos\theta_1 = \delta/(4J), \phi_1 = 0, \pi)$ is an elliptic point.

The above stability analysis are summarized in Tab. 2.2.

2.4.3 Qualitative picture from the phase portrait

After the fixed point analysis, we are in the position to plot the phase portrait of the classical two-spin system. As shown in Fig. 2.8.a, in the dephased regime before the bifurcation ($J = 0.1\delta$), the system has rather simple dynamical behaviors. In this regime, the system has two elliptic fixed points at the north and south pole $\theta = 0, \pi$ when $J = 0.1\delta < 0.25\delta$. Consequently the trajectories of spin 1 would be mainly circles rotating around these two fixed points. And we observe therefore the periodical circles around the z-axis.

If the interaction strength is increased to the transition point $J \geq \delta/4$, another two elliptic fixed point emerge at $((n_1^x = \sqrt{1 - (\delta/(4J))^2}), n_1^y = 0, n_1^z = \delta/(4J))$ from the north pole, and the north pole becomes a saddle point with a negative and a positive eigenvalues for the linear expansion equations, characterizing a separatrix which goes through it (see the green trajectory in Fig. 2.8.b). A bifurcation transition occurs. Then the phase space of spin 1 would be separated into two regions by the separatrix passing the north pole. In one of the two regions that contains the newly emerged fixed points, the trajectories rotate around the newly emerged fixed points because of the elliptic nature of these two points. In this region, the spin number 1 can not pass the yz plane, and n_t^x is always positive or negative (depending on $\phi_i = 0$ or π). We call this region synchronized region because the movement in this region would lead to synchronization of contrast. In the other region, the trajectories perform periodic circular movement around the south pole as before. Moving in the region, n_t^x vanishes periodically when spin number 1 go from the front hemisphere ($x > 0$) to the back hemisphere ($x < 0$). This region will be called dephased region hereafter. The surface of the synchronized region has a positive correlation with the quantity $J - J_{bif} (= \delta/4)$. Increasing J would induce larger synchronized region. When

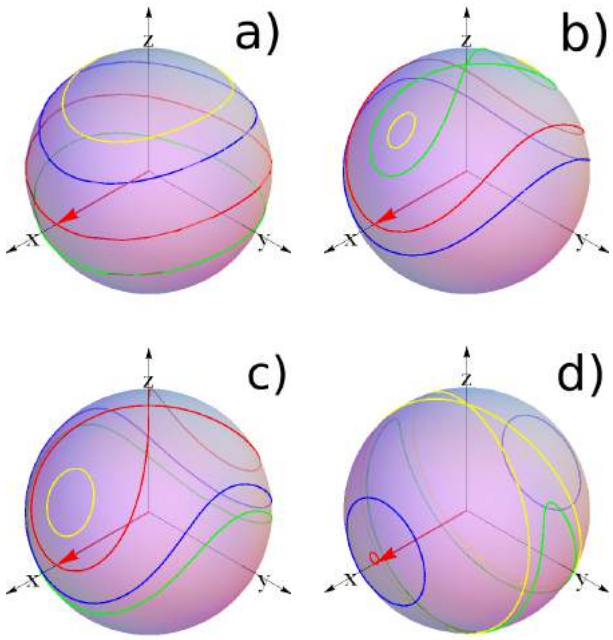

Figure 2.8: The phase portrait for spin number 1 of the two-spin system with the additional symmetry between the two spins $n_1^x(\tilde{t}) = n_2^x(\tilde{t})$, $n_1^y(\tilde{t}) = -n_2^y(\tilde{t})$, and $n_1^z(\tilde{t}) = -n_2^z(\tilde{t})$. a) The dephased regime before bifurcation ($J = 0.1\delta$), the four curves represent trajectories with different energies. The red one depicts the trajectory with energy $E = 0.1\delta$ (coinciding with the trajectory of the initial condition considered in the most part of this thesis), the blue one with $E = 0.5\delta$, the green one with $E = -0.3\delta$ and the yellow one with $E = 0.7\delta$. b) The dephased regime after bifurcation($J = 0.35\delta$). The red curve has energy $E = 0.35\delta$, the blue one has energy $E = 0.1\delta$, the yellow one has energy $E = 0.7\delta$, and the green one has energy $E = 0.65\delta$. c) The critical point ($J = 0.5\delta$). The red curve (separatrix) has energy $E = 0.5\delta$ (the initial condition considered), the blue one (dephased) has energy $E = 0.1\delta$, the yellow one (synchronized) has energy $E = 0.7\delta$, and the green one has energy $E = -0.1\delta$. d) The synchronized regime ($J = 5\delta$). For the red curve (synchronized), the energy is $E = 5\delta$. For the yellow curve (separatrix), the energy is $E = -4\delta$. For the blue curve (synchronized), the energy is $E = -5\delta$. And for the green curve (dephased), the energy is $E = -0.45\delta$. The red arrow indicates the initial state of spin number 1 and the red curve corresponds to the trajectory of the initial condition. For the meaning of separatrix, dephased and synchronized region, see text.

$\delta/4 < J < \delta/2$ (see Fig. 2.8.b), the initial condition we take is still contained in the dephased region, so there is no synchronization observed yet.

At the critical point $J = \delta/2$, the synchronized region is extended to such a degree that the chosen initial state lies just on the separatrix passing the north pole (see Fig. 2.8.c). And then it takes an infinite amount of time for the spin 1 to reach the north pole. This corresponds to the critical behavior of the contrast. If the interaction is further increased (see Fig. 2.8.d), the initial condition will be contained in the synchronized region and synchronization will be observed.

2.5 Relation to the Bose-Hubbard dimer and the Lipkin-Meshkov-Glick model

With the x-axis symmetry

$$\begin{aligned} n_1^x =& n_2^x, \\ n_1^y =& -n_2^y, \\ n_1^z =& -n_2^z, \end{aligned} \tag{2.61}$$

our Hamiltonian reduces to

$$H_{xsym} = \frac{\delta}{2}(n_1^z - n_2^z) + J(n_1^x n_2^x + n_1^y n_2^y + n_1^z n_2^z) = \delta n_1^z + 2J(n_1^x)^2 + \text{Const} \tag{2.62}$$

with Const $= -J$ since $(n_1^x)^2 + (n_1^y)^2 + (n_1^z)^2 = 1$ by our rescaling. This Hamiltonian is equivalent to that of the symmetric Lipkin-Meshkov-Glick (LMG) model[33], which intially describes a system consisting of N interacting fermions in two N-fold degenerate levels. The symmetric LMG Hamiltonian reads

$$H_{LMG} = \epsilon S^z + 2V(S^x)^2. \tag{2.63}$$

If we make the transformation

$$\begin{aligned} S\epsilon \to& \delta, \\ \frac{S^i}{S} \to& n^i, \quad \text{for } i = x, y, z \\ S^2 V \to& J, \end{aligned} \tag{2.64}$$

then the symmetric LMG model is identical to the two-spin model with x-axis symmetry.

However, the two-spin model with x-axis symmetry can also describe the classical dynamics of the Bose-Hubbard dimer (BHD) model. The BHD model is a two-site Bose-Hubbard model with the Hamiltonian[34, 35]

$$H_{BHD} = (E_1 a_1^\dagger a_1 + E_2 a_2^\dagger a_2) + K(a_1^\dagger a_2 + a_2^\dagger a_1) + [U_1 (a_1^\dagger)^2 a_1^2 + U_2 (a_2^\dagger)^2 a_2^2], \quad (2.65)$$

where E_i is the energy level or the chemical potential of the two sites, K the tunneling rate between the two sites, and U_i the interaction strength in the two sites. The BHD model, though describing a very different physical system, is equivalent to the LMG model. To show this, we use the Schwinger boson representation of spin operators[36]

$$\begin{aligned} S^x &= \frac{1}{2}(a_1^\dagger a_2 + a_2^\dagger a_1), \\ S^y &= \frac{i}{2}(a_1^\dagger a_2 - a_2^\dagger a_1), \\ S^z &= \frac{1}{2}(a_1^\dagger a_1 - a_2^\dagger a_2). \end{aligned} \quad (2.66)$$

Then substituting the above equalities into the BHD Hamiltonian in Eq. 2.65, and assuming symmetric sites, i.e. $E_1 = E_2 = E$ and $U_1 = U_2 = U$, the BHD Hamiltonian takes the form

$$H_{BHD} = 2KS^x + 2U(S^z)^2 + \text{Const.} \quad (2.67)$$

because the number of bosons N in the system is a constant. Then this Hamiltonian is the same as the symmetric LMG Hamiltonian if we make the transformation

$$\begin{aligned} 2K &\to \epsilon, \\ U &\to V. \end{aligned} \quad (2.68)$$

As a result, the BHD model is equivalent to the symmetric LMG model. Their classical limit is the same as that of the two-spin system with x-axis. The relation between the three is shown in Fig. 2.9. The bifurcation transition has also been found in the BHD model[37, 38].

In passing, we note that in [35], it is argued that the classical dynamics of the BHD model can be described as a non-rigid and nonlinear pendulum. This point of view is correct but less intuitive. The phase space of the non-rigid (z, ϕ) and nonlinear pendulum can be shown equivalent to that of a spin $(\cos\theta, \phi)$[39].

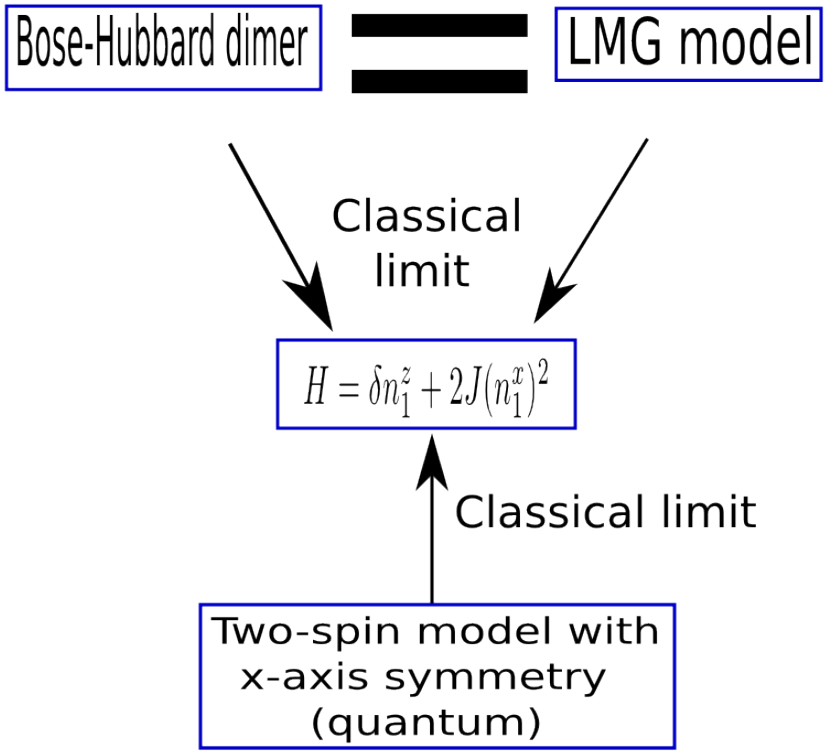

Figure 2.9: Relations between the LMG model, BHD model, and two-spin model with x-axis symmetry.

2.6 Summary

In this chapter, the model is defined together with the initial condition. Its solution is presented with an emphasis on the experimental measurable quantities, the contrast. In this simplistic model, two regimes are found depending on the ratio between the interaction strength and the inhomogeneity of the magnetic field. The two regimes are separated by a dynamical phase transition which depends on the initial condition. In one regime ($J < \delta/2$), the dephased phase, the two spins would dephase completely, and the contrast reaches zero periodically. In the other regime ($J > \delta/2$), the two spins are synchronized and rotate mainly around the total spin. There, the contrast is always finite, with oscillation period determined mainly by the interaction strength. Phase portraits have been used to reveal the underlying mechanism of this phase transition: bifurcation. At the transition point ($J_{tr} = \delta/4$), two

new fixed points emerge from the north pole and a separatrix separates the phase space into synchronized region and dephased region. At the critical point ($J = \delta/2$), our initial condition lies right on the separatrix, which goes to the north pole, the saddle point.

It has also been shown that our Hamiltonian, together with the x-axis symmetry constraint, is equivalent to the classical dynamics of the LMG model in the context of nuclear physics and BHD model in the context of cold atoms. However, it should be noted that our model consisting of two spins has richer dynamical behaviors than the classical LMG model or the classical BHD model in the sense that the phase space of our two-spin model is four dimensional, while the LMG model and BHD model have a two dimensional phase space. Only with the x-axis symmetry does the two-spin model reduce to the two other models consisting of a single spin.

Chapter 3

Quantum dynamics and absence of synchronization

In the previous chapter, we have solved the classical dynamics and found that the different dynamical behaviors in the classical system are caused by a bifurcation. Now we turn to the quantum system with the same Hamiltonian and initial condition. It describes two quantum spins lying initially parallel in the transverse plane of an inhomogeneous magnetic field. They interact with each other through an exchange interaction. The Hamiltonian of the system is

$$H = \frac{\delta_S}{2}(S_1^z - S_2^z) + J_S \vec{S}_1 \cdot \vec{S}_2, \tag{3.1}$$

and the initial condition

$$|\Psi(0)\rangle = |m_1^x = S, m_2^x = S\rangle, \tag{3.2}$$

where we have used the eigenstate of the x-component of spin operators. In the above Hamiltonian, the spin components should be considered as quantum operators. The dimension of the underlying Hilbert space is determined by the size S of the spins via Dim $= (2S+1)^2$. A difference between classical mechanics and quantum mechanics is the fact that the cumulant $\langle S_i^\alpha S_j^\beta \rangle_c \equiv \langle S_i^\alpha S_j^\beta \rangle - \langle S_i^\alpha \rangle \langle S_j^\beta \rangle$ is not zero in quantum mechanics. This has motivated the idea of cumulant expansion[40, 41, 42], which we will apply to our model in a later section.

We can define the single spin contrast as

$$C_i(t) \equiv \frac{|\langle \vec{S}_i \rangle|}{S}, \quad i = 1, 2. \tag{3.3}$$

For our special initial condition, we have $C_1(t) = C_2(t)$, so we will use C_1 to denote the single spin contrast for both spins. And the single spin unit vector is defined as

$$\vec{n}_i(t) \equiv \frac{\langle \vec{S}_i \rangle}{|\langle \vec{S}_i \rangle|} = \frac{\langle \vec{S}_i \rangle}{SC_i}, \quad i = 1, 2. \tag{3.4}$$

The measured Ramsey contrast in the cold atom experiments corresponds to the contrast defined as

$$C(t) \equiv \frac{|\langle \vec{S}_1 + \vec{S}_2 \rangle|}{2S}. \tag{3.5}$$

Since $C_1(t) = C_2(t)$, we have

$$C(t) = C_1(t)\sqrt{\frac{1 + \vec{n}_1 \cdot \vec{n}_2}{2}}. \tag{3.6}$$

Another quantity we want to define is the effective spreading of the quantum spins

$$D_1(t) \equiv \frac{\langle (\vec{S}_1 - \langle \vec{S}_1 \rangle)^2 \rangle}{S^2} = \frac{S(S+1) - (\langle \vec{S}_1 \rangle)^2}{S^2}. \tag{3.7}$$

This quantity is a measure of the deviation of the single spin contrast from that of a coherent state through the relation

$$C_1^2(t) = 1 + \frac{1}{S} - D_1(t). \tag{3.8}$$

For a coherent spin state[43], we have

$$\begin{aligned} D_{1coh} &= \frac{1}{S}, \\ C_{1coh} &= 1. \end{aligned} \tag{3.9}$$

If $S \to \infty$, $D_{1coh} \to 0$. Thus the coherent state approaches the classical state in the semiclassical limit. For a general quantum state, $C_1 < 1$ and $D_1 < 1/S$.

We also rescale the systems in order to get rid of the spin-size dependence. However, here the rescaling constant is not the same as that in the classical systems. For the quantum system we have

$$\begin{aligned} \tilde{t} &= \frac{t}{\Lambda_S}, \\ \delta &= \Lambda_S \delta_S, \\ J &= \Lambda_S^2 J_S, \\ \hat{\vec{n}}_i &= \frac{\vec{S}_i}{\Lambda_S}, \end{aligned} \tag{3.10}$$

where $\Lambda_S = \sqrt{S(S+1)}$ is used instead of $\Lambda_S = S$ in the classical system. And $\hat{\vec{n}}_i$ is the rescaled spin operator. We have used a hat here to distinguish it from the single spin unit vector. This different constant is employed under the consideration that the norm of a quantum spin should be defined through $\sqrt{\langle \vec{S}^2 \rangle} = S(S+1)$, which is a constant of motion during the entire dynamics and should thus serve as a straightforward rescaling constant.

3.1 Spin One Half

The simplest case of quantum dynamics is a system consisting of two spin $S = 1/2$ particles. This situation is exactly solvable because of the small dimension of the Hilbert space. In solving the problem, we first use the unrescaled quantities and only in the end do we transform to the rescaled quantities so as to compare the obtained results with the classical ones. The Hamiltonian is given in Eq. 3.1 and the initial condition is

$$|\Psi(0)\rangle = |S_1^x = 1/2, S_2^x = 1/2\rangle = \frac{1}{\sqrt{2}}(|\uparrow\rangle + |\downarrow\rangle) \otimes \frac{1}{\sqrt{2}}(|\uparrow\rangle + |\downarrow\rangle)$$

Using the vectors $\{|S_1^z, S_2^z\rangle\}$ as basis, we obtain the matrix form of the Hamiltonian:

$$H = \begin{pmatrix} \frac{J_S}{4} & 0 & 0 & 0 \\ 0 & \frac{\delta_S}{2} - \frac{J_S}{4} & \frac{J_S}{2} & 0 \\ 0 & \frac{J_S}{2} & -\frac{\delta_S}{2} - \frac{J_S}{4} & 0 \\ 0 & 0 & 0 & \frac{J_S}{4} \end{pmatrix}. \tag{3.11}$$

And the initial state is $|\Psi(0)\rangle = 1/2(|\uparrow\uparrow\rangle + |\uparrow\downarrow\rangle + |\downarrow\uparrow\rangle + |\downarrow\downarrow\rangle)$. Written in column vector form, it reads:

$$|\Psi(0)\rangle = 1/2 \begin{pmatrix} 1 \\ 1 \\ 1 \\ 1 \end{pmatrix} \tag{3.12}$$

The eigenvalues and eigenvectors of the Hamiltonian can be found as:

$$\begin{aligned} E_1 &= \frac{J_S}{4}, & |e_1\rangle &= |\uparrow\uparrow\rangle, \\ E_2 &= \frac{J_S}{4}, & |e_2\rangle &= |\downarrow\downarrow\rangle, \\ E_3 &= -\frac{J_S}{4} + \frac{\omega}{2}, & |e_3\rangle &= \sin\alpha|\uparrow\downarrow\rangle + \cos\alpha|\downarrow\uparrow\rangle, \\ E_4 &= -\frac{J_S}{4} - \frac{\omega}{2}, & |e_4\rangle &= -\cos\alpha|\uparrow\downarrow\rangle + \sin\alpha|\downarrow\uparrow\rangle, \end{aligned} \tag{3.13}$$

where $\omega = \sqrt{J_S^2 + \delta_S^2}$ and $\tan\alpha = J_S/(\omega - J_S)$. The contrast can be calculated as:

$$\mathrm{C}(\tilde{t}) = \left|\cos\left(\frac{J\tilde{t}}{\sqrt{3}}\right)\cos\left(\frac{\sqrt{3}}{4}\omega\tilde{t}\right) + \frac{4J}{3\omega}\sin\left(\frac{J\tilde{t}}{\sqrt{3}}\right)\sin\left(\frac{\sqrt{3}}{4}\omega\tilde{t}\right)\right|, \tag{3.14}$$

with $\omega = \sqrt{J_S^2 + \delta_S^2} = (2/3)\sqrt{4J^2 + 3\delta^2}$. In the above expression, we have used the rescaled quantities:

$$\begin{aligned} \tilde{t} =& \frac{2t}{\sqrt{3}}, \\ \delta =& \frac{\sqrt{3}}{2}\delta_S, \\ J =& \frac{3}{4}J_S. \end{aligned} \tag{3.15}$$

Expanding this solution to second order in rescaled time, we find for short time

$$\mathrm{C}(\tilde{t}) \approx \left|1 - \frac{(\delta\tilde{t})^2}{8}\right|. \tag{3.16}$$

Therefore, the initial decay of the contrast is still given by $\mathrm{C}(\tilde{t}) \approx 1 - (\tilde{t}/\tilde{t}_i)^2$, with $\tilde{t}_i = 2\sqrt{2}/\delta$. This decay is the same as that found in the classical case. The very short time dynamics is determined entirely by the inhomogeneous magnetic field because during this time interval, the two spins are almost perfectly aligned such that the interaction between them does not affect the dynamics. As a result, the dynamics of the two spins is independent of each other and is simply the movement of two coherent states in external magnetic field. This movement is the same as that of two classical spins in the external magnetic field as long as there is no interaction between them to dephase the coherent states.

For longer time, the dynamics is not the same as the classical systems. There is no more the regime of synchronization as in the classical system because in the quantum $S = 1/2$ case the contrast always vanishes at a certain time. But we can still distinguish two different regimes depending on the ratio between the rescaled interaction and the inhomogeneity of the magnetic field, in which the contrast behaves differently for large(small) interaction. In the following, we stick to the terms ``dephased'' regime and ``synchronized'' regime though there is no synchronization in the strict sense that ``the contrast should not vanish at any time''. In both regimes, there exist a fast oscillation corresponding to the classical oscillation and an envelope modulating the contrast which is purely of quantum origin.

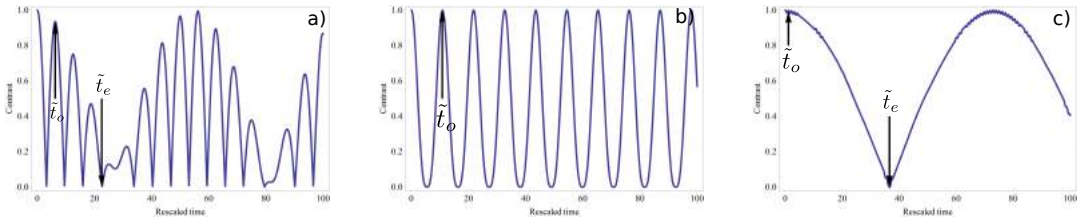

Figure 3.1: Contrast for $S = 1/2$ system as a function of the rescaled time $\tilde{t}$ in unit of $1/\delta$. a) $J = 0.1\delta$, b) $J = 0.5\delta$, and c)$J = 5\delta$. The oscillating time and envelope time have been indicated for the dephased regime a) and synchronized regime c). The critical point b) is special in that the dynamics is periodic and only the oscillating time is indicated.

If the interaction is small compared to the inhomogeneity ($J \ll \delta/2$), the approximate expression for the contrast

$$\mathrm{C}(\tilde{t}) \approx \left|\cos\left(\delta\tilde{t}/2\right)\cos\left(J\tilde{t}/\sqrt{3}\right)\right| \tag{3.17}$$

representing rapid oscillations with such large amplitude that the contrast goes down to zero rapidly after the onset of the dynamics. The period of the fast oscillation is $\tilde{t}_o = 2\pi/\delta$. This time is the equivalent of the classical period $\tilde{t}_p = 4K(2J/\delta)/\delta \approx 2\pi/\delta$ when $J \ll \delta/2$. In addition, the oscillating amplitude is modulated by an envelope such that there is an additional time scale, which we call the envelope time, characterizing the time at which the envelope reaches zero. In this dephased regime, the envelope time is given by the second term in the above approximate expression $\tilde{t}_e = \sqrt{3}\pi/J$.

On the other hand, when the interaction is large ($J \gg \delta/2$), the contrast takes the following approximate form

$$\mathrm{C}(\tilde{t}) \approx \left|\cos\left(\frac{\sqrt{3}\delta^2}{8J}\tilde{t}\right)\left[1 - \frac{3\delta^2}{8J^2}\sin^2\left(\frac{J\tilde{t}}{\sqrt{3}}\right)\right]\right|. \tag{3.18}$$

The contrast oscillates with small amplitude ($\sim 3\delta^2/(8J^2)$) close to 1 at short time. The period for this fast oscillation is $\tilde{t}_o = \sqrt{3}\pi/J$ corresponding to the classical period in the synchronized regime $\tilde{t}_p = 2K(\delta/(2J))/J \approx \pi/J$. However, this correspondence is not exact in the sense that the oscillating time of the $S = 1/2$ systems is not the same as the classical period. At longer time, the contrast is modulated by an envelope which eventually leads to its vanishing at an envelope time $\tilde{t}_e \sim 4J\pi/(\sqrt{3}\delta^2)$. As in the dephased regime, this characteristic time scale has no classical equivalent.

	Initial decay ($\tilde{t}_i$)	Oscillating time ($\tilde{t}_o$)	Envelope time ($\tilde{t}_e$)
Dephased regime($J \ll \delta/2$)	$2\sqrt{2}/\delta$	$2\pi/\delta$	$\sqrt{3}\pi/J$
Critical point ($J = \delta/2$)	$2\sqrt{2}/\delta$	$2\sqrt{3}\pi/\delta$	
Synchronized regime ($J \gg \delta/2$)	$2\sqrt{2}/\delta$	$\sqrt{3}\pi/J$	$4J\pi/\sqrt{3}\delta^2$

Table 3.1: Characteristic time scales for $S = 1/2$.

At the critical point $J = \delta/2$, the $S = 1/2$ case is special. The contrast is

$$\mathrm{C}(\tilde{t}) = \left|\cos^3\left(\frac{J\tilde{t}}{\sqrt{3}}\right)\right| = \left|\cos^3\left(\frac{\delta\tilde{t}}{2\sqrt{3}}\right)\right|. \tag{3.19}$$

It is periodic with the period $\tilde{t}_p = \sqrt{3}\pi/J = 2\sqrt{3}\pi/\delta$. In either the dephased or the synchronized regime, the contrast for $S = 1/2$ system is not periodic unless $J/\sqrt{3}$ and $\sqrt{3}\omega/4$ are commensurate, which is rare. Compared to the classical system, this behavior is also quite unusual. In the classical systems, the period of the contrast diverges logarithmically as $J \to \delta/2$: $\tilde{t}_p \approx 2\log(\delta/(2|J - \delta/2|))/\delta$.

In passing, we also plot the trajectory of a single spin on the Bloch sphere as done in the previous chapter. We designate by the trajectory the expectation value of $\vec{S}_1/S = C_1\vec{n}_1$, whose norm (the single spin contrast C_1) may change in time. The expressions for the components of spin 1, normalized to unity at initial time, read:

$$\begin{cases} \langle\hat{n}_1^x\rangle(\tilde{t}) = & \cos\left(\frac{J\tilde{t}}{\sqrt{3}}\right)\cos\left(\frac{\sqrt{3}}{4}\omega\tilde{t}\right) + \frac{4J}{3\omega}\sin\left(\frac{J\tilde{t}}{\sqrt{3}}\right)\sin\left(\frac{\sqrt{3}}{4}\omega\tilde{t}\right), \\ \langle\hat{n}_1^y\rangle(\tilde{t}) = & \frac{2\delta}{\sqrt{3}\omega}\cos\left(\frac{J\tilde{t}}{\sqrt{3}}\right)\sin\left(\frac{\sqrt{3}}{4}\omega\tilde{t}\right), \\ \langle\hat{n}_1^z\rangle(\tilde{t}) = & \frac{8J\delta}{3\sqrt{3}\omega}\sin^2\left(\frac{\sqrt{3}}{4}\omega\tilde{t}\right). \end{cases} \tag{3.20}$$

Then in this graphical representation (see Fig. 3.2), it is clear that there are two mechanisms in the temporal evolution changing the contrast. The first one is the rotation of the individual spin direction ($\vec{n}_1$), which resembles the classical movement and thus determines the fast oscillation. The other is the change of the single spin contrast (C_1), which is now purely quantum and prescribes the envelope time. In the dephased regime ($J < \delta/2$, see Fig. 3.2.a) or the synchronized regime ($J > \delta/2$, see Fig. 3.2.c), the individual spin would first rotate on the Bloch sphere as in the classical systems with the fast oscillating time $\tilde{t}_o$. Meanwhile, it diminishes in norm, spiraling inside towards the center region of the Bloch sphere. This induces the diminishment of the oscillating amplitude in the dephased regime, and the diminishment of contrast in the synchronized regime. At the envelope time $\tilde{t}_e$, the spin reaches innermost region and the contrast is zero too. After this, the spin

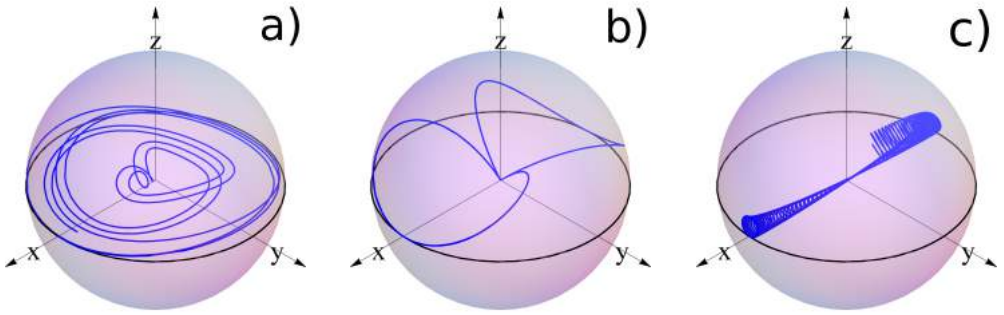

Figure 3.2: Bloch sphere representation of a single normalized spin $\vec{n}_1$ for the $S = 1/2$ system for $0 \leq \tilde{t} \lessapprox \tilde{t}_e$. a) $J = 0.1\delta$, b) $J = 0.5\delta$, and c) $J = 5\delta$.

spirals outward and at about $2\tilde{t}_e$, it almost regains its norm though this is not exact, due to the uncommensurability of the two frequencies. And the trajectory is not periodic as can be seen in Fig. 3.2.c, where the spin continues in a different path after $2\tilde{t}_e$, reaching the opposite part of its initial position on the Bloch sphere. However, at $J = \delta/2$ (see Fig. 3.2.b), the situation is different. The dynamics becomes periodic and the rotation and the change of single spin contrast share the same period $\tilde{t}_p = \tilde{t}_o = 2\sqrt{3}\pi/\delta$.

3.2 Large spins: numerics

In the previous section, we have seen that the dynamics for the quantum system $S = 1/2$ deviates from the classical dynamics solved in the previous chapter. The classical dynamics demonstrates only two characteristic time scales while the quantum $S = 1/2$ system has three. Besides, there is no synchronization in the quantum $S = 1/2$ system no matter how large the exchange interaction is. To understand why the quantum system is different from the classical system and how the classical limit emerges in the quantum dynamics, we carry out numerical simulations investigating the temporal evolution of the quantum systems with S larger than $1/2$, ranging from 1, $3/2$, to 10. The dimension of the Hilbert space of the whole system increases with the size of spin S as $(2S + 1)^2 \sim \mathcal{O}(S^2)$.

First, we concentrate on the contrast for $S = 10$ (see Fig. 3.3). There are still two regimes where the behavior of the contrast is different, as is the case in the $S = 1/2$ system. In addition, the critical point marking the transition between the two regimes remains $J = \delta/2$. In the dephased regime ($J < \delta/2$, see Fig. 3.3.a and d), fast oscillations with amplitude large enough to kill the contrast completely are observed. This behavior is reminiscent of the corre-

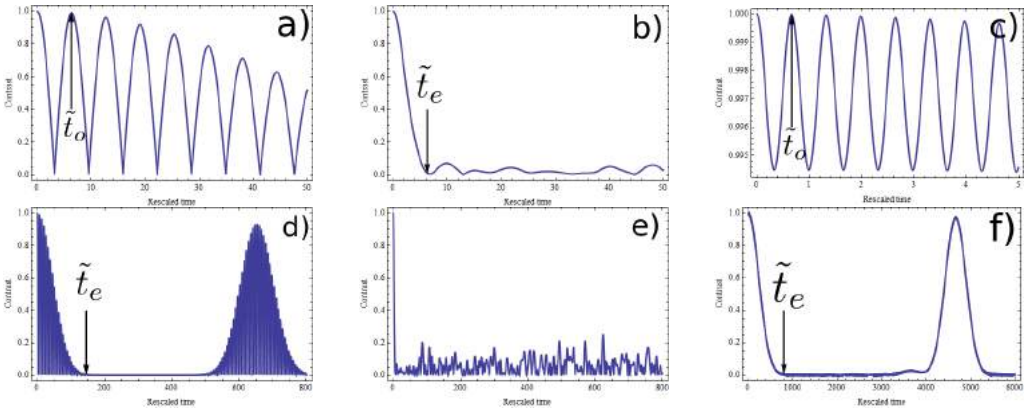

Figure 3.3: Contrast as a function of rescaled time in units of $1/\delta$ for a system with spin size $S = 10$. a)Short time behavior in the dephased regime ($J = 0.1\delta$), the fast oscillation time $\tilde{t}_o$ is indicated by the black arrow. b)Short time behavior for the critical point ($J = 0.5\delta$), the envelope time $\tilde{t}_e$ is showed. c)Short time behavior in the synchronized regime ($J = 5\delta$), the fast oscillation time is indicated. d) Long time behavior in the dephased regime ($J = 0.1\delta$), the envelope time $\tilde{t}_e$ is indicated. e)Long time behavior for the critical point ($J = 0.5\delta$). f)Long time behavior in the synchronized regime ($J = 5\delta$), the envelope time $\tilde{t}_e$ is indicated.

sponding classical dynamics where the contrast vanish periodically because of the large oscillation. Besides, the quantum nature of the system manifests itself by the existence of an envelope which fixes the amplitude of these classical oscillations with the characteristic time $\tilde{t}_e$. In the synchronized regime ($J > \delta/2$, see Fig. 3.3.c and f), the fast classical oscillation is not large enough to make the contrast vanish and the contrast oscillates around its initial value 1. However, at longer time, the contrast is instead determined mainly by an envelope modulating the dynamics, which originates from quantum effects. At the envelope time $\tilde{t}_e$, this envelope brings the contrast to zero. At the critical point ($J = \delta/2$, see Fig. 3.3.b and e), the contrast falls towards zero and then stays close to zero oscillating with small amplitude. From these qualitative pictures, it is evident that the dynamics for larger spin systems ($S = 10$) resembles that of the classical one during short time, and reveals quantum characters at longer times. The dynamics for the $S = 10$ systems also shows richer dynamics which has not appeared in the quantum $S = 1/2$ systems. For example, when $J > \delta/2$ (see Fig. 3.3.f), there is a plateau after the envelope time $\tilde{t}_e$ where the contrast stays around zero before restoring to almost 1 at a much larger time. The time when the contrast almost attains 1 is called approximate recurrence time $\tilde{t}_{ar}$. This new temporal behavior indi-

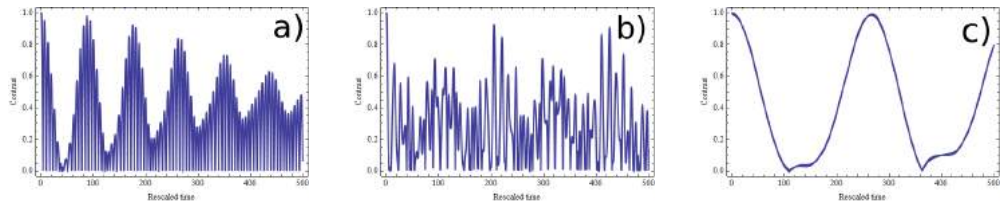

Figure 3.4: Contrast for spin size $S = 1$. The red lines are the classical trajectories, the dotted blue lines quantum trajectories, and the thikc black lines the equators. a) Dephased regime ($J = 0.1\delta$), b) critical point ($J = 0.5\delta$), and c) synchronized regime ($J = 5\delta$).

cates two points: a) the dynamics for the quantum systems is multi-scaled, and b) as the spin size S of the system increases, the number of characteristic time scales also increases.

It is also constructive to compare the dynamics of quantum systems with different spin sizes in order to show that the dynamics becomes richer with the increasing spin size. The contrast for $S = 1$ system in different regimes is shown in Fig. 3.4. Comparing Fig. 3.4 with Fig. 3.1, we can infer that in either the dephased regime or the synchronized regime, the dynamics of $S = 1$ system is richer than that of $S = 1/2$ system in that in addition to the envelope with a slow modulating effect on the contrast, an envelope of the envelope exists. The maximum of the contrast in each small envelope changes with time. And if we look at the difference between the $S = 1$ (Fig. 3.4) and $S = 10$ (Fig. 3.3) systems, an evident difference in the behavior of the two systems is that there is a plateau where the contrast stays near zero in the $S = 10$ system. This justifies our earlier speculation that the dynamics becomes richer with increasing spin sizes. The critical point, however, is worth special attention. At this point, the behavior of the contrast after first attaining zero eludes explanation. The best we can say is that the quantum dynamics follows roughly the classical one, with a quantum fluctuation, which leads to the noisy contrast after the first zero. In the $S = 1/2$ case, the quantum fluctuation is so strong that the contrast can restore its full amplitude after certain time (see Fig. 3.1.b). Or the quantum recurrence is small because of the small dimension of the Hilbert space and we can observe it. The amplitude of the quantum fluctuation diminishes when spin size goes larger. For $S = 10$, the variation of contrast after the time $\tilde{t}_e$ is smaller than 0.1 most of the time as can be seen from Fig. 3.3.e.

Following the same token as for the $S = 1/2$ system, we can similarly use the Bloch sphere representation to interpret qualitatively the dynamical process. This is done for the $S = 10$ systems as shown in Fig. 3.5. The behavior

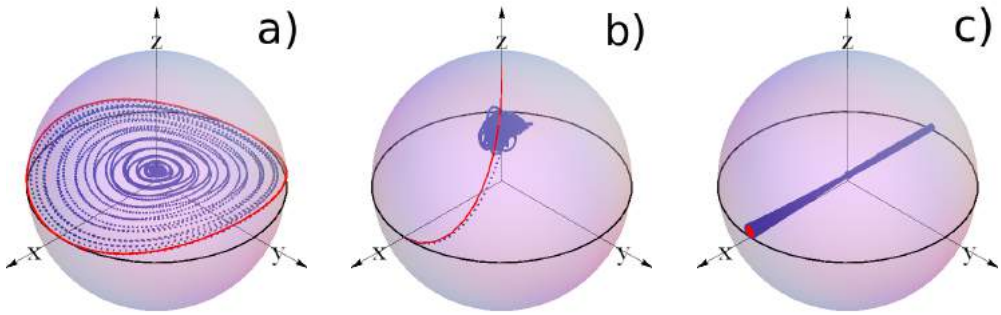

Figure 3.5: Bloch sphere representation of a single normalized spin for spin size $S = 10$. a) Dephased regime ($J = 0.1\delta$), b) critical point ($J = 0.5\delta$), and c) synchronized regime ($J = 5\delta$).

is also similar to that for $S = 1/2$, with a more complicated trajectory on the Bloch sphere. In the dephased regime (Fig. 3.5.a), the movement of the spin number 1 is determined mainly by the external dephasing magnetic field which rotates the spin around the z-axis. At the same time, the norm $C_1(\tilde{t})$ decreases as a manifestation of the quantum effects which can be conceived as the spreading of the wave packet on the Bloch sphere (For a more detailed discussion on the spreading of the wave packet, see Sec. 3.5). When the spin approaches the central region of the Bloch sphere at the envelope time ($\tilde{t}_e$), it starts oscillating with small amplitude for a long time before leaving this region and spiraling out. This long period of small oscillation can be better understood if we look at the contrast: the plateau between two envelopes is a clear signal of this staying near the center. The spin continues spiraling outward until it almost fully restores the amplitude. This time is the approximate recurrence time ($\tilde{t}_{ar}$). In the synchronized regime (Fig. 3.5.c), the spin rotates mainly around the direction of the total spin, the x-axis. But quantum effect diffuses the wave packet on the Bloch sphere, inducing the diminishment of the norm. And the spin retreats correspondingly toward the center. The long staying near the center also exists in this regime. And then the spin rotates outward to $-x$-axis reaching almost the point $(-1, 0, 0)$ at the approximate recurrence time $\tilde{t}_{ar}$. At the critical point (Fig. 3.5.b), the spin first follows the classical trajectory, and then deviates from this trajectory due to quantum fluctuation moving toward the z-axis. After arriving at the center region, the spin stays there forever, oscillating because of quantum uncertainty.

After the qualitative understanding, we now begins a more quantitative study. Since the dynamics is more complicated and a larger number of char-

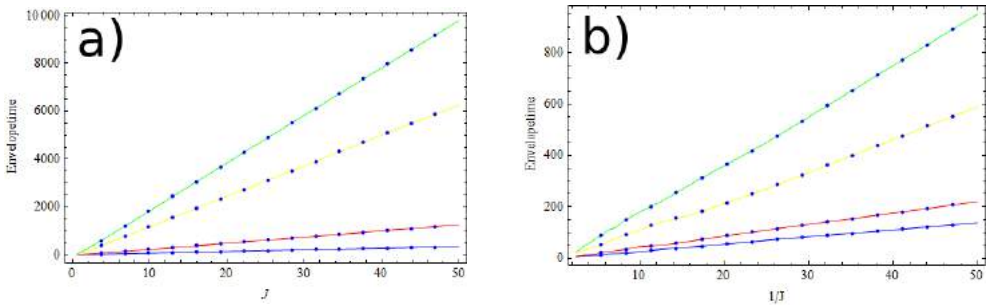

Figure 3.6: a)Envelope time as a function of the interaction strength in the synchronized regime ($J > \delta$). b)Envelope time as a function of the inverse of interaction strength in the dephased regime ($J < \delta/2$). The blue line is for $S = 1/2$, red line $S = 1$, yellow line $S = 5$, and green line $S = 10$.

acteristic time scales, which are essentially quantum time scales, emerge as the spin size is increased, we confine ourselves to the smallest quantum times scale: the envelope time $\tilde{t}_e$. The first thing to note is that in the synchronized regime ($J > \delta/2$) the envelope time is proportional to the interaction strength, while in the dephased regime, we have $\tilde{t}_e \propto 1/J$. This is best illustrated with the figure of the envelope as a function of (the inverse of) the interaction strength for a specific spin size (see Fig. 3.6). It is also obvious from this figure that the envelope time has a spin size dependence. As S increases, the envelope time also increases. In the synchronized regime, we can fit the envelope time as a function of the interacting as

$$\tilde{t}_e(J, S) = i_{syn}(S) + f_{syn}(S)J, \tag{3.21}$$

which gives the proportionality $f_{syn}(S)$. Then we can fit this proportionality

$$f_{syn}(S) = a_{syn} + b_{syn}S^{c_{syn}}, \tag{3.22}$$

and obtain $c_{syn} = 0.500928 \approx 1/2$. Therefore, we have

$$\tilde{t}_e \sim \sqrt{S}\frac{J}{\delta^2} \tag{3.23}$$

in the synchronized regime. In the dephased regime, we carry out the same fitting for envelope time

$$\tilde{t}_e(J, S) = i_{dep}(S) + f_{dep}(S)1/J, \tag{3.24}$$

and then fit

$$f_{dep}(S) = a_{dep} + b_{dep}S^{c_{dep}} \tag{3.25}$$

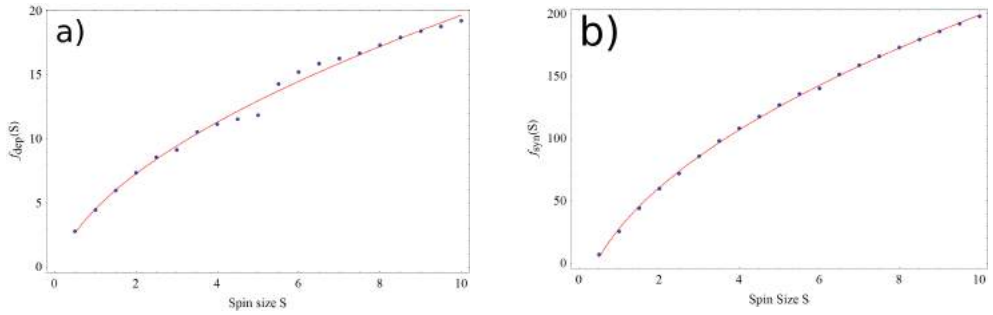

Figure 3.7: The slope of the envelope time as a function of spin size S. a)Dephased regime. b)Synchronized regime. For the meaning of $f_{dep}(S)$ and $f_{syn}(S)$, see text.

to obtain $c_{deph} = 0.551247 \approx 1/2$ (see Fig. 3.7). Thus we obtain

$$\tilde{t}_e \sim \sqrt{S}\frac{1}{J} \tag{3.26}$$

in the dephased regime. In the next section, we will see that $\tilde{t}_e \propto \sqrt{S}$ and $\tilde{t}_{ar} \propto S$.

3.3 Effective models for the dynamics

In the previous section, we have seen that the dynamics of the quantum spin system is very complicated and that there is an increasing number of characteristic time scales as the spin size augments. Instead of trying to gain a complete understanding of this complex phenomenon, we concentrate on the two smallest quantum time scales and make some approximations in the model to capture these two quantum time scales. In the dephased regime ($J < \delta/2$) and the synchronized regime ($J > \delta/2$), we employ two different effective Hamiltonians which give a good agreement with the numerical results till the first approximate recurrence time. Near the critical point, however, the underlying physics is not well understood. In this section, we will use the unrescaled quantities for computational convenience and only in the end restore the rescaled expressions.

3.3.1 Effective model in the dephased regime

In the dephased regime ($J \ll \delta/2$), the main mechanism of the dynamics is the inhomogeneity of the external magnetic field. The exchange interaction

between the two spins, therefore, can be treated as a small perturbation in a first place. The unperturbed eigenstates and eigenenergies are

$$\frac{\delta_S}{2}(S_1^z - S_2^z)|m_1, m_2\rangle = \frac{\delta_S}{2}(m_1 - m_2)|m_1, m_2\rangle. \tag{3.27}$$

where we have omitted the quantum number of spin size S for the sake of simplicity, as there would be no ambiguity. In the basis of the unperturbed Hamiltonian, the perturbation has the matrix elements

$$\begin{aligned}
&\langle m_1' m_2'|(S_1^x S_2^x + S_1^y S_2^y)|m_1, m_2\rangle \\
=&\frac{1}{2}\Big(\sqrt{(S - m_1)(S + m_1 + 1)(S + m_2)(S - m_2 + 1)}\delta_{m_1', m_1+1}\delta_{m_2', m_2-1} \\
&+\sqrt{(S + m_1)(S - m_1 + 1)(S - m_2)(S + m_2 + 1)}\delta_{m_1', m_1-1}\delta_{m_2', m_2+1}\Big)
\end{aligned} \tag{3.28}$$

and

$$\begin{aligned}
&\langle m_1', m_2'|S_1^z S_2^z|m_1, m_2\rangle \\
=&m_1, m_2\delta_{m_1', m_1}\delta_{m_2', m_2}
\end{aligned} \tag{3.29}$$

Then the interaction in the xy-plane has no diagonal element in this basis. As a first order approximation, we can neglect them and get an effective Hamiltonian

$$H_{dep} = \frac{\delta_S}{2}(S_1^z - S_2^z) + J_S S_1^z S_2^z. \tag{3.30}$$

In this effective Hamiltonian, not only is the z-component of the total spin conserved as a result of the rotational invariance around the z-axis, but also that of each individual spin is also conserved as the Hamiltonian now commutes with the single spin operator in the z-axis, $[H, S_i^z] = 0$. The eigenvalues and eigenvectors of the effective Hamiltonian are

$$|e_i\rangle = |m_1, m_2\rangle, \quad E_i = \frac{\delta_S}{2}(m_1 - m_2) + J_S m_1 m_2, \tag{3.31}$$

with i the ensemble of quantum number (m_1, m_2). These eigenvectors clearly separate the two spins, i.e., the operator of an individual spin would not change the state of the other spin when applied onto such an eigenvector. The initial state is two spins each in a coherent state pointing in the x-axis direction with the direction angle $\theta_1 = \theta_2 = \pi/2$, and $\phi_1 = \phi_2 = 0$. A

coherent state for spin S with the direction angle (θ, ϕ) can be written as (see [43, 44])

$$|\theta,\phi\rangle = \sum_{m=-S}^{S} \sqrt{\binom{2S}{S+m}} (\cos\frac{\theta}{2})^{S+m} (\sin\frac{\theta}{2})^{S-m} e^{i(S-m)\phi} |S,m\rangle, \quad (3.32)$$

where we have used the binomial coefficient

$$\binom{2S}{S+m} = \frac{(2S)!}{(S+m)!(S-m)!}. \quad (3.33)$$

Then the initial state can be written as

$$|\Psi(0)\rangle = \left(\frac{1}{2}\right)^{2S} \sum_{m_1,m_2=-S}^{S} \sqrt{\binom{2S}{S+m_1}\binom{2S}{S+m_m}} |m_1,m_2\rangle. \quad (3.34)$$

Then at time t, the temporal evolution of the effective Hamiltonian would lead to the state

$$|\Psi(t)\rangle = \left(\frac{1}{2}\right)^{2S} \sum_{m_1,m_2=-S}^{S} \sqrt{\binom{2S}{S+m_1}\binom{2S}{S+m_m}} e^{-iE_i t} |m_1,m_2\rangle, \quad (3.35)$$

as $|m_1, m_2\rangle$ is nothing but the eigenvectors of the effective Hamiltonian. Now we are ready to calculate the expectation of the x-component of the total spin

$$\langle S_t^x\rangle(t) = \langle\Psi(t)|S_t^x|\Psi(t)\rangle = \langle\Psi(t)|S_1^x|\Psi(t)\rangle + \langle\Psi(t)|S_2^x|\Psi(t)\rangle. \quad (3.36)$$

Leaving the details of calculation to the appendix, we only write the result

$$\begin{aligned}
\langle S_1^x(t)\rangle &= S\cos(\frac{\delta_S t}{2})\cos^{2S}(\frac{J_S t}{2}) = \langle S_2^x(t)\rangle, \\
\langle S_1^y(t)\rangle &= S\sin(\frac{\delta_S t}{2})\cos^{2S}(\frac{J_S t}{2}) = -\langle S_2^y(t)\rangle, \\
\langle S_1^z(t)\rangle &= 0 = -\langle S_2^z(t)\rangle.
\end{aligned} \quad (3.37)$$

And the contrast, written in the rescaled quantities, takes the form

$$\text{Contrast} = \left|\cos\left(\frac{\delta_S t}{2}\right)\cos^{2S}\left(\frac{J_S t}{2}\right)\right|. \quad (3.38)$$

In the above result, the first term on the right hand side $\cos(\delta_S t/2)$ gives the fast oscilaltion with the fast oscillation time $\tilde{t}_o = 2\pi/\delta$. The second term

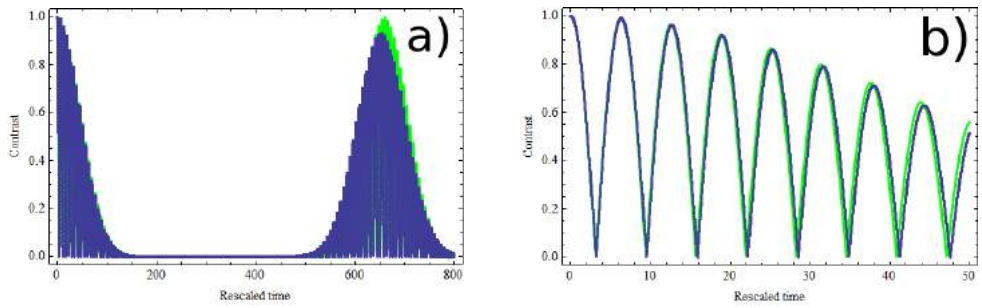

Figure 3.8: The contrast as a function of rescaled time in units of $1/\delta$ obtained by the effective model and the numerical methods for $S = 10$, $J = 0.1\delta$. The dotted blue curve is the numerical result, the thick green the analytical contrast for the effective model. a)Long time comparison. b)Short time comparison.

$\cos^{2S}(J_S t/2)$ gives the approximate recurrence time $\tilde{t}_{ar}$ and the envelope time $\tilde{t}_e$. For the approximate recurrence time, we have

$$\cos^{2S}\left(\frac{J_S t_{ar}}{2}\right) = 1 \rightarrow \tilde{t}_{ar} = \frac{2\pi\sqrt{S(S+1)}}{J}. \tag{3.39}$$

In the limit $S \gg 1$, $J = \text{const.}$ and $\delta = \text{const.}$, we get

$$\tilde{t}_{ar} \approx \frac{2\pi S}{J}. \tag{3.40}$$

For the envelope time, taking the limit $S \rightarrow \infty$, $J = \text{const.}$, and $\delta = \text{const.}$, we have

$$\cos^{2S}(J_S t/2) \approx e^{2S\ln(1-\frac{1}{2}\frac{J_S^2 t^2}{4})} \approx e^{-\frac{SJ_S^2 t^2}{4}}, \tag{3.41}$$

yielding

$$t_e \approx \frac{2}{J_S\sqrt{S}} \rightarrow \tilde{t}_e \approx 2\sqrt{S}/J. \tag{3.42}$$

The first thing to note from the result in Eq. 3.38 is that the agreement with numerical simulations is excellent till the first approximate recurrence time $\tilde{t}_{ar}$ (see Fig. 3.8). At $\tilde{t}_{ar}$, the analytical contrast obtained above deviates from the numerical one. The analytical approach has not properly taken into account the multi-scale dynamics of the system, but has instead focused on the first time scales. Thus the complex phenomena, such as the envelope of the envelope, are not obtained. In the analytical solution of the effective

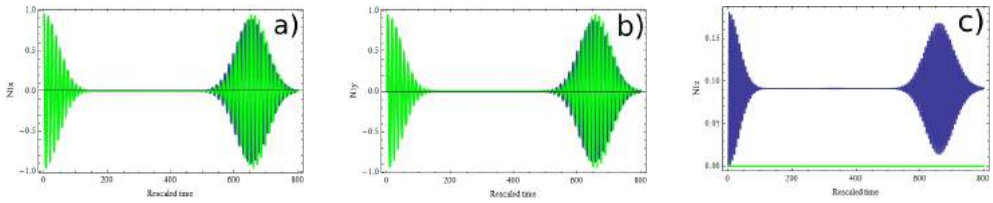

Figure 3.9: Comparison of components of spin number 1 between the numerical simulations and the effective model as a function of rescaled time $1/\delta$ for $S = 10$ and $J = 0.1\delta$. The blue lines are the numerics and the green ones analytical results. a) n_1^x. b) n_1^y. c) n_1^z. Note that the vertical scale for n_1^z is different from those for n_1^x and n_1^y.

model, only three time scales are revealed, the fast oscillation time, the envelope time, and the first approximate recurrence time. The fast oscillation time is given as $\tilde{t}_o \sim 1/\delta$. This is a reminiscent of the classical period $\tilde{t}_p$. The envelope time in the effective model is $\tilde{t}_e \sim \sqrt{S}/J$, giving the right behavior of numerical results. And the first approximate recurrence time takes the form $\tilde{t}_{ar} \approx 2\pi\sqrt{S(S+1)}/J \approx 2\pi S/J$. The latter two are purely quantum time scales.

Another remarkable point is that in this effective model, the z-component of the individual spin is always zero instead of following the dynamics in the numerical simulations. However, this difference does not have a great impact on the dynamics and the other components obtained from the effective model agree very well with the numerics till the first approximate recurrence time. This can be understood by noting that the z-component of the individual spin operator is small. For $S = 10$, $J = 0.1\delta$, the maximum value of the $\langle n_1^z(\tilde{t})\rangle$ is about 0.18 (see Fig. 3.9). For a single spin, we can write

$$C_1(\tilde{t}) \approx \left|\cos^{2S}\left(\frac{J\tilde{t}}{2\sqrt{S(S+1)}}\right)\right|, \tag{3.43}$$

and

$$\vec{n}_1 \approx \begin{pmatrix} \cos\left(\delta\tilde{t}/2\right) \\ \sin\left(\delta\tilde{t}/2\right) \\ 0 \end{pmatrix}. \tag{3.44}$$

We can compare the result of this effective model with that of the $S = 1/2$ case obtained exactly. In the spin $S = 1/2$ case, if $J \ll \delta/2$, the contrast can be written as

$$\mathrm{C}_{1/2} \approx \left|\cos\left(\delta\tilde{t}/2\right)\cos\left(\frac{J\tilde{t}}{\sqrt{3}}\right)\right|.$$

And the contrast obtained by the effective model reads

$$\mathrm{C}_{dep} \approx \left| \cos\left(\delta\tilde{t}/2\right) \cos^{2S}\left(\frac{J\tilde{t}}{2\sqrt{S(S+1)}}\right) \right|. \tag{3.45}$$

If we take $S = 1/2$, we recover the exact result for $S = 1/2$.

3.3.2 Effective model in the synchronized regime

Contrary to the dephased regime, the dominant mechanism of dynamics in the synchronized regime ($J \gg \delta/2$) is the exchange interaction. The interaction term in the original Hamiltonian in Eq. 6.1 can be written as

$$\vec{S}_1 \cdot \vec{S}_2 = \frac{1}{2}\left[\left(\vec{S}_1 + \vec{S}_2\right)^2 - \left(\vec{S}_1\right)^2 - \left(\vec{S}_2\right)^2\right]. \tag{3.46}$$

The second and third term in the square bracket are constant because of the identity

$$\left(\vec{S}_i\right)^2 \equiv S(S+1)\mathbb{1}, \tag{3.47}$$

where $\mathbb{1}$ is the identity operator. If we neglect the constant terms in the Hamiltonian, the original Hamiltonian reduces to

$$H = \frac{\delta_S}{2}(S_1^z - S_2^z) + \frac{J_S}{2}\left(\vec{S}_1 + \vec{S}_2\right)^2. \tag{3.48}$$

The interaction is nothing but the square of the total spin operator $\vec{S}_t \equiv \vec{S}_1 + \vec{S}_2$. In the synchronized regime, the inhomogeneity of the external magnetic field is small and can therefore be treated as a perturbation. The unperturbed Hamiltonian with only the interaction term takes the form

$$H_0 = \frac{J_S}{2}\left(\vec{S}_t\right)^2, \tag{3.49}$$

and therefore it is more suitable to consider the total spin as a good quantum number instead of the individual spins. This Hamiltonian has eigenenergies and eigenvectors

$$E_i^0 = \frac{J_S}{2}S_t^2, \quad |E_i^0\rangle = |S_t, m_t^z\rangle, \tag{3.50}$$

with $S_t \in [0, 2S]$ and $m_t^z \in [-S_t, S_t]$. The eigenvectors are the eigenvectors of the total spin operator $\vec{S}_t$, and are $(2S_t+1)$-fold degenerate where S_t is the

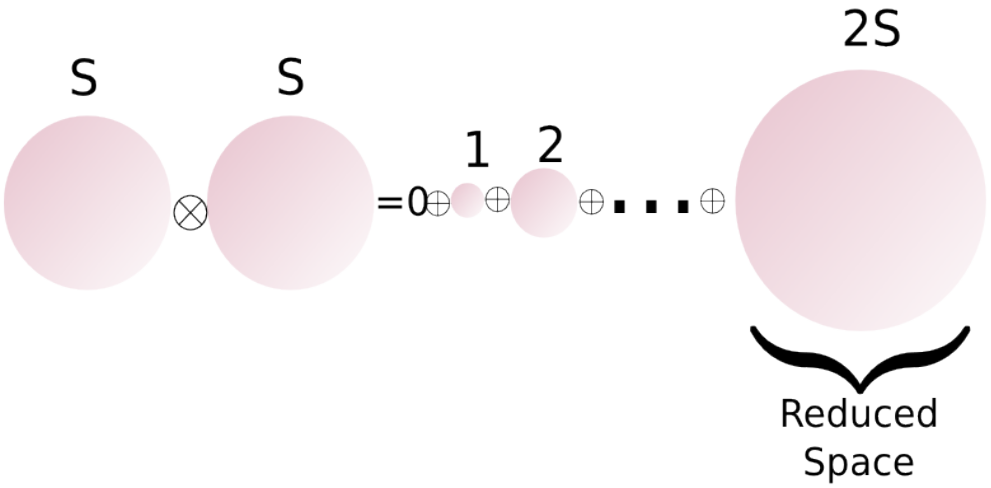

Figure 3.10: A schematic illustration of the Bloch spheres of the two-spin system and the corresponding radii. The system of two spins with size S can be considered as the product of two spheres with radii S. And this is equivalent to the sum of $2S+1$ spheres with radii 0, 1, $\ddots$, $2S$. As a first approximation, we only consider the Bloch sphere with $S_t = 2S$.

quantum number of total spin. It is equivalent to say that the eigenvectors of the unperturbed Hamiltonian are grouped according to their total spin size. Each group is on a different Bloch sphere of the total spin.

The initial state is two spin of size S pointing in the x-direction. Using the total spin basis, this is the state $|S_t = 2S, m_{tx} = 2S\rangle$. This can be seen readily if we consider transformation between the basis $\{|m_1^x, m_2^x\rangle\}$ and $\{|S_t, m_t^x\}$ for two spins of size S. For the state $|S_t = 2S, m_t^x = 2S\rangle$, the only non-vanishing Clebsch-Gordan coefficient is $\langle m_1^x = S, m_2^x = S|S_t = 2S, m_t^x = 2S\rangle$ (where for simplicity, we have omitted the quantum number S_1 and S_2 in the Clebsch-Gordan coefficient) because of the property of the Clebsch-Gordan coefficient that $\langle m_1^x, m_2^x|S_t, m_t^x\rangle = 0$ unless $m_1^x + m_2^x = m_t^x$. Thus $|S_t = 2S, m_t^x = 2S\rangle \propto |m_1^x = S, m_2^x = S\rangle$. And since both $|S_t = 2S, m_t^x = 2S\rangle$ and $|m_1^x = S, m_2^x = S\rangle$ are normalized, we have $|S_t = 2S, m_t^x = 2S\rangle = |m_1^x = S, m_2^x = S\rangle$. Therefore the initial state under consideration is on the outermost Bloch sphere with $S_t = 2S$. The energy difference between this subspace of the complete Hilbert space and the neighboring subspace with $S_t = 2S - 1$ is

$$\Delta E = \frac{J_S}{2}\left[4S - 1 + \mathcal{O}(\frac{\delta_S}{J_S})\right], \tag{3.51}$$

where the second term comes from the perturbation, should the perturbation theory work. In the synchronized regime and in the large interaction limit $J \gg \delta/2$, which is equivalent to $J_S S \gg \delta_S$, this energy difference is large and the perturbation from the external field is unlikely to couple the initial state with states from different Bloch sphere. As a first approximation, we constrain ourselves to the outermost Bloch sphere and project the complete Hamiltonian onto this subspace to get an effective Hamiltonian (see Fig. 3.10).

The perturbation term in the Hamiltonian, when acting on the basis $\{|S_t, m_t^z\rangle\}$, has no diagonal terms. Besides, it only couples two states with S_t and $S_t \pm 1$. The details of these are left to the appendix. With this information, the full Hamiltonian, written in the eigenvectors of the unperturbed Hamiltonian H_0, takes the form

$$H = \begin{pmatrix} \frac{J_S}{2}(\vec{S}_t)^2(S_t = 2S) & \frac{\delta_S}{2}(S_1^z - S_2^z)\ (S_t = 2S, 2S-1) \\ \frac{\delta_S}{2}(S_1^z - S_2^z)^T\ (S_t = 2S, 2S-1) & \frac{J_S}{2}(\vec{S}_t)^2(S_t \neq 2S) \end{pmatrix}. \tag{3.52}$$

In the above symbolical expression, the term $\frac{J_S}{2}(\vec{S}_t)^2(S_t = 2S)$ designates the diagonal block of the interaction in the subspace $S_t = 2S$, and $\frac{J_S}{2}(\vec{S}_t)^2(S_t \neq 2S)$ the diagonal block of the interaction in the remaining subspace $S_t \neq 2S$. The two off-diagonal terms represent the perturbations. Though the perturbation also contributes to the diagonal part in the subspace $S_t \neq 2S$, they have no impact on the perturbation calculation. And for simplicity, they are not written explicitly in the above Hamiltonian.

To carry out the perturbative calculation, we use the projection operator method developed by Bloch and Horowitz [45], and later with contribution from Löwdin [46]. Leaving the details of this approach to the appendix, we can write the Hamiltonian in the subspace $S_t = 2S$ as follows

$$H_{syn} = \frac{J_S}{2}\left(\vec{S}_t\right)^2 + \delta V, \tag{3.53}$$

with the perturbation

$$\delta V = \frac{\delta_S^2}{8S(4S-1)J_S}\left[(2S)^2\mathbb{1} - (S_t^z)^2\right]. \tag{3.54}$$

This term is obtained from second order perturbation theory, and can be considered as describing virtual transitions to the second outermost Bloch spheres $S_t = 2S - 1$. Neglecting the term proportional to the identity operator, the Hamiltonian reduces to

$$H'_{eff} = -\frac{\delta_S^2}{8S(4S-1)J_S}\,(S_t^z)^2, \tag{3.55}$$

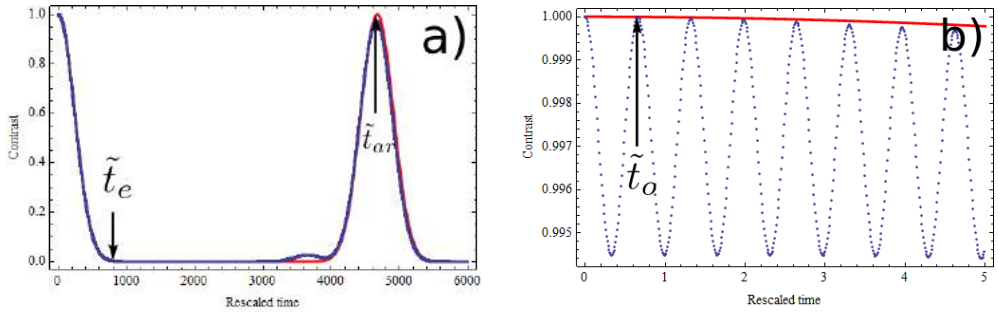

Figure 3.11: Contrast as a function of rescaled time in unit of $1/\delta$. The analytical results from perturbation theory is compared to the numerics for $S = 10$, $J = 5\delta$. The red line is the analytical result and the dotted blue numerics. a) Long time behavior. b) Short time behavior.

with the eigenvectors and eigenenergies

$$E_i = -\left(S_t^z\right)^2 m^2, \quad |E_i\rangle = |S_t = 2S, m_t^z = m\rangle. \tag{3.56}$$

And the contrast takes the form

$$\text{Contrast}(\tilde{t}) = \left|\cos^{4S-1}\left(\frac{\delta^2\sqrt{S(S+1)}\tilde{t}}{8S(4S-1)J}\right)\right|, \tag{3.57}$$

where we have already restored the rescaled quantities. This result gives good agreement with the numerics, as shown in Fig. 3.11. The envelope time and first approximate recurrence are well described by this perturbative calculation.

In the deep synchronized regime ($J \gg \delta$), and for large spin size S, the contrast reduces to

$$\text{Contrast}(\tilde{t}) \approx \cos\left(\frac{\delta^2\tilde{t}}{32SJ}\right)^{4S}. \tag{3.58}$$

When $S \to \infty$, we have

$$\begin{aligned} \mathrm{C}(t) \approx & e^{4S\ln\left(\cos\left(\frac{\delta^2\tilde{t}}{32SJ}\right)\right)} \\ \approx & e^{4S\ln\left(1-\frac{1}{2}\left(\frac{\delta^2\tilde{t}}{32SJ}\right)^2\right)} \\ \approx & e^{-2S\left(\frac{\delta^2\tilde{t}}{32SJ}\right)^2} \\ \approx & e^{(\tilde{t}/\tilde{t}_e)^2}. \end{aligned} \tag{3.59}$$

Then the envelope time reads

$$\tilde{t}_e \approx \frac{16\sqrt{2S}J}{\delta^2} \sim \sqrt{S}\frac{J}{\delta^2}. \tag{3.60}$$

Also, the first approximate recurrence time $\tilde{t}_{ar}$ can be obtained from the approximate expression of contrast in Eq. 3.57 from the requirement

$$\frac{\delta^2\sqrt{S(S+1)}\tilde{t}}{8S(4S-1)J} = \pi. \tag{3.61}$$

Then $\tilde{t}_{ar}$ is found to be

$$\tilde{t}_{ar} = \frac{32\pi S^2(1-1/(4S))}{\sqrt{S(S+1)}}\frac{J}{\delta^2} \approx 32\pi S\frac{J}{\delta^2}. \tag{3.62}$$

However, from Fig. 3.11.b, it is clear that this single sphere approach does not yield the right short time behavior. The fast oscillating corresponding to the classical dynamics are completely absent in this approximation. A remedy to this is to include higher orders in the perturbative calculation or make a truncation in the Hilbert space, including the matrix elements from other Bloch spheres.

3.3.3 Improved method in the synchronized regime

In the preceding subsection, we have obtained an effective Hamiltonian with a perturbation describing the virtual transition between the Bloch spheres $S_t = 2S$ and $S_t = 2S-1$. In this subsection, we carry out a truncation in the Hilbert space and consider the subspace of $S_t = 2S, 2S+1$, treating the transition exactly but neglecting all the other subspaces. In this subspace, we can show that the perturbation term $\delta_S/2(S_1^z - S_2^z)$ only couples the state $|S_t = 2S, m_t\rangle$ and $|S_t = 2S-1, m_t\rangle$. Thus we can first confine ourselves to the small subspace consisting of the two states. In this small subspace, the Hamiltonian reads

$$H = \begin{pmatrix} J_S S^2 & \frac{\delta_S}{2}\sqrt{\frac{4S^2-m^2}{4S-1}} \\ \frac{\delta_S}{2}\sqrt{\frac{4S^2-m^2}{4S-1}} & J_S S(S-2) \end{pmatrix} \tag{3.63}$$

The eigenenergies are

$$\begin{aligned} E_m^+ =& J_S S(S-1) + \frac{1}{2}\sqrt{4J_S^2S^2 + \delta_S^2\frac{4S^2-m^2}{4S-1}}, \\ E_m^- =& J_S S(S-1) - \frac{1}{2}\sqrt{4J_S^2S^2 + \delta_S^2\frac{4S^2-m^2}{4S-1}}. \end{aligned} \tag{3.64}$$

And the eigenstates are

$$\begin{aligned} |e_m^+\rangle &= s_m|2S,m\rangle + c_m|2S-1,m\rangle, \\ |e_m^-\rangle &= -c_m|2S,m\rangle + s_m|2S-1,m\rangle, \end{aligned} \tag{3.65}$$

with $s_m = \sin\alpha_m$, $c_m = \cos\alpha_m$ and

$$\tan\alpha_m = \delta_S\sqrt{(4S^2-m^2)/(4S-1)}/(E_{m+}-J_S S^2). \tag{3.66}$$

To first order, we have

$$\begin{aligned} E_m^+ \approx & J_S S^2 + \frac{\delta_S^2(4S^2-m^2)}{8J_S S(4S-1)}, \\ E_m^- \approx & J_S S(S-2) - \frac{\delta_S^2(4S^2-m^2)}{8J_S S(4S-1)}, \\ s_m \approx & 1 \\ c_m \approx & \frac{\delta_S}{4J_S S}\sqrt{\frac{4S^2-m^2}{4S-1}}. \end{aligned} \tag{3.67}$$

Then the contrast reads

$$\langle S_t^x\rangle(\tilde{t}) \approx 2S\cos^{4S-1}\left(\frac{\delta^2\sqrt{S(S+1)}\tilde{t}}{8S(4S-1)J}\right) + \frac{\delta^2(S+1)}{16J^2}\cos\left(\frac{2J\tilde{t}}{\sqrt{1+1/S}}\right). \tag{3.68}$$

However, the above result does not satisfy

$$\langle S_t^x\rangle(0) = 2S, \tag{3.69}$$

as it should, because of the second term. We can expand the second term

$$\begin{aligned} & \frac{\delta^2(S+1)}{16J^2}\cos\left(\frac{2J\tilde{t}}{\sqrt{1+1/S}}\right) \\ = & \frac{\delta^2(S+1)}{16J^2}\left[1-2\sin^2\left(\frac{2J\tilde{t}}{\sqrt{1+1/S}}\right)\right]. \end{aligned} \tag{3.70}$$

If we neglect the constant term, then we get

$$\begin{aligned} & \langle S_t^x\rangle(\tilde{t}) \\ \approx & 2S\cos^{4S-1}\left(\frac{\delta^2\sqrt{S(S+1)}\tilde{t}}{8S(4S-1)J}\right) \\ & - \frac{\delta^2(S+1)}{8J^2}\sin^2\left(\frac{2J\tilde{t}}{\sqrt{1+1/S}}\right). \end{aligned} \tag{3.71}$$

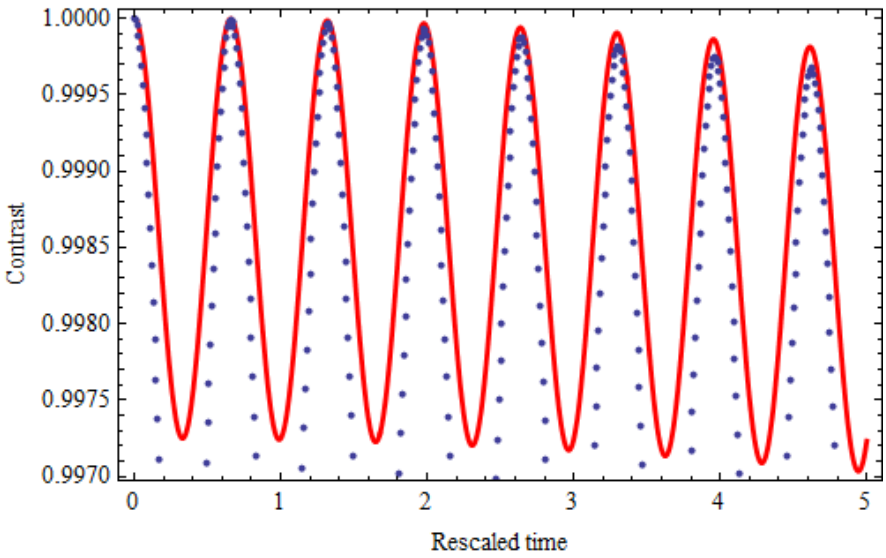

Figure 3.12: Contrast as a function of rescaled time in units of $1/\delta$ for $S = 10$, $J = 5$. The red line is the contrast in Eq. 3.71, the blue dots are the result of numerical simulation.

At time $t = 0$, the above expression gives correctly

$$\langle S_t^x \rangle(0) = 2S. \tag{3.72}$$

From Fig. 3.12, we can see that the expression in Eq. 3.71 does not fit exactly to the numerical simulations. We need to improve further. Recall from the calculation for the $S = 1/2$ case that, in the synchronized regime ($J \gg \delta/2$), the contrast reads

$$\mathrm{C}_{1/2} \approx \left| \cos\left(\frac{\sqrt{3}\delta^2}{8J}\tilde{t}\right) \left[1 - \frac{3\delta^2}{8J^2} \sin^2\left(\frac{J\tilde{t}}{\sqrt{3}}\right)\right] \right|,$$

which can be written as

$$\mathrm{C}_{1/2} \approx \left| \cos^{4S-1}\left(\frac{\delta^2\sqrt{1+\frac{1}{S}}}{8J(4S-1)}\tilde{t}\right) \left[1 - \frac{\delta^2(1+\frac{1}{S})}{8J^2} \sin^2\left(\frac{J\tilde{t}}{\sqrt{1+\frac{1}{S}}}\right)\right] \right|, \quad \text{with } S = 1/2. \tag{3.73}$$

In addition, the contrast for the limit $S \to \infty$ (classical system) is

$$\mathrm{C}(\tilde{t}) \approx 1 - \frac{\delta^2}{8J^2} \sin^2(J\tilde{t}). \tag{3.74}$$

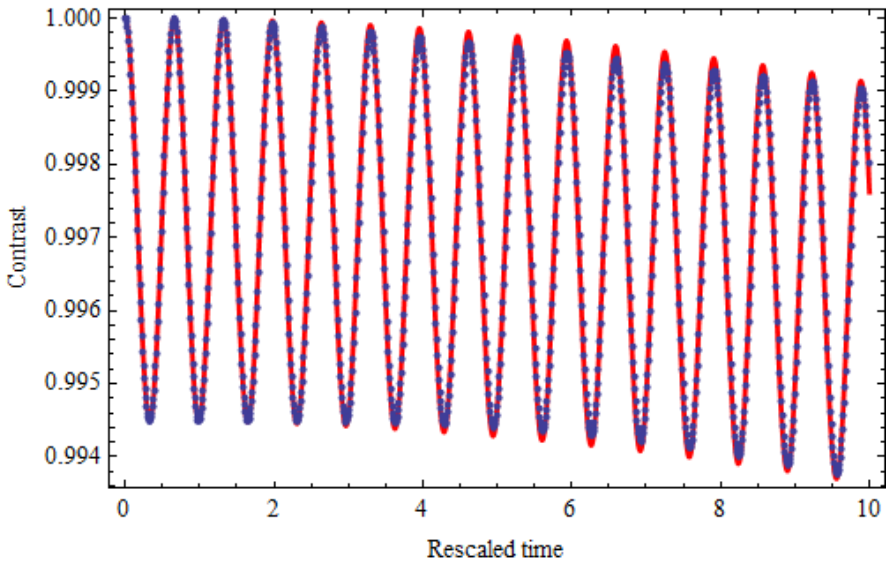

Figure 3.13: Contrast as a function of rescaled time in units of $1/\delta$ for $S = 10$, $J = 5$. The red line is the contrast in Eq. 3.75, the blue dots are the result of numerical simulation.

	$\tilde{t}_i$	$\tilde{t}_o$	$\tilde{t}_e$	$\tilde{t}_{ar}$
Dephased regime ($J \ll \delta/2$)	$2\sqrt{2}/\delta$	$\approx 2\pi/\delta$	$2\sqrt{S}/J$	$2\pi S/J$
Synchronized regime ($J \gg \delta/2$)	$2\sqrt{2}/\delta$	$\approx \sqrt{1+\frac{1}{S}}\pi/J$	$\approx 16\sqrt{2S}J/\delta^2$	$\approx 32\pi SJ/\delta^2$

Table 3.2: Characteristic time scales in the quantum two-spin model.

Then we guess that the contrast should take the form

$$\mathrm{C} \approx \left| \cos^{4S-1}\left(\frac{\delta^2\sqrt{1+\frac{1}{S}}}{8J(4S-1)}\tilde{t}\right)\left[1-\frac{\delta^2(1+\frac{1}{S})}{8J^2}\sin^2\left(\frac{J\tilde{t}}{\sqrt{1+\frac{1}{S}}}\right)\right]\right|. \tag{3.75}$$

From Fig. 3.13, we can see that the guessed result in Eq. 3.75 agrees very well with the numerical simulations. And we can get the fast oscillation time

$$\tilde{t}_o = \sqrt{1+\frac{1}{S}}\frac{\pi}{J}. \tag{3.76}$$

Now we summarize the characteristic time scales in the quantum dynamics of the two-spin system in Tab. 3.2.

3.4 Cumulant expansion method

A semiclassical approach to the spin dynamics problem is the cumulant expansion, developed by Garanin and collaborators (see [40, 41, 42]). In particular, we follow closely the approach in [42]. The basic idea is to expand the Heisenberg equations of motions for spin operators, and treat the quantum average as classical average plus a quantum correction which take the form of cumulants of spin operators.

3.4.1 Direct expansion

For our model, the equations of motion for the first order spin operators read

$$\begin{aligned}\frac{d}{d\tilde{t}}\vec{n}_t =&\frac{\delta}{2}\hat{e}_z \times \vec{n}_d,\\ \frac{d}{d\tilde{t}}\vec{n}_d =&\frac{\delta}{2}\hat{e}_z \times \vec{n}_t + \frac{J}{2}\left(\vec{n}_t \times \vec{n}_d - \vec{n}_d \times \vec{n}_t\right).\end{aligned} \tag{3.77}$$

In the above equations, the term $\vec{n}_t \times \vec{n}_d - \vec{n}_d \times \vec{n}_t$, which contains second order spin operators, needs to be treated quantum mechanically. We define the second order spin operators as

$$\begin{aligned}M^{\alpha\beta} &= n_t^\alpha n_d^\beta + n_d^\beta n_t^\alpha,\\ M_t^{\alpha\beta} &= n_t^\alpha n_t^\beta + n_t^\beta n_t^\alpha,\\ M_d^{\alpha\beta} &= n_d^\alpha n_d^\beta + n_d^\beta n_d^\alpha.\end{aligned} \tag{3.78}$$

Then the equations of motion for second order spin operators can be written as

$$\begin{aligned}\frac{d}{d\tilde{t}}M_t^{\alpha\beta} =& -\frac{\delta}{2}\left(\epsilon_{z\alpha\delta}M^{\beta\delta} + \epsilon_{z\beta\delta}M^{\alpha\delta}\right),\\ \frac{d}{d\tilde{t}}M^{\alpha\beta} =& -\frac{\delta}{2}\left(\epsilon_{z\alpha\delta}M_d^{\delta\beta} + \epsilon_{z\beta\delta}M_t^{\alpha\delta}\right) + \frac{J}{2}\epsilon_{\beta\gamma\delta}T_t^{\alpha\gamma\delta},\\ \frac{d}{d\tilde{t}}M_d^{\alpha\beta} =& -\frac{\delta}{2}\left(\epsilon_{z\alpha\delta}M^{\delta\beta} + \epsilon_{z\beta\delta}M^{\delta\alpha}\right) + \frac{J}{2}\left(\epsilon_{\alpha\gamma\delta}T_d^{\beta\gamma\delta} + \epsilon_{\beta\gamma\delta}T_d^{\alpha\gamma\delta}\right),\end{aligned} \tag{3.79}$$

where we have used the anti-symmetric Levi-Civita symbol $\epsilon_{\alpha\beta\gamma}$ and have defined the third order operators

$$\begin{aligned}T_t^{\alpha\beta\delta} =& S_t^\alpha M^{\beta\delta} + M^{\beta\delta}S_t^\alpha,\\ T_d^{\alpha\beta\delta} =& S_d^\alpha M^{\beta\delta} + M^{\beta\delta}S_d^\alpha.\end{aligned} \tag{3.80}$$

And the equations of motion for the third order spin operators need also to be calculated using Heisenberg equations, which in turn leads to fourth order operators. Continuing this approach, we would obtain an infinite series of coupled equations of motion. However, we will not calculate higher orders and truncate the equations of motion at second orders, which gives an error of the order S^{-1}. At first order, we will recover the classical limit and the second order cumulants are the minimum to take into account the quantum corrections. The expectation values are

$$\begin{aligned}
\frac{d}{d\tilde{t}}\langle n_t^\alpha\rangle =& -\frac{\delta}{2}\epsilon_{z\alpha\beta}\langle n_d^\beta\rangle,\\
\frac{d}{d\tilde{t}}\langle n_d^\alpha\rangle =& -\frac{\delta}{2}\epsilon_{z\alpha\beta}\langle n_t^\beta\rangle + \frac{J}{2}\epsilon_{\alpha\beta\gamma}\langle M^{\beta\gamma}\rangle,\\
\frac{d}{d\tilde{T}}\langle M_t^{\alpha\beta}\rangle =& -\frac{\delta}{2}\left(\epsilon_{z\alpha\delta}\langle M^{\beta\delta}\rangle + \epsilon_{z\beta\delta}\langle M^{\alpha\delta}\rangle\right),\\
\frac{d}{d\tilde{T}}\langle M^{\alpha\beta}\rangle =& -\frac{\delta}{2}\left(\epsilon_{z\alpha\delta}\langle M_d^{\delta\beta}\rangle + \epsilon_{z\beta\delta}\langle M_t^{\alpha\delta}\rangle\right) + \frac{J}{2}\epsilon_{\beta\gamma\delta}\langle T_t^{\alpha\gamma\delta}\rangle,\\
\frac{d}{d\tilde{T}}\langle M_d^{\alpha\beta}\rangle =& -\frac{\delta}{2}\left(\epsilon_{z\alpha\delta}\langle M^{\delta\beta}\rangle + \epsilon_{z\beta\delta}\langle M^{\delta\alpha}\rangle\right) + \frac{J}{2}\left(\epsilon_{\alpha\gamma\delta}\langle T_d^{\beta\gamma\delta}\rangle\right.\\
&\left. +\epsilon_{\beta\gamma\delta}\langle T_d^{\alpha\gamma\delta}\rangle\right),
\end{aligned} \tag{3.81}$$

We define the cumulants of first and second order as follows

$$\begin{aligned}
m_t^\alpha =& \langle n_t^\alpha\rangle,\\
m_d^\alpha =& \langle n_d^\alpha\rangle,\\
m^{\alpha\beta} =& \frac{1}{2}\langle M^\alpha\rangle - m_t^\alpha m_d^\beta,\\
m_t^{\alpha\beta} =& \frac{1}{2}\langle M_t^\alpha\rangle - m_t^\alpha m_t^\beta,\\
m_d^{\alpha\beta} =& \frac{1}{2}\langle M_d^\alpha\rangle - m_d^\alpha m_d^\beta.
\end{aligned} \tag{3.82}$$

From the above definition, we can see that the second order cumulants $m_t^{\alpha\beta}$ and $m_d^{\alpha\beta}$ are symmetric. It has been shown that the n-th order cumulants for the spin operators are of the order S^{1-n}[41, 47], negligible for large spin size S. Therefore, if we truncate at terms of order $\mathcal{O}(S^{-2})$, we can expand the expectation values for third order operators as

$$\begin{aligned}
\langle T_t^{\alpha\beta\delta}\rangle \approx& 4\left(m_t^\alpha m_t^\beta m_d^\delta + m_t^{\alpha\beta} m_d^\delta + m^{\alpha\delta} m_t^\beta + m^{\beta\delta} m_t^\alpha\right),\\
\langle T_d^{\alpha\beta\delta}\rangle \approx& 4\left(m_d^\alpha m_t^\beta m_d^\delta + m^{\beta\alpha} m_d^\delta + m^{\beta\delta} m_d^\alpha + m_d^{\alpha\delta} m_t^\beta\right).
\end{aligned} \tag{3.83}$$

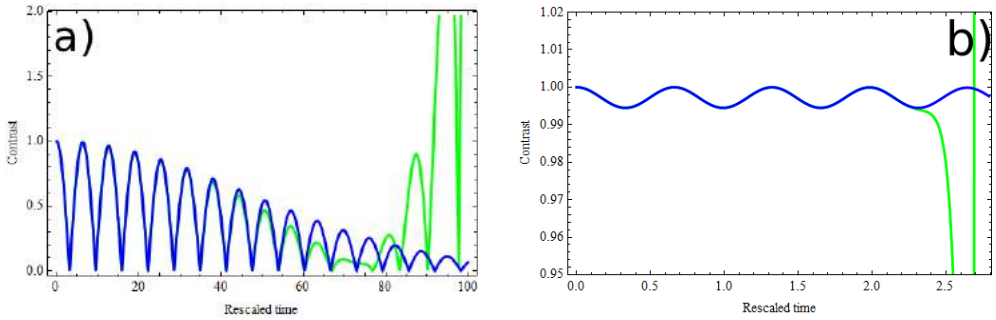

Figure 3.14: The numerical results of contrast as a function of rescaled time (in units of $1/\delta$) obtained from the cumulant expansion equations of motion. a) $S = 10$, $J = 0.1\delta$. b) $S = 10$, $J = 5\delta$. The blue line is the results of exact diagonalization. The green one is the solution of the cumulant equations obtained from Eq. 3.84.

Then the equations of motion for operators reduce to

$$\begin{aligned}
\frac{d}{d\tilde{t}}m_t^{\alpha} =& -\frac{\delta}{2}\epsilon_{z\alpha\beta}m_d^{\beta},\\
\frac{d}{d\tilde{t}}m_d^{\alpha} =& -\frac{\delta}{2}\epsilon_{z\alpha\beta}m_t^{\beta} + J\epsilon_{\alpha\beta\gamma}\left(m_d^{\gamma}m_t^{\beta} + m^{\beta\gamma}\right),\\
\frac{d}{d\tilde{t}}m_t^{\alpha\beta} =& -\frac{\delta}{2}\left(\epsilon_{z\alpha\gamma}m^{\beta\gamma} + \epsilon_{z\beta\gamma}m^{\alpha\gamma}\right),\\
\frac{d}{d\tilde{t}}m^{\alpha\beta} =& -\frac{\delta}{2}\left(\epsilon_{z\alpha\gamma}m_d^{\gamma\beta} + \epsilon_{z\beta\gamma}m_t^{\alpha\gamma}\right) + J\epsilon_{\beta\gamma\delta}\left(m_t^{\gamma}m^{\alpha\delta} + m_d^{\delta}m_t^{\gamma\alpha}\right),\\
\frac{d}{d\tilde{t}}m_d^{\alpha\beta} =& -\frac{\delta}{2}\left(\epsilon_{z\alpha\gamma}m^{\gamma\beta} + \epsilon_{z\beta\gamma}m^{\gamma\alpha}\right) + J\left[\epsilon_{\alpha\gamma\delta}\left(m_t^{\gamma}m_d^{\beta\delta} + m_d^{\delta}m^{\gamma\beta}\right)\right.\\
&\left.+\epsilon_{\beta\gamma\delta}\left(m_t^{\gamma}m_d^{\alpha\delta} + m_d^{\delta}m^{\gamma\alpha}\right)\right],
\end{aligned} \tag{3.84}$$

which form a closed set of equations. The initial conditions are

$$\begin{aligned}
m_t^{\alpha}(0) =& \frac{2S\delta_{\alpha x}}{\sqrt{S(S+1)}},\\
m_d^{\alpha}(0) =& 0,\\
m^{\alpha\beta}(0) =& 0,\\
m_t^{\alpha\beta}(0) =& \frac{1}{S+1}\left(\delta_{\alpha y}\delta_{\beta y} + \delta_{\alpha z}\delta_{\beta z}\right),\\
m_d^{\alpha\beta}(0) =& \frac{1}{S+1}\left(\delta_{\alpha y}\delta_{\beta y} + \delta_{\alpha z}\delta_{\beta z}\right).
\end{aligned} \tag{3.85}$$

We can solve the above equations of motion numerically. The results are shown in Fig 3.14. From the results, we can see that in the dephased regime

(i.e. $J = 0.1\delta$), the contrast obtained by the cumulant expansion agrees well with the one obtained by exact diagonalization before diverging to infinity at approximately the envelope time. In the opposite regime, however, the cumulant expansion leads to unphysical result at very short time ($\tilde{t} \sim 2.5/\delta$). This clearly indicates that the cumulant expansion to second order does not describe correctly the real physics of the synchronized regime. We need to either expand further or find other physical constraints that would give a more physically consistent set of equations. If we go to further orders of cumulants, the number of equations increases exponentially, which is undesirable.

3.4.2 Improved cumulant expansion

As an alternative approach, we seek the physical constraints that might lift the irregular behavior of the solution in the large interaction regime. To do so, we first note that the total energy of the system is conserved since the Hamiltonian of the system is independent of time. Then due to the rotation symmetry around the z-axis, $\langle n_t^z(\tilde{t})\rangle$ is a constant of motion. Besides, for the two individual spins, we have

$$\langle \vec{n}_i \rangle = 1. \tag{3.86}$$

These constraints lead to

$$\begin{aligned}
&E = \left\langle \frac{\delta}{2} n_d^z + \frac{J}{4}\left((\vec{n}_t)^2 - (\vec{n}_d)^2\right) \right\rangle = J\frac{S}{S+1}, \\
&\langle n_t^z \rangle = 0, \\
&\langle (n_t^z)^2 \rangle = 0, \\
&\langle \vec{n}_t \cdot \vec{n}_d + \vec{n}_d \cdot \vec{n}_t \rangle = 0, \\
&\langle (\vec{n}_t)^2 + (\vec{n}_d)^2 \rangle = 4.
\end{aligned} \tag{3.87}$$

In the cumulant language, the above constraints are equivalent to

$$\begin{aligned}
&(m_d^x)^2 + (m_d^y)^2 + (m_d^z)^2 + m_d^{xx} m_d^{yy} + m_d^{zz} - \frac{\delta}{J} m_d^z = \frac{2}{S+1}, \\
&m_t^z = 0, \\
&m_t^{zz} = \frac{1}{S+1}, \\
&m_t^x m_d^x + m_t^y m_d^y + m_t^z m_d^z + m^{xx} + m^{yy} + m^{zz} = 0, \\
&(m_t^x)^2 + (m_t^y)^2 + (m_t^z)^2 + m_t^{xx} + m_t^{yy} + m_t^{zz} + \frac{\delta}{J} m_d^z = 2\frac{2S+1}{S+1}.
\end{aligned} \tag{3.88}$$

Now we need some supplementary information that does not come from the physical argument, but rather from the numerical simulations by exact diagonalization. First of all, in the numerical simulation, the first order operators have the property that

$$\begin{aligned} m_t^y(\tilde{t}) &= 0, \\ m_d^x(\tilde{t}) &= 0, \end{aligned} \tag{3.89}$$

because $\langle n_1^x \rangle = \langle n_2^x \rangle$, $\langle n_1^y \rangle = -\langle n_2^y \rangle$, and $\langle n_1^z \rangle = -\langle n_2^z \rangle$. Then the constraints in Eq 3.88 reduce to

$$\begin{aligned} &(m_d^y)^2 + (m_D^z)^2 + m_D^{xx} + m_d^{yy} + m_d^{zz} = \frac{2}{S+1}, \\ &m_t^z = 0, \\ &m_t^z z = \frac{1}{S+1}, \\ &m^{xx} + m^{yy} + m^{zz} = 0, \\ &(m_t^x)^2 + m_t^{xx} + m_t^{yy} + \frac{\delta}{J} m_d^z = \frac{4S+1}{S+1}. \end{aligned} \tag{3.90}$$

The fact that $m_d^x \equiv 0$ leads to

$$\frac{d}{d\tilde{t}} m_d^x = \frac{J}{2}(m^{yz} - m^{zy}) \equiv 0, \tag{3.91}$$

since $m_t^y \equiv m_t^z \equiv 0$. Besides, exact diagonalization simulation also shows that for the second order cumulants, we have

$$\begin{aligned} m^{yz}(\tilde{t}) &= 0, \\ m^{zy}(\tilde{t}) &= 0, \\ m^{xx}(\tilde{t}) &= 0, \\ m^{yy}(\tilde{t}) &= 0. \end{aligned}$$

From these, we can show that

$$\begin{aligned} m_t^{xy} &= 0, \\ m_t^{xz} &= 0, \\ m_d^{xy} &= 0, \\ m_d^{xz} &= 0. \end{aligned} \tag{3.92}$$

So finally, the equations of motion with the second order cumulants reduce to 14 coupled differential equations

$$
\begin{aligned}
\frac{d}{d\tilde{t}}m_t^x =& -\frac{1}{2}m_d^y,\\
\frac{d}{d\tilde{t}}m_d^y =& \frac{\delta}{2}m_t^x + J(m^{zx} - m^{xz}) - Jm_d^z m_t^x,\\
\frac{d}{d\tilde{t}}m_d^z =& Jm_d^y m_t^x + J(m^{xy} - m^{yx}),\\
\frac{d}{d\tilde{t}}m_t^{xx} =& -m^{xy},\\
\frac{d}{d\tilde{t}}m_t^{yy} =& \delta m^{yz},\\
\frac{d}{d\tilde{t}}m_t^{yz} =& \frac{\delta}{2}m^{zx},\\
\frac{d}{d\tilde{t}}m_d^{xx} =& -\delta m^{yx} + 2J(m_d^z m^{yx} - m_d^y m^{zx}),\\
\frac{d}{d\tilde{t}}m_d^{yy} =& \delta m^{xy} - 2J(m_d^z m^{xy} - m_d^y m^{zx}),\\
\frac{d}{d\tilde{t}}m_d^{zz} =& 2J(m_d^y m^{xz} + m_t^x m_d^{yz}),\\
\frac{d}{d\tilde{t}}m_d^{yz} =& \frac{\delta}{2}m^{xz} + J[m_d^y m^{xy} - m_d^z m^{xz} + m_t^x(m_d^{yy} - m_d^{zz})],\\
\frac{d}{d\tilde{t}}m_{xy} =& -\frac{\delta}{2}(m_d^{yy} - m_t^{xx}) + J(-m_d^z m_t^{xx} - m_t^x m^{xz}),\\
\frac{d}{d\tilde{t}}m^{yx} =& \frac{\delta}{2}(m_d^{xx} - m_t^{yy}) + J(m_d^z m_t^{yy} - m_d^y m_t^{yz}),\\
\frac{d}{d\tilde{t}}m^{xz} =& -\frac{\delta}{2}m_d^{yz} + J(m_d^y m_t^{xx} + m_t^x m^{xy}),\\
\frac{d}{d\tilde{t}}m^{yx} =& -\frac{\delta}{2}m_t^{yz} + J(m_d^z m_t^{yz} - m_d^y m_t^{zz}),
\end{aligned}
\tag{3.93}
$$

which form a closed set of equations. The numerical solution of the above equations is shown in Fig. 3.15. The improved cumulant expansion does not diverge, which compares favorably to the original cumulant expansion. We can also note that in the dephased regime ($J = 0.1\delta$), the contrast obtained from the improved cumulant expansion agrees well with that of the exact diagonalization simulation until the envelope time where the contrast of the improved cumulant begins reviving earlier, the same as the previous cumulant method. In the synchronized regime ($J = 5\delta$), the improved cumulant expansion first follows well the quantum dynamics and then at a certain time

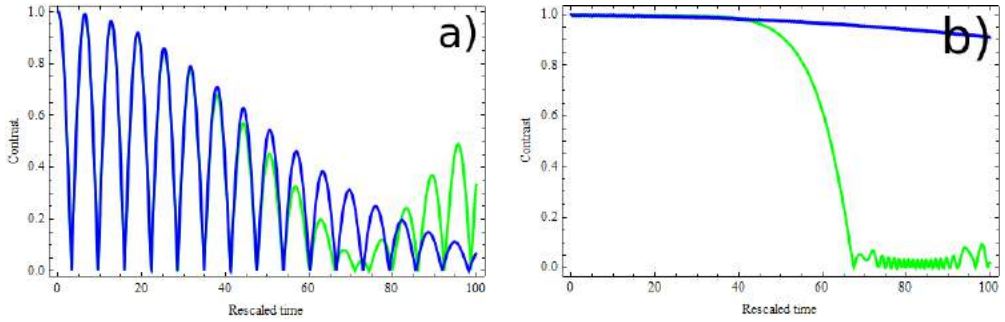

Figure 3.15: Contrast as a function of rescaled time in units of $1/\delta$. a) $S = 10$, $J = 0.1\delta$. b) $S = 10$, $J = 5\delta$. The blue line is the exact diagonalization, the green one the improved cumulant expansion from Eq. 3.93.

($\tilde{t} \sim 50/\delta$), the contrast relaxes to zero and stays close zero oscillating with small amplitude.

3.4.3 Comments on the cumulant expansion

Before proceeding to another method, we need to make some remarks. First, in [41, 47] it is argued that the nth-order cumulants should be of the order S^{1-n}. But we have seen that the cumulants expansion failed to describe the envelope behavior, which is of the order $\sqrt{S}$. One possible explanation is that since we have only simulated a system of spin size $S = 10$, and that this is not large enough to compensate the possible prefactors. To see this, we need to compare the cumulant expansion with exact diagonalization for systems with larger spins. Another possible explanation is that the system considered by Kladko et. al.[41] and Garanin et. al.[47] is at equilibrium, or at least in adiabatic limit, where the state vector is not far away from a coherent state. The spin components in their system can be characterized by a reference frame following the direction of external field. In our model, however, the effective magnetic field acting on each spin depends on the dynamics of the whole system, and thus may not follow their conclusion. This also indicates the answer to the question why the cumulant expansion method has worse performance in the synchronized regime. In the synchronized regime, the exchange interaction between the two spins are very strong and plays a dominant role in the temporal evolution of the system. Unlike the external magnetic field, which preserves a coherent spin state, the interaction between the two spins generates correlation between the two spins and deforms the wave packet of the two spins such that they are not in coherent states anymore. The stronger the interaction, the faster the deviation of the spin states

from coherent states. Therefore, the cumulant expansion does not apply in strongly interacting systems.

Second, if the conclusion in [41, 47] is correct for our model, we may still fail to get the correct envelope time behavior. This is due to the fact in cumulant expansion, we get a series of the form

$$\sum_S a_n S^{-n}, \tag{3.94}$$

but the envelope time $\tilde{t}_e \propto \sqrt{S}$, which can not be approximated by such a series.

Third, the cumulant method may not be self-contained when treating certain time dependent systems or systems out of equilibrium. To get the right behavior, certain quantum information is needed. For example, in the article [42], Garanin used a technique similar to moving average tricks in data analysis and we have used some complementary information from our quantum simulations. This does not invalidate the cumulant expansion, but makes it a less appealing approach since no universal methods are found and we need to complement the method with other approaches.

However, as we can see from the cumulant expansion method, the $S \to \infty$ limit gives the classical dynamics. For $1 \ll S < \infty$, the correction of order $1/S$ to the classical dynamics destroys the synchronization in the synchronized regime.

3.5 Phase-space method

In the previous sections, we have seen that the quantum dynamics of the two-spin problem demonstrates considerable differences from the classical model. New characteristic time scales emerge which do not have classical equivalents. In this section, we will try to understand the origin of the quantum corrections to the classical dynamics. In order to achieve this goal, we need to carry out analysis of the quantum phase space, which is described by the quasiprobability functions. The phase-space approach in quantum mechanics was initially used in the quantum optics, where it was applied to the Dicke model using the quasiprobability distribution $P(\theta, \phi, t)$, the diagonal weighting function of the density operator, by Narducci et al[48]. And then Gilmore et al developed a similar approach using the Husimi Q function and compared the two approaches, arriving at the conclusion that the two functions are related by a convolution integral[49].

In the literature, there are mainly three types of quasiprobability functions used in the description of quantum dynamics. In the following, we

define them with respect to a single spin. But generalization to two spins is evident. For a review on the quasiprobability functions, see [50, 51] and references therein. The quasiprobability function is based on the density operator $\hat{\rho}(t)$ which describes the statistical ensemble of the quantum system. But since we do not consider dissipation effects and work at zero temperature, the density operator is given by

$$\hat{\rho}(t) = |\Psi(t)\rangle\langle\Psi(t)|, \tag{3.95}$$

where $|\Psi(t)\rangle$ is the state vector.

The first one of the three quasiprobability functions is the Wigner function, introduced by Eugene Wigner[52] as a quantum analog to the classical phase space density. The generalization to spin systems was done by Agarwal[53] and Dowling et al[54]. The Wigner function W is defined as

$$W(\theta,\phi,t) = \sum_{l=0}^{2S}\sum_{m=-l}^{l} \rho_{lm}(t) Y_l^m(\theta,\phi), \tag{3.96}$$

with (θ,ϕ) specifying the coordinate on the Bloch sphere, $Y_l^m(\theta,\phi)$ the spherical harmonic functions, and $\rho_{lm}(t) = Tr(\hat{\rho}(t)\hat{T}_l^{m\dagger})$ the reduced density operator. In the preceding expression, we have used the multipole operator

$$T_l^m \equiv \sum_{n,n'=-S}^{S} (-1)^{S-n}\sqrt{2l+1}\begin{pmatrix} S & l & S \\ -n & m & n' \end{pmatrix} |S,n\rangle\langle S,n'|, \tag{3.97}$$

where we have used the Wigner $3j$ symbol.

Another quasiprobability function is the Husimi function (see [55]) defined as

$$Q(\theta,\phi,t) \equiv \langle\theta,\phi|\hat{\rho}(t)|\theta,\phi\rangle, \tag{3.98}$$

where $\hat{\rho}(t)$ is the density operator at time t.

The third one is the Glauber-Sudarshan distribution $P(\theta,\phi,t)$ defined as (see [56, 57])

$$\hat{\rho}(t) = \int P(\theta,\phi,t)|\theta,\phi\rangle\langle\theta,\phi| d\mu(\theta,\phi), \tag{3.99}$$

with $d\mu(\theta,\phi)$ being the measure of the phase space.

In practice, the Wigner function is used less often because it is not definite positive and gives negative values at some region under certain circumstances, which makes it a bad probability although the negativity points directly to quantum effects. Besides, Wigner function can also change abruptly

in certain region, rendering it more difficult to compute. The Glauber-Sudarshan distribution shares the same problems. On the contrary, the Husimi function is semi definite positive and can be viewed as an average of the Wigner function in a small cell of phase space of the surface $\hbar$, and thus behaves more benignly. Consequently, in the following, we will use this function as the desired quasiprobability and derive the equation of motion for it. This method has been first proposed by Brif and Mann [58], and then developed by Trimborn et al [59, 60] in the system of Bose-Einstein condensate trapped in a double well potential. This approach has also been applied to the Dicke model by Altland and Haake [61, 62].

Before proceeding, we need to use a different parametrization of the coherent states. Instead of using the angle specifying the coordinate on the Bloch sphere, we use the stereographic projection on the complex plane of the points on the Bloch sphere. The complex parameter is defined as

$$z = \tan\frac{\theta}{2}e^{i\phi}, \tag{3.100}$$

with (θ, ϕ) the coordinate of the end point of the spin state on the Bloch sphere. This is the stereographic projection of the spin vector on the equator complex plane from the south pole (see Fig. 3.16). The points on the north hemisphere are projected onto the region $|z| < 1$, while the points on the south hemisphere are projected onto the region $|z| > 1$. The south pole is a singular point in this projection and is projected to ∞.

Using this parametrization, the spin coherent state is now expressed as

$$|z\rangle = |\theta, \phi\rangle = \sum_{m=-S}^{S} \sqrt{\binom{2S}{S+m}} \frac{z^{S-m}}{(1+|z|^2)^S} |S, m\rangle. \tag{3.101}$$

Then the Husimi function for a single spin is

$$Q(z, t) \equiv \langle z|\hat{\rho}|z\rangle, \tag{3.102}$$

which is just a change of variable. Note that, since the Husimi function is a quasiprobability function and follows most normal properties of a probability distribution function, if we want to change the variables, we need to introduce a corresponding Jacobian as a prefactor. In the above expression, this is not done explicitly, because we will normalize the obtained function to unit. But later, when deriving the equation of motion for this quasiprobability function for the canonical variables, we should not forget this factor. Otherwise, the obtained equation of motion would not take the correct form.

Another element needed to derive the equation of motion for the quasiprobability function is the differential operator resulting from the action of an

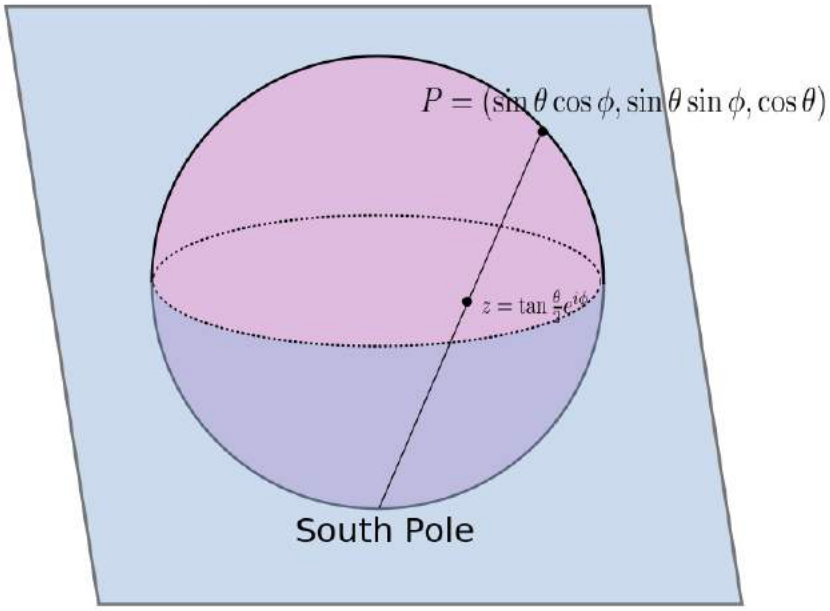

Figure 3.16: Schematic illustration of the stereographic projection used to parametrize the Bloch sphere of unit radius. A spin vector pointing in the direction $(\sin\theta\cos\phi, \sin\theta\sin\phi, \cos\theta)$ is projected onto the equator plane at $z = \tan(\theta/2)e^{i\phi}$.

arbitrary Hermitian operator on the coherent state projector. This is in analogy with the classical phase-space distribution theory and the algebra is called coherent state D algebra (see [43]). There are different types of D algebra defined as

$$\begin{aligned} B|\Omega\rangle &= D^k(B)|\Omega\rangle, \\ \langle\Omega|B &= \langle\Omega|D^b(B), \\ B|\Omega\rangle\langle\Omega| &= D^l(B)|\Omega\rangle\langle\Omega|, \\ |\Omega\rangle\langle\Omega|B &= |\Omega\rangle\langle\Omega|D^r(b), \end{aligned} \tag{3.103}$$

where $|\Omega\rangle$ is a generic coherent state and B a Hermitian operator. From the above definitions, it is clear that we have the relations

$$\begin{aligned} D^k(b) &= [D^b(b)]^*, \\ D^r(b) &= [D^l(b)]^*. \end{aligned} \tag{3.104}$$

Besides, we also have

$$|\Omega\rangle\langle\Omega|B = |\Omega\rangle\langle\Omega|D^r(b) = D^r(b)|\Omega\rangle\langle\Omega| = [D^l(b)]^*|\Omega\rangle\langle\Omega|. \tag{3.105}$$

For our purpose, to derive the equation of motion for the Husimi function, it is more suitable to use the D^l algebra. And the D^l algebra for the spin coherent state in the z representation reads (for a detailed derivation, see Sect. 3.8)

$$\begin{aligned} S^+|z\rangle\langle z| &= \left(-z^2\partial_z + 2S\frac{z}{1+|z|^2}\right)|z\rangle\langle z|, \\ S^-|z\rangle\langle z| &= \left(\partial_z + 2S\frac{z^*}{1+|z|^2}\right)|z\rangle\langle z|, \\ S^z|z\rangle\langle z| &= \left(-z\partial_z + S\frac{1-|z|^2}{1+|z|^2}\right)|z\rangle\langle z|. \end{aligned} \tag{3.106}$$

And the right action of the spin operators are

$$\begin{aligned} |z\rangle\langle z|S^+ &= \left(-(z^*)^2\partial_{z^*} + 2S\frac{z^*}{1+|z|^2}\right)|z\rangle\langle z|, \\ |z\rangle\langle z|S^- &= \left(\partial_{z^*} + 2S\frac{z}{1+|z|^2}\right)|z\rangle\langle z|, \\ |z\rangle\langle z|S^z &= \left(-z^*\partial_{z^*} + S\frac{1-|z|^2}{1+|z|^2}\right)|z\rangle\langle z|. \end{aligned} \tag{3.107}$$

Now we are in the position to derive the equation of motion for the quasiprobability function of the two-spin system. The Husimi function for our two-spin model is defined as

$$Q(z_1, z_2, t) \equiv C(z_1, z_2)\langle z_1, z_2|\hat{\rho}(t)|z_1, z_2\rangle, \tag{3.108}$$

with the coherent state $|z_1, z_2\rangle = |z_1\rangle \otimes |z_2\rangle$ and the time-independent normalization factor

$$C(z_1, z_2) = \frac{(2S+1)^2}{\pi^2(1+|z_1|^2)^2(1+|z_2|^2)^2}.$$

Then the equation of motion for this function can be derived as

$$\begin{aligned}
&d_tQ(z_1,z_2,t)\\
=&C(z_1,z_2)\langle z_1,z_2|d_t\hat{\rho}|z_1,z_2\rangle\\
=&C(z_1,z_2)\langle z_1,z_2|(-i)[H,\hat{\rho}]|z_1,z_2\rangle\\
=&-iC(z_1,z_2)(\langle z_1,z_2|H\hat{\rho}|z_1,z_2\rangle-\langle z_1,z_2|\hat{\rho}H|z_1,z_2\rangle)\\
=&-iC(z_1,z_2)\left(\sum_n\langle z_1,z_2|H|n\rangle\langle n|\hat{\rho}|z_1,z_2\rangle-\sum_n\langle z_1,z_2|n\rangle\langle n|\hat{\rho}H|z_1,z_2\rangle\right)\\
=&-iC(z_1,z_2)\left(\sum_n\langle n|\hat{\rho}|z_1,z_2\rangle\langle z_1,z_2|H|n\rangle-\sum_n\langle n|\hat{\rho}H|z_1,z_2\rangle\langle z_1,z_2|n\rangle\right)\\
=&-iC(z_1,z_2)Tr\left(\hat{\rho}[|z_1,z_2\rangle\langle z_1,z_2|,H]\right)\\
=&-2Im[D^l(\Omega)]Q(z_1,z_2,t).
\end{aligned}\tag{3.109}$$

After some algebra, we obtain the equation of motion for the quasiprobability Husimi function as

$$d_tQ(z_1,z_2,t)=\left(\mathcal{L}_{drift}+\mathcal{L}_{diff}\right)Q(z_1,z_2,t)\tag{3.110}$$

with the drift term

$$\begin{aligned}
&\mathcal{L}_{drift}\\
=&-i\frac{\delta_S}{2}(z_1\partial_{z_1}-z_2\partial_{z_2})+iJ_SS\left(\frac{z_2}{1+|z_2|^2}-\frac{z_2^*}{1+|z_2|^2}z_1^2\right.\\
&\left.-\frac{1-|z_2|^2}{1+|z_2|^2}z_1\right)\partial_{z_1}+iJ_SS\left(\frac{z_1}{1+|z_1|^2}-\frac{z_1^*}{1+|z_1|^2}z_2^2\right.\\
&\left.-\frac{1-|z_1|^2}{1+|z_1|^2}z_2\right)\partial_{z_2}+c.c.
\end{aligned}\tag{3.111}$$

and the diffusion term

$$\mathcal{L}_{diff}=-i\frac{J_S}{2}\left(z_1^2-2z_1z_2+z_2^2\right)\partial^2_{z_1z_2}+c.c.\tag{3.112}$$

The above equation of motion for Husimi function takes the form of a Fokker-Planck equation. The drift term corresponds to the classical movement, and the diffusion is the quantum correction, as we will see later.

In the following, we demonstrate that the drift term does indeed correspond to the classical movement. To this end, we need to first reduce the

drift term to its standard form and then change to canonical variable representation. But before that, we need to express the unrescaled quantities in the rescaled quantities. Using the relations

$$\begin{aligned}\delta =&\frac{\delta_S}{\sqrt{S(S+1)}},\\ J =&\frac{J_S}{S(S+1)},\end{aligned} \tag{3.113}$$

and neglecting the difference between S and $S+1$ (since we consider the semiclassical limit), the equation of motion for the Husimi function reduces to

$$d_{\tilde{t}}Q(z_1,z_2,\tilde{t}) = \left(\tilde{\mathcal{L}}_{drift}+\tilde{\mathcal{L}}_{diff}\right)Q(z_1,z_2,\tilde{t}), \tag{3.114}$$

with the drift term

$$\begin{aligned}&\tilde{\mathcal{L}}_{drift}\\ =&-i\frac{\delta}{2}(z_1\partial_{z_1}-z_2\partial_{z_2})+iJ\left(\frac{z_2}{1+|z_2|^2}-\frac{z_2^*}{1+|z_2|^2}z_1^2\right.\\ &\left.-\frac{1-|z_2|^2}{1+|z_2|^2}z_1\right)\partial_{z_1}+iJ\left(\frac{z_1}{1+|z_1|^2}-\frac{z_1^*}{1+|z_1|^2}z_2^2-\frac{1-|z_1|^2}{1+|z_1|^2}z_2\right)\partial_{z_2}\\ &+c.c.\end{aligned} \tag{3.115}$$

and the diffusion time

$$\begin{aligned}&\tilde{\mathcal{L}}_{diff}\\ =&-i\frac{J}{2S}\left(z_1^2-2z_1z_2+z_2^2\right)\partial^2_{z_1z_2}+c.c.\end{aligned} \tag{3.116}$$

From the above expression, we can already see that the quantum effects, i.e. the diffusion term, is negligible in the semiclassical limit $S\to\infty$, $J=$ Const. and $\delta=$ Const..

The first drift term originates from the inhomogeneous magnetic field, and can be written as

$$\begin{aligned}&-i\frac{\delta_S}{2}(z_1\partial_{z_1}-z_2\partial_{z_2})\\ =&-i\frac{\delta}{2}\left(\partial_{z_1}z_1-\partial_{z_2}z_2\right).\end{aligned} \tag{3.117}$$

The second term is

$$\begin{aligned}
&iJ\left(\frac{z_2}{1+|z_2|^2}-\frac{z_2^*}{1+|z_2|^2}z_1^2-\frac{1-|z_2|^2}{1+|z_2|^2}z_1\right)\partial_{z_1}\\
=&iJ\partial_{z_1}\left(\frac{z_2}{1+|z_2|^2}-\frac{z_2^*}{1+|z_2|^2}z_1^2-\frac{1-|z_2|^2}{1+|z_2|^2}z_1\right)\\
&+iJ\left(2\frac{z_1z_2^*}{1+|z_2|^2}+\frac{1-|z_2|^2}{1+|z_2|^2}\right).
\end{aligned}\tag{3.118}$$

Similarly, the third term is

$$\begin{aligned}
&iJ\left(\frac{z_1}{1+|z_1|^2}-\frac{z_1^*}{1+|z_1|^2}z_2^2-\frac{1-|z_1|^2}{1+|z_1|^2}z_2\right)\partial_{z_2}\\
=&iJ\partial_{z_2}\left(\frac{z_1}{1+|z_1|^2}-\frac{z_1^*}{1+|z_1|^2}z_2^2-\frac{1-|z_1|^2}{1+|z_1|^2}z_2\right)\\
&+iJ\left(2\frac{z_1^*z_2}{1+|z_1|^2}+\frac{1-|z_1|^2}{1+|z_2|^2}\right).
\end{aligned}\tag{3.119}$$

As a result, the drift term can be written as

$$\begin{aligned}
&\tilde{\mathcal{L}}_{drift}\\
=&i\partial_{z_1}\left[-\frac{\delta}{2}z_1+J\left(\frac{z_2}{1+|z_2|^2}-\frac{z_2^*}{1+|z_2|^2}z_1^2-\frac{1-|z_2|^2}{1+|z_2|^2}z_1\right)\right.\\
&\left.+i\partial_{z_2}\left[\frac{\delta_S}{2}z_2+J\left(\frac{z_1}{1+|z_1|^2}-\frac{z_1^*}{1+|z_1|^2}z_2^2-\frac{1-|z_1|^2}{1+|z_1|^2}z_2\right)\right]+c.c.\right.
\end{aligned}\tag{3.120}$$

Now we are in the position to change the variables to the canonical variables $(\cos\theta_1,\phi_1,\cos\theta_2,\phi_2)$. From the transformation rule in Eq. 3.100

$$z_i=\tan\frac{\theta_i}{2}e^{i\phi_i},$$

we can get the transformation rule for the derivatives

$$\partial_{z_i}=-\frac{1}{2}\left[\partial_{c_i}(1+c_i)\sqrt{1-c_i^2}+i\partial_{\phi_i}\sqrt{\frac{1+c_i}{1-c_i}}\right]e^{-i\phi_i}+\sqrt{1-c_i^2}e^{-i\phi_i}.\tag{3.121}$$

The above result has been found in [62], and we have followed their convention using c_i to denote $\cos\theta_i$. A detailed derivation of the above expression is given in Sect. 3.8. However, given the Jacobian arising from the transformation $(z_i,z_i^*)\to(c_i,\phi_i)$, we should use

$$\partial_{z_i}\to-\frac{1}{2}\left[\partial_{c_i}(1+c_i)\sqrt{1-c_i^2}+i\partial_{\phi_i}\sqrt{\frac{1+c_i}{1-c_i}}\right]e^{-i\phi_i}.\tag{3.122}$$

Then the drift term in the equation of motion for the Husimi function can be expressed in canonical variables as

$$\hat{\mathcal{L}}_{drift} = \partial_{c_1} d_{c_1} + \partial_{\phi_1} d_{\phi_1} + \partial_{c_2} d_{c_2} + \partial_{\phi_2} d_{\phi_2}, \tag{3.123}$$

with

$$\begin{aligned} d_{c_1} &= J \sin\theta_1 \sin\theta_2 \sin(\phi_2 - \phi_1), \\ d_{\phi_1} &= -\frac{\delta}{2} - J\left[\cos\theta_2 - \sin\theta_2 \cos(\phi_1 - \phi_2)\frac{\cos\theta_1}{\sin\theta_1}\right], \\ d_{c_2} &= J \sin\theta_1 \sin\theta_2 \sin(\phi_1 - \phi_2), \\ d_{\phi_2} &= \frac{\delta}{2} - J\left[\cos\theta_1 - \sin\theta_1 \cos(\phi_1 - \phi_2)\frac{\cos\theta_2}{\sin\theta_2}\right]. \end{aligned} \tag{3.124}$$

Then according to the standard theory of stochastic processes (see for example [63, 64]), for a drift term of the form

$$-\frac{\partial}{\partial x_i}\left[A_i(x)\right], \tag{3.125}$$

the corresponding evolution equations are

$$\frac{dx_i}{dt} = A_i(x). \tag{3.126}$$

It is clear that the evolution equations for the canonical variables $(\cos\theta_i, \phi_i)$ correspond to the classical dynamics:

$$\begin{aligned} \frac{d}{d\tilde{t}}\cos\theta_1 =& J \sin\theta_1 \sin\theta_2 \sin(\phi_1 - \phi_2), \\ \frac{d}{d\tilde{t}}\phi_1 =& \frac{\delta}{2} + J\left[\cos\theta_2 - \sin\theta_2 \cos(\phi_1 - \phi_2)\frac{\cos\theta_1}{\sin\theta_1}\right], \\ \frac{d}{d\tilde{t}}\cos\theta_1 =& J \sin\theta_1 \sin\theta_2 \sin(\phi_2 - \phi_1), \\ \frac{d}{d\tilde{t}}\phi_1 =& -\frac{\delta}{2} + J\left[\cos\theta_1 - \sin\theta_1 \cos(\phi_1 - \phi_2)\frac{\cos\theta_2}{\sin\theta_2}\right], \end{aligned} \tag{3.127}$$

the same as the classical dynamics of the two-spin model discussed in the previous chapter.

3.5.1 Remarks on the phase-space method

In summary, we have shown that the evolution of the Husimi function which determines uniquely the system can be described with a Fokker-Planck type

equation in the limit $S \to \infty$. In the semiclassical limit, the drift term reflects the underlying classical dynamics while the diffusion term is the quantum correction to this system. The Fokker-Planck equation has been extensively studied and we can find well developed method to solve this problem.

The advantage of the phase-space approach is that the obtained equation of evolution can be solved numerically to obtain the correct dynamics in the semiclassical limit, which is the future direction of this work. Besides, if we use exact diagonalization to simulate the system, the dimension of the Hilbert space is $(2S+1)^2$, increasing fast when considering the semiclassical limit $S \to \infty$. With the phase-space method, this is no longer a problem, because the phase space of the system is always $SU(2) \otimes SU(2)$.

The quantum aspects manifest themselves in three points. First, the rescaling factor is different from that of the classical dynamics. Thus the drift term is equivalent to the classical dynamics only in the limit $S \to \infty$ such that we can neglect the difference between $\sqrt{S(S+1)}$ and S. Second, there is a diffusion term in addition to the drift term, which is purely of quantum origin. Third, the initial state in the quantum dynamics is a Gaussian wave packet in the phase space. In the classical dynamics, the initial state is a Dirac point.

3.6 Summary

In this chapter, we have studied the quantum model which has the same Hamiltonian and initial conditions as the classical problem we considered in the preceding chapter. Unlike the classical system, in the quantum system, there is no synchronization transition in the strict sense for finite spin size S. Besides, we have seen that the dynamics of the quantum system is characterized by a multi-scale behavior. The smallest time scales correspond to the classical time scales, and the other time scales are purely of quantum origin as they have an explicit dependence on the size of the spin. We then concentrated on the smallest quantum time scales and derived two effective models which describe correctly the fast oscillation time $\tilde{t}_o$, the envelope time $\tilde{t}_e$, and the $\tilde{t}_{ar}$ in the dephased and synchronized regimes respectively. However, near the critical point $J = \delta/2$, the dynamics is very complicated and eludes simple explanation.

In addition, we have used the cumulant expansion method, which is basically a semiclassical approach, to study the quantum corrections. The results obtained by the direct expansion diverge and we are forced to use an improved version combining information obtained from quantum simulations. The improved method works more or less well in the dephased regime, but deviates from the exact result quickly in the synchronized regime.

Another promising approach we considered is the phase-space method, originating from quantum optics. This work is not finished yet, but we can see clearly that it separates the classical movement and the quantum corrections in the evolution equation of the quasiprobability function, which determines the state vector. Since this is an approach in the phase space, the critical point, which is shown to be a separatrix in the classical dynamics, can also be included in this approach. The separatrix in other systems has been studied with the phase-space method already in [65, 66].

3.7 Appendix: Details of calculation for the effective models

In Sec. 3.3, the results are given without the details of calculation. Here, we write explicitly the omitted intermediate steps.

3.7.1 Dephased regime ($J \ll \delta/2$): $\{|m_1, m_2\rangle\}$ basis

In the dephased regime, the terms like $\langle\Psi(t)|S_1^x|\Psi(t)\rangle$ and $\langle\Psi(t)|S_2^x|\Psi(t)\rangle$ in Eq. 3.36 can be obtained as follows

$$\begin{aligned}
&\langle S_1^x\rangle(t)\\
=&\langle\Psi(t)|S_1^x|\Psi(t)\rangle\\
=&\left(\frac{1}{2}\right)^{4S}\sum_{m_1',m_2',m_1,m_2}\sqrt{\binom{2S}{S+m_1'}\binom{2S}{S+m_2'}\binom{2S}{S+m_1}\binom{2S}{S+m_2}}\\
&\times\exp\left[i\left(E_i'-E_i\right)t\right]\langle m_1',m_2'|S_1^x|m_1,m_2\rangle
\end{aligned}\tag{3.128}$$

The term $\langle m_1', m_2'|S_1^x|m_1, m_2\rangle$ can be written as

$$\begin{aligned}
&\langle m_1',m_2'|S_1^x|m_1,m_2\rangle\\
=&\frac{1}{2}\left(\langle m_1',m_2'|S_1^+|m_1,m_2\rangle+\langle m_1',m_2'|S_1^-|m_1,m_2\rangle\right)\\
=&\frac{1}{2}\delta_{m_2,m_2'}\Big(\sqrt{(S-m_1)(S+m_1+1)}\delta_{m_1',m_1+1}\\
&+\sqrt{(S+m_1)(S-m_1+1)}\delta_{m_1',m_1-1}\Big).
\end{aligned}\tag{3.129}$$

Substituting back into the expression for $\langle S_1^x \rangle(t)$, and summing over m_1' and m_2', we get

$$\begin{aligned}
&\langle S_1^x \rangle(t) \\
=&\left(\frac{1}{2}\right)^{4S+1} \sum_{m_1,m_2} \binom{2S}{S+m_2} \left(\sqrt{\binom{2S}{S+m_1+1}\binom{2S}{S+m_1}} \right. \\
&\times \sqrt{(S-m_1)(S+m_1+1)} \exp\left[i \left(\frac{\delta_S}{2} + J_S m_2 \right) t \right] \\
&+ \sqrt{\binom{2S}{S+m_1-1}\binom{2S}{S+m_1}} \sqrt{(S+m_1)(S-m_1+1)} \\
&\left. \times \exp\left[-i \left(\frac{\delta_S}{2} + J_S m_2 \right) t \right] \right).
\end{aligned} \tag{3.130}$$

For the sum over m_1, the first term in the bracket can be calculated as

$$\begin{aligned}
&\sum_{m_1} \sqrt{\binom{2S}{S+m_1+1}\binom{2S}{S+m_1}} \sqrt{(S-m_1)(S+m_1+1)} \\
=&\sum_{m_1} \sqrt{\binom{2S}{S+m_1+1}\binom{2S}{S-m_1}} \sqrt{(S-m_1)(S+m_1+1)} \\
=&\sum_{m_1} 2S \sqrt{\binom{2S-1}{S+m_1}\binom{2S-1}{S-m_1-1}} \\
=&\sum_{m_1} 2S \binom{2S-1}{S+m_1} \\
=&2^{2S} S.
\end{aligned} \tag{3.131}$$

Similarly, the second term in the bracket yields

$$\begin{aligned}
&\sum_{m_1} \sqrt{\binom{2S}{S+m_1-1}\binom{2S}{S+m_1}} \sqrt{(S+m_1)(S-m_1+1)} \\
=&2^{2S} S.
\end{aligned} \tag{3.132}$$

And the sum over m_2 yields

$$\begin{aligned}
&\sum_{m_2} \binom{2S}{S+m_2} \exp\left(iJ_S t\right) \\
=&\sum_{m_2} \binom{2S}{S+m_2} \exp\left(i\frac{J_S t}{2}(S+m_2)\right) \exp\left(i\frac{J_S t}{2}(S-m_2)\right) \\
=&2^{2S}\left(\cos\left(\frac{J_S t}{2}\right)\right)^{2S}.
\end{aligned} \tag{3.133}$$

Then

$$\langle S_1^x\rangle(t) = S\cos\left(\frac{\delta_S t}{2}\right)\cos^{2S}\left(\frac{J_S t}{2}\right). \tag{3.134}$$

$\langle S_2^x\rangle(t)$ can be calculated the same way and the result is

$$\langle S_2^x\rangle(t) = S\cos\left(\frac{\delta_S t}{2}\right)\cos^{2S}\left(\frac{J_S t}{2}\right). \tag{3.135}$$

Therefore, we obtain

$$\langle S_t^x\rangle(t) = 2S\cos\left(\frac{\delta_S t}{2}\right)\cos^{2S}\left(\frac{J_S t}{2}\right). \tag{3.136}$$

The other components can be computed alike.

3.7.2 Synchronized regime ($J \gg \delta/2$): $\{|S_t, m_t\rangle\}$ basis

If we have an Hamiltonian with unperturbed eigenvectors grouped into different subspaces which are separated far away in energy, then we can treat the subspace as a single state. But the perturbation from other subspaces, instead of being just numbers, take the form of operators. For example, if the Hamiltonian has the generic form

$$H = H_0 + V, \tag{3.137}$$

where H_0 is the unperturbed Hamiltonian and V the perturbation. If the subspace S_1 is degenerate under the unperturbed Hamiltonian and is far separated from its complement space S_2, then we can write the complete Hamiltonian in the eigenvectors of H_0 as

$$H = \begin{pmatrix} H_1 & V \\ V & H_2 \end{pmatrix}, \tag{3.138}$$

where we have assumed that the perturbation V has no diagonal part. This blockwise form of the Hamiltonian is quite convenient. If we define the projection operators P_1 and P_2, onto the subspaces S_1 and S_2 respectively, then the effective Hamiltonian [45] for the eigenenergy E in the subspace S_1 is

$$H_1 = P_1 H_0 P_1 + P_1 V \frac{1}{E - H_0} V P_1. \tag{3.139}$$

Note that this Hamiltonian is not a real Hamiltonian in that it depends itself on the energy E. To lowest order, the above Hamiltonian can be approximated as

$$H_1 \approx P_1 H_0 P_1 + P_1 V \frac{1}{E_0^{S_1} - E_0^{S_2}} V P_1, \tag{3.140}$$

where E_0 is the eigenenergy of the unperturbed Hamiltonian. Here $E_0^{S_1} = J_S S^2$.

The previous paragraph outlines the general philosophy of the approximation scheme for a degenerate perturbation problem. Returning to the two-spin model in the synchronized regime, the unperturbed Hamiltonian is the exchange interaction term $H_0 = J_S \vec{S}_1 \cdot \vec{S}_2$, and the weak perturbation is the external magnetic field $V = (\delta_S/2)(S_1^z - S_2^z)$. The eigenvectors of the exchange interaction is $\{|S_t, m_t^z\rangle\}$. And the perturbation does not have diagonal term because

$$\begin{aligned} &\langle S_t', m_t'|V|S_t, m_t\rangle \\ =&\frac{\delta_S}{2}\delta_{m_t,m_t'} \sum_{m_1} m_1 \langle S_t', m_t|m_1, m_t - m_1\rangle\langle m_1, m_t - m_1|S_t, m_t\rangle \\ &\times \left(1 - (-1)^{4S - S_t - S_t'}\right). \end{aligned} \tag{3.141}$$

In the above expression, the terms $\langle m_1, m_t - m_1|S_t, m_t\rangle$ are Clebsch-Gordan coefficients. And we have used the property of Clebsch-Gordan coefficients that

$$\langle m_1, m_2|S_t, m_t\rangle = 0, \quad \text{unless } m_1 + m_2 = m_t. \tag{3.142}$$

And since S_t and S_t' are integers, $\langle S_t', m_t'|V|S_t, m_t\rangle = 0$ if $S_t = S_t' \pm 2n$ with $n = 0, 1, 2, \ldots$. So V has no diagonal term. And it only couples two Bloch spheres with $S_t - S_t' = 2n + 1$. Besides, the delta function in front also indicates that the the perturbation couples only two states with similar z-component of total spin.

Numerical computation of the matrix of the perturbation shows further that the perturbation couples only the nearest neighboring Bloch sphere of the total spin, i.e.

$$\langle S_t', m_t'|V|S_t, m_t\rangle = 0, \quad \text{unless } S_t' = S_t \pm 1. \tag{3.143}$$

The only $E_0^{S_2}$ we need to consider is $E_0^{S_2} = J_S S(S-2)$. Then to calculate the perturbation in the Bloch sphere $S_t = 2S$, we need to calculate the matrix elements like

$$\begin{aligned}&\langle S_t = 2S, m_t|(S_1^z - S_2^z)|S_t = 2S-1, m_t\rangle,\\ &\langle S_t = 2S-1, m_t|(S_1^z - S_2^z)|S_t = 2S, m_t\rangle.\end{aligned} \tag{3.144}$$

These can be done numerically, and the final form of the effective Hamiltonian takes the form

$$H_{syn} = H_0 + \delta V, \tag{3.145}$$

with

$$\delta V = \frac{\delta_S^2}{8S(4S-1)J_S}\left[(2S)^2\mathbb{1} - (S_t^z)^2\right]. \tag{3.146}$$

Then the contrast can be computed as in the dephased regime. However, the components of the individual spin are not easy to calculate because of the complicated form of the Clebsch-Gordan coefficients.

3.7.3 Improved method in the synchronized regime ($J \gg \delta/2$)

In this subsection, we give the details in Sect. 3.3.3. The state vector at $t = 0$ is

$$\begin{aligned}&|\Psi(0)\rangle\\ &= \left(\frac{1}{2}\right)^{2S}\sum_{m=-2S}^{2S}\sqrt{\binom{4S}{2S+m}}|2S, m\rangle\\ &= \left(\frac{1}{2}\right)^{2S}\sum_{m=-2S}^{2S}\sqrt{\binom{4S}{2S+m}}\left(s_m|e_m^+\rangle + c_m|e_m^-\rangle\right).\end{aligned} \tag{3.147}$$

Then at t, the state is

$$\begin{aligned}
&|\Psi(t)\rangle \\
=&(\frac{1}{2})^{2S}\sum_{m=-2S}^{2S}\sqrt{\binom{4S}{2S+m}}\left(s_m e^{-iE_m^+t}|e_m^+\rangle - c_m e^{-iE_m^-t}|e_m^-\rangle\right) \\
=&(\frac{1}{2})^{2S}\sum_{m=-2S}^{2S}\sqrt{\binom{4S}{2S+m}}\Big[\left(s_m^2 e^{-iE_m^+t}+c_m^2 e^{-iE_m^-t}\right)|2S,m\rangle \\
&+s_m c_m\left(e^{-iE_m^+t}-e^{-iE_m^-t}\right)|2S-1,m\rangle\Big].
\end{aligned} \tag{3.148}$$

Then $\langle S_t^x\rangle$ is

$$\begin{aligned}
&\langle S_t^x\rangle(t) \\
=&\left(\frac{1}{2}\right)^{4S}\sum_{m,m'=-2S}^{2S}\sqrt{\binom{4S}{2S+m}\binom{4S}{2S+m'}} \\
&\times\Big\{\left(s_m^2 e^{iE_m^+t}+c_m^2 e^{iE_m^-t}\right)\left(s_m'^2 e^{-iE_{m'}^+t}+c_m'^2 e^{-iE_{m'}^-t}\right) \\
&\times\langle 2S,m|S_t^x|2S,m'\rangle + s_m c_m s_m' c_m'\left(e^{iE_m^+t}-e^{iE_m^-t}\right) \\
&\times\left(e^{-iE_{m'}^+t}-e^{-iE_{m'}^-t}\right)\langle 2S-1,m|S_t^x|2S-1,m'\rangle\Big\}
\end{aligned} \tag{3.149}$$

The first sum in the curly bracket can be rewritten as

$$\begin{aligned}
&\sum_{m,m'}\sqrt{\binom{4S}{2S+m}\binom{4S}{2S+m'}}\left(s_m^2 e^{iE_m^+t}+c_m^2 e^{iE_m^-t}\right) \\
&\times\left(s_m'^2 e^{-iE_{m'}^+t}+c_m'^2 e^{-iE_{m'}^-t}\right)\langle 2S,m|S_t^x|2S,m'\rangle \\
=&2S\sum_m\binom{4S-1}{2S+m}\Big[\left(s_{m+1}^2 e^{iE_{(m+1)^+}t}+c_{m+1}^2 e^{iE_{(m+1)^-}t}\right) \\
&\times\left(s_m^2 e^{-iE_{m^+}t}+c_m^2 e^{-iE_{m^-}t}\right)+c.c\Big] \\
=&2S\sum_m\binom{4S-1}{2S+m}\Big[(s_m^2 s_{m+1}^2 e^{i(E_{m+1}^+-E_m^+)t}+c.c.) \\
&+(s_{m+1}^2 c_m^2 e^{i(E_{m+1}^+-E_m^-)t}+c.c.)+(s_m^2 c_{m+1}^2 e^{i(E_m^+-E_{m+1}^-)t}+c.c.)\Big]
\end{aligned} \tag{3.150}$$

Using Eq. 3.67, we get

$$\begin{aligned}
&\sum_m \binom{4S-1}{2S+m} (s_m^2 s_{m+1}^2 e^{i(E_{m+1}^+ - E_m^+)t} + c.c.) \\
\approx& 2^{4S} \cos^{4S-1}\left(\frac{\delta_S^2 t}{8S(4S-1)J_S}\right), \\
&\sum_m \binom{4S-1}{2S+m} (s_{m+1}^2 c_m^2 e^{i(E_{m+1}^+ - E_m^-)t} + c.c.) \\
\approx& (2S) 2\cos(2J_S S t) \frac{\delta_S^2}{16 J_S^2 S^2 (4S-1)} \sum_m \binom{4S-1}{2S+m} (4S^2 - m^2), \\
&\sum_m \binom{4S-1}{2S+m} (s_m^2 c_{m+1}^2 e^{i(E_m^+ - E_{m+1}^-)t} + c.c.) \\
\approx& (2S) 2\cos(2J_S S t) \frac{\delta_S^2}{16 J_S^2 S^2 (4S-1)} \sum_m \binom{4S-1}{2S+m} (4S^2 - (m+1)^2).
\end{aligned} \tag{3.151}$$

For the second sum, we have

$$\begin{aligned}
&\sum_{m,m'=-2S}^{2S} \sqrt{\binom{4S}{2S+m}\binom{4S}{2S+m'}} s_m c_m s'_m c'_m \left(e^{iE_m^+ t} - e^{iE_m^- t}\right) \\
&\times \left(e^{-iE_{m'}^+ t} - e^{-iE_{m'}^- t}\right) \langle 2S-1, m | S_t^x | 2S-1, m' \rangle \\
\approx& (2S) 4(1 - \cos(2J_S S t)) \frac{\delta_S^2}{16 J_S^2 S^2 (4S-1)} \\
&\times \sum_m \sqrt{\binom{4S}{2S+m}\binom{4S}{2S+m'}} \sqrt{(4S^2 - m^2)(4S^2 - (m-1)^2)}.
\end{aligned} \tag{3.152}$$

We can check numerically that

$$\begin{aligned}
&\sum_m \binom{4S-1}{2S+m} (4S^2 - m^2) + \sum_m \binom{4S-1}{2S+m} (4S^2 - (m+1)^2) \\
&- 2\sum_m \sqrt{\binom{4S}{2S+m}\binom{4S}{2S+m'}} \sqrt{(4S^2 - m^2)(4S^2 - (m-1)^2)} \\
\sim& 2^{4S-2}(4S-1).
\end{aligned} \tag{3.153}$$

And for the constant term in Eq. 3.152, we have

$$\begin{aligned}&\sum_m \sqrt{\binom{4S}{2S+m}\binom{4S}{2S+m'}}\sqrt{(4S^2-m^2)(4S^2-(m-1)^2)} \\ \sim& 2^{4S-1}S(4S-1).\end{aligned} \tag{3.154}$$

This term is too large by a factor S, so we neglect it. Then, we get

$$\begin{aligned}&\langle S_t^x\rangle(t) \\ \approx& 2S\cos^{4S-1}\left(\frac{\delta^2\sqrt{S(S+1)}\tilde{t}}{8S(4S-1)J}\right) \\ &-\frac{\delta^2(S+1)}{8J^2}\sin^2\left(\frac{2J\tilde{t}}{\sqrt{1+1/S}}\right).\end{aligned}$$

3.8 Appendix: Coherent states

In this section, we give some key elements in deriving the D algebra, and the change of variables to canonical variables. For simplicity, we consider the single spin case, but the results can be readily generalized to two-spin systems.

3.8.1 D algebra of coherent state

The D algebra for spin coherent states, or atomic coherent states, has been derived by Gilmore et al[49], and Zhang[67], where they used group theoretical approach and obtained the algebra in terms of the variables (θ, ϕ). But the pair of variables (θ, ϕ) are not canonical variables. To make the link between the phase-space approach and the classical dynamics, it is better to use the canonical variables $(\cos\theta, \phi)$ instead. This is the very approach adopted by Altland and Haake[61]. They first derived the D algebra for the complex number z parametrizing the Bloch sphere, and then changed to the canonical variables. We follow their approach and give some computational details. The coherent states $|z\rangle$ can be written explicitly as

$$|z\rangle = \sum_{m=-S}^{S}\sqrt{\binom{2S}{S+m}}\frac{z^{S-m}}{(1+|z|^2)^S}|S,m\rangle. \tag{3.155}$$

For the sake of simplicity, we will use the unnormalized coherent states in deriving the D algebra, which read

$$||z\rangle = \sum_{m=-S}^{S} \sqrt{\binom{2S}{S+m}} z^{S-m}|S,m\rangle = (1+|z|^2)^S|z\rangle. \tag{3.156}$$

Then we have for the spin operator S^+

$$\begin{aligned}
&S^+||z\rangle\langle z|| \\
=&\sum_{m_1,m_2} \sqrt{\binom{2S}{S+m_1}\binom{2S}{S+m_2}} S^+ z^{S-m_1}|m_1\rangle\langle m_2|(z^*)^{S-m_2} \\
=&\sum_{m_1,m_2} \sqrt{\binom{2S}{S+m_1}\binom{2S}{S+m_2}} \sqrt{(S-m_1)(S+m_1+1)} z^{S-m_1} \\
&\times |m_1+1\rangle\langle m_2|(z^*)^{S-m_2} \\
=&\sum_{m_1,m_2} \sqrt{\binom{2S}{S+m_1+1}\binom{2S}{S+m_2}} (S+m_1+1) z^{S-m_1} \\
&\times |m_1+1\rangle\langle m_2|(z^*)^{S-m_2} \\
=&\sum_{m_1,m_2} \sqrt{\binom{2S}{S+m_1}\binom{2S}{S+m_2}} z(S+m_1) z^{S-m_1}|m_1\rangle\langle m_2|(z^*)^{S-m_2}.
\end{aligned} \tag{3.157}$$

In the last line of the above expression, we have changed m_1+1 to m_1. And the factor $(S+m_1)$ can be obtained as

$$\begin{aligned}
&(S+m_1)z^{S-m_1} \\
=&[2S-(S-m_1)]z^{S-m_1} \\
=&(2S-z\partial_z)z^{S-m_1}.
\end{aligned} \tag{3.158}$$

As a result, we have the following algebra

$$S^+||z\rangle\langle z|| = (2Sz - z^2\partial_z)||z\rangle\langle z||. \tag{3.159}$$

Similarly, we can get the other two expressions

$$\begin{aligned}
S^-||z\rangle\langle z|| =&\partial_z||z\rangle\langle z||, \\
S^z||z\rangle\langle z|| =&(S-z\partial_z)||z\rangle\langle z||.
\end{aligned} \tag{3.160}$$

It is simple to get the D algebra for the normalized coherent states. For example, for S^+ operator, we have

$$\begin{aligned}
&S^+|z\rangle\langle z| \\
=&S^+\left(\frac{1}{(1+|z|^2)^{2S}}||z\rangle\langle z||\right) \\
=&(2Sz-z^2\partial_z)\left(\frac{1}{(1+|z|^2)^{2S}}||z\rangle\langle z||\right)-z^2\left(\partial_z\frac{1}{(1+|z|^2)^{2S}}||z\rangle\langle z||\right) \\
=&(2Sz-z^2\partial_z)|z\rangle\langle z|-\frac{2Sz^2z^*}{(1+|z|^2)}|z\rangle\langle z| \\
=&(-z^2\partial_z+2S\frac{z}{1+|z|^2}|z\rangle\langle z|.
\end{aligned} \tag{3.161}$$

And we obtain finally

$$\begin{aligned}
S^+|z\rangle\langle z| &= \left(-z^2\partial_z+2S\frac{z}{1+|z|^2}\right)|z\rangle\langle z|, \\
S^-|z\rangle\langle z| &= \left(\partial_z+2S\frac{z^*}{1+|z|^2}\right)|z\rangle\langle z|, \\
S^z|z\rangle\langle z| &= \left(-z\partial_z+S\frac{1-|z|^2}{1+|z|^2}\right)|z\rangle\langle z|.
\end{aligned}$$

3.8.2 The equation of motion for Husimi function

The equation of motion for the Husimi function is

$$d_tQ(z_1,z_2,t)=iTr\left(\hat{\rho}(t)H|z_1,z_2\rangle\langle z_1,z_2|-\hat{\rho}(t)|z_1,z_2\rangle\langle z_1,z_2|H\right). \tag{3.162}$$

We first calculate the term $Tr(\hat{\rho}(t)H|z_1,z_2\rangle\langle z_1,z_2|)$ as follows

$$\begin{aligned}
&Tr\left(\hat{\rho}(t)H|z_1,z_2\rangle\langle z_1,z_2|\right) \\
=&Tr\left(\hat{\rho}(t)\frac{\delta_S}{2}(S_1^z-S_2^z)|z_1,z_2\rangle\langle z_1,z_2|\right) \\
&+Tr\left(\hat{\rho}(t)\frac{J_S}{2}(S_1^+S_2^-+S_1^-S_2^+)|z_1,z_2\rangle\langle z_1,z_2|\right) \\
&+Tr\left(\hat{\rho}(t)J_SS_1^zS_2^z|z_1,z_2\rangle\langle z_1,z_2|\right).
\end{aligned} \tag{3.163}$$

The magnetic field can be written as

$$\begin{aligned}
&Tr\left(\hat{\rho}(t)\frac{\delta_S}{2}(S_1^z - S_2^z)|z_1,z_2\rangle\langle z_1,z_2|\right)\\
=&Tr\left(\hat{\rho}(t)\frac{\delta_S}{2}(-z_1\partial_{z_1} + S\frac{1-|z_1|^2}{1+|z_1|^2})|z_1,z_2\rangle\langle z_1,z_2|\right)\\
&- Tr\left(\hat{\rho}(t)\frac{\delta_S}{2}(-z_2\partial_{z_2} + S\frac{1-|z_2|^2}{1+|z_2|^2})|z_1,z_2\rangle\langle z_1,z_2|\right)\\
=&Tr\left(\hat{\rho}(t)\frac{\delta_S}{2}(-z_1\partial_{z_1} + z_2\partial_{z_2})|z_1,z_2\rangle\langle z_1,z_2|\right)\\
&+ Tr\left(\hat{\rho}(t)\frac{\delta_S S}{2}(\frac{1-|z_1|^2}{1+|z_1|^2} - \frac{1-|z_2|^2}{1+|z_2|^2})|z_1,z_2\rangle\langle z_1,z_2|\right)\\
=&-\frac{\delta_S}{2}\left(z_1\partial_{z_1} - z_2\partial_{z_2}\right)Q(z_1,z_2,t)\\
&+\frac{\delta_S S}{2}\left(\frac{1-|z_1|^2}{1+|z_1|^2} - \frac{1-|z_2|^2}{1+|z_2|^2}\right)Q(z_1,z_2,t).
\end{aligned} \tag{3.164}$$

The term originating from $S_1^+ S_2^-$ is

$$\begin{aligned}
&Tr\left(\hat{\rho}(t)\frac{J_S}{2}S_1^+ S_2^-|z_1,z_2\rangle\langle z_1,z_2|\right)\\
=&Tr\left(\hat{\rho}(t)\frac{J_S}{2}(-z_1^2 + 2S\frac{z_1}{1+|z_1|^2})(\partial_{z_2} + 2S\frac{z_2^*}{1+|z_2|^2})|z_1,z_2\rangle\langle z_1,z_2|\right)\\
=&Tr\left(\hat{\rho}(t)\frac{J_S}{2}(4S^2\frac{z_1 z_2^*}{1+|z_2|^2} - 2S\frac{z_1^2 z_2^*}{1+|z_2|^2}\partial_{z_1})|z_1,z_2\rangle\langle z_1,z_2|\right)\\
&+ Tr\left(\hat{\rho}(t)\frac{J_S}{2}(2S\frac{z_1}{1+|z_1|^2}\partial_{z_2} - z_1^2\partial^2_{z_1 z_2})|z_1,z_2\rangle\langle z_1,z_2|\right)\\
=&J_S S\left(-\frac{z_1^2 z_2^*}{1+|z_2|^2}\partial_{z_1} + \frac{z_1}{1+|z_1|^2}\partial_{z_2}\right)Q(z_1,z_2,t)\\
&-\frac{J_S}{2}z_1^2\partial^2_{z_1 z_2}Q(z_1,z_2,t) + 2J_S S\frac{z_1 z_2^*}{1+|z_2|^2}Q(z_1,z_2,t).
\end{aligned} \tag{3.165}$$

The term containing $S_1^- S_2^+$ is similarly

$$\begin{aligned}
&Tr\left(\hat{\rho}(t)\frac{J_S}{2}S_1^- S_2^+|z_1,z_2\rangle\langle z_1,z_2|\right)\\
=&J_S S\left(-\frac{z_2^2 z_1^*}{1+|z_1|^2}\partial_{z_2} + \frac{z_2}{1+|z_2|^2}\partial_{z_1}\right)Q(z_1,z_2,t)\\
&-\frac{J_S}{2}z_2^2\partial^2_{z_1 z_2}Q(z_1,z_2,t) + 2J_S S\frac{z_1^* z_2}{1+|z_1|^2}Q(z_1,z_2,t).
\end{aligned} \tag{3.166}$$

The $S_1^z S_2^z$ term is

$$\begin{aligned}
&Tr\left(\hat{\rho}(t) J_S S_1^z S_2^z |z_1, z_2\rangle\langle z_1, z_2|\right) \\
=&Tr\left(\hat{\rho}(t) J_S(-z_1\partial_{z_1} + S\frac{1-|z_1|^2}{1+|z_1|^2})\right. \\
&\left.\times\ (-z_2\partial_{z_2} + S\frac{1-|z_2|^2}{1+|z_2|^2})|z_1, z_2\rangle\langle z_1, z_2|\right) \\
=&-J_S S\left(\frac{1-|z_2|^2}{1+|z_2|^2} z_1\partial_{z_1} + \frac{1-|z_1|^2}{1+|z_1|^2} z_2\partial_{z_2}\right) Q(z_1, z_2, t) \\
&-J_S z_1 z_2 \partial^2_{z_1 z_2} Q(z_1, z_2, t) + J_S S^2 \frac{1-|z_1|^2}{1+|z_1|^2}\frac{1-|z_2|^2}{1+|z_2|^2} Q(z_1, z_2, t).
\end{aligned} \tag{3.167}$$

Summing over all the four terms, we get the equation of motion for the Husimi function

$$d_t Q(z_1, z_2, t) = \left(\mathcal{L}_{drift} + \mathcal{L}_{diff}\right) Q(z_1, z_2, t) \tag{3.168}$$

with the drift term and diffusion term as in Eq. 3.111 and Eq. 3.112.

3.8.3 Change of variables to canonical variables

As mentioned earlier, the conjugate variables (z, z^*) are not canonical variables. In order to change to the canonical variables $(\cos\theta, \phi)$, we need to find the inverse transformation of the variable

$$\begin{aligned}
z =& \tan\frac{\theta}{2} e^{i\phi}, \\
z^* =& \tan\frac{\theta}{2} e^{-i\phi}.
\end{aligned} \tag{3.169}$$

First, we can calculate the Jacobian between these two variables

$$\begin{aligned}
&\left|\frac{\partial(z, z^*)}{\partial(\cos\theta, \phi)}\right| \\
=&\begin{vmatrix} -\frac{e^{i\phi}}{(1+\cos\theta)\sin\theta} & i\frac{\sin\theta e^{i\phi}}{1+\cos\theta} \\ -\frac{e^{-i\phi}}{(1+\cos\theta)\sin\theta} & -i\frac{\sin\theta e^{-i\phi}}{1+\cos\theta} \end{vmatrix} \\
=&\frac{2}{(1+\cos\theta)^2}.
\end{aligned} \tag{3.170}$$

After some algebra, the inverse transformation can be found to be

$$\begin{aligned}
\cos\theta =& \frac{1-zz^*}{1+zz^*}, \\
\phi =& \arccos\left(\frac{z+z^*}{2\sqrt{zz^*}}\right).
\end{aligned} \tag{3.171}$$

The derivatives are

$$\begin{aligned}\frac{\partial \cos\theta}{\partial z} &= -\frac{1}{2}\sin\theta(1+\cos\theta)e^{-i\phi},\\ \frac{\partial\phi}{\partial z} &= -\frac{i}{2}\frac{\cos\theta}{\sin\theta}e^{-i\phi.}\end{aligned} \tag{3.172}$$

Then using the chain rule, we get

$$\begin{aligned}&\partial_z\\ =&\frac{\partial\cos\theta}{\partial z}\frac{\partial}{\partial\cos\theta}+\frac{\partial\phi}{\partial z}\frac{\partial}{\partial\phi}\\ =&-\frac{1}{2}\left[\partial_{\cos\theta}(1+\cos\theta)\sin\theta+i\partial_\phi\frac{\cos\theta}{\sin\theta}\right]+\sin\theta e^{-i\phi}\\ =&-\frac{1}{2}\left[\partial_{\cos\theta}(1+\cos\theta)\sqrt{1-\cos^2\theta}+i\partial_\phi\sqrt{\frac{1+\cos\theta}{1-\cos\theta}}\right]e^{-i\phi}\\ &+\sqrt{1-\cos^2\theta}e^{-i\phi}.\end{aligned} \tag{3.173}$$

The last term is a constant term, and may indicate dissipation effects of quantum jumps. However, this is artificial because if we take into account the Jacobian factor which is indispensable to keep the quasiprobability function a well-behaved one, this term would cancel out. And the final form of the derivative is

$$\partial_z \to -\frac{1}{2}\left[\partial_{\cos\theta}(1+\cos\theta)\sqrt{1-\cos^2\theta}+i\partial_\phi\sqrt{\frac{1+\cos\theta}{1-\cos\theta}}\right]e^{-i\phi}. \tag{3.174}$$

This result has been obtained by Altland and Haake[62].

Chapter 4

Squeezing and quantum entanglement in the two spin model

In the previous chapter, we have studied the quantity $\langle \vec{S}_t \rangle$ which is the quantum mechanical equivalent to the classical spin vector. In this chapter, we study the quantum operators of higher order and the phenomena of spin squeezing.

4.1 Introduction to spin squeezing

The squeezing phenomena describe the redistribution of quantum fluctuations. At first the squeezing phenomena were studied in bosonic systems in the context of quantum optics(see e.g. [68], and see [69] for a review). And then the concept of squeezing was generalized to spin systems[70, 71, 72]. For a general treatment of spin squeezing, see [73] for a review. Below, we first briefly review spin squeezing.

Let us consider a spin coherent state pointing in the z-direction, which is a state with minimum uncertainty. For the operator S^z, we have

$$\langle S^z \rangle = S, \quad \langle (\Delta S^z)^2 \rangle = 0, \tag{4.1}$$

where we have defined

$$\Delta S^z \equiv S^z - \langle S^z \rangle. \tag{4.2}$$

For the operators S^x and S^y, we have

$$\langle (\Delta S^x)^2 \rangle \langle (\Delta S^y)^2 \rangle = \frac{|\langle S^z \rangle|^2}{4} = \frac{S^2}{4}, \tag{4.3}$$

where we have defined similarly

$$\Delta S^x \equiv S^x - \langle S^x \rangle, \Delta S^y \equiv S^y - \langle S^y \rangle. \tag{4.4}$$

Furthermore, we have

$$\langle (\Delta S^x)^2 \rangle = \langle (\Delta S^y)^2 \rangle = \frac{S}{2}. \tag{4.5}$$

The quantity $S/2$ is called the standard quantum limit (SQD). The quantum fluctuations are distributed isotropically in the transverse plane of the mean spin direction for the coherent state. If the quantum fluctuations are redistributed and become anisotropic, it is possible that in one direction, for example the x-direction, the fluctuation is less than $S/2$ as long as

$$\langle (\Delta S^x)^2 \rangle \langle (\Delta S^y)^2 \rangle \geq \frac{S^2}{4}. \tag{4.6}$$

In this case, we have

$$\langle (\Delta S^x)^2 \rangle < \frac{\langle S^z \rangle}{2} = \frac{S}{2} < \langle (\Delta S^y)^2 \rangle. \tag{4.7}$$

The quantum fluctuation in the x-direction is smaller the the SQD. We say that the system is spin squeezed in the x-direction. In the following, we give two more rigorous definitions of spin squeezing.

4.1.1 Spin squeezing parameter of Kitagawa and Ueda

The spin squeezing parameter of Kitagawa and Ueda[71] is

$$\xi_S^2 = \frac{\min(\langle (\Delta S_{n_\perp})^2 \rangle)}{S/2}, \tag{4.8}$$

where $S_{n_\perp}$ denotes the spin operator perpendicular to the mean spin direction. If $\xi_S^2 < 1$, the spin is squeezed according to Kitagawa and Ueda. According to this criteria, the spin squeezing means that in the transverse plane of the mean spin direction, there exists a direction in which the quantum fluctuation is smaller than the SQD of a coherent state.

To calculate this spin squeezing parameter (see [73]), we first need to determine the mean spin direction by computing the quantum average of the spin vector operator. This gives us the mean spin direction $\vec{n}_0$. Then we can define two orthogonal spin operators in the transverse plane of the mean spin direction $\vec{n}_1$ and $\vec{n}_2$. Then the spin squeezing parameter is

$$\xi_S^2 = \frac{1}{2S}\left[\langle S_{\vec{n}_1}^2 + S_{\vec{n}_2}^2 \rangle - \sqrt{\left(\langle S_{\vec{n}_1}^2 - S_{\vec{n}_2}^2 \rangle\right)^2 + 4\mathrm{Cov}(S_{\vec{n}_1}, S_{\vec{n}_2})^2}\right], \tag{4.9}$$

where we have defined the covariance of spin operators $S_{\vec{n}_1}$ and $S_{\vec{n}_2}$

$$\begin{aligned} &\mathrm{Cov}(S_{\vec{n}_1}, S_{\vec{n}_2}) \\ =&\frac{1}{2}\left\langle [S_{\vec{n}_1}, S_{\vec{n}_2}]_+ \right\rangle - \langle S_{\vec{n}_1}\rangle\langle S_{\vec{n}_2}\rangle \\ =&\frac{1}{2}\left\langle [S_{\vec{n}_1}, S_{\vec{n}_2}]_+ \right\rangle, \end{aligned} \tag{4.10}$$

since

$$\langle S_{\vec{n}_1}\rangle = \langle S_{\vec{n}_2}\rangle = 0. \tag{4.11}$$

4.1.2 Spin squeezing parameter of Wineland et al

Soon after the proposition of the spin squeezing by Kitagawa and Ueda, Wineland et al have proposed another definition of spin squeezing[72]. Their definition of spin squeezing is related to the precision in the Ramsey spectroscopy measurement. They consider a system of trapped atoms with two internal degrees of freedom. These atoms can be treated as an ensemble of N spins $1/2$ and thus a macro-spin of spin size $S = N/2$. When performing Ramsey spectroscopy experiments, the precision is of primary interest. However, there is an intrinsic precision, which is that of the initial coherent state given by

$$\Delta\phi_{DS} = \frac{1}{N^{1/2}} = \frac{1}{\sqrt{2S}}, \tag{4.12}$$

where the subscript DS indicates the Dicke state of the constituting spin $1/2$ particles. In the experiment, if we can achieve in one direction a better precision

$$\Delta\phi = \frac{\sqrt{\min(\langle(\Delta S_{n_\perp})^2\rangle)}}{|\langle\vec{S}\rangle|} < \Delta\phi_{DS}, \tag{4.13}$$

then we say that we have spin squeezing. The spin squeezing parameter is given by

$$\xi_R^2 = \left|\frac{\Delta\phi}{\Delta\phi_{DS}}\right|^2 = \frac{2S\min(\langle(\Delta S_{n_\perp})^2\rangle)}{|\langle\vec{S}\rangle|^2}. \tag{4.14}$$

From the above definition, we can rewrite the spin squeezing parameter of Wineland et al. as the follows

$$\xi_R^2 = \left(\frac{S}{|\langle\vec{S}\rangle|}\right)^2 \frac{\min(\langle(\Delta S_{n_\perp})^2\rangle)}{S/2} = \left(\frac{1}{\mathrm{C}}\right)^2 \xi_S^2, \tag{4.15}$$

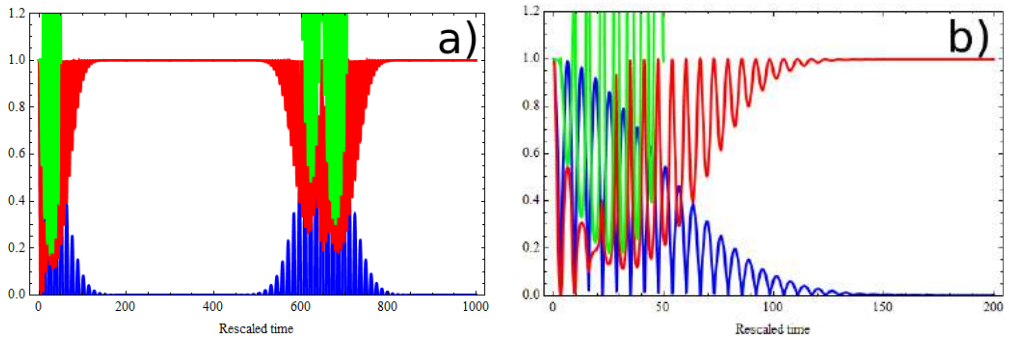

Figure 4.1: Numerical results of spin squeezing and contrast as a function of rescaled time (in units of $1/\delta$) for $S = 10$ and $J = 0.1\delta$. The unit of rescaled time is $1/\delta$. The blue line is the contrast, the red line the spin squeezing parameter ξ_S^2, and the green line ξ_R^2. a) shows the long time behavior till the approximate recurrence time $\tilde{t}_{ar}$ and b) the short time behavior till the envelope time $\tilde{t}_e$.

where C is the contrast. If $\xi_R^2 < 1$, the spin is squeezed. The physical interpretation of this squeezing is that the measured noise of the spectroscopy is less than that of the independent atoms. The correlation or entanglement between the atoms has increased the precision of measurement.

Since $S \geq |\langle \vec{S} \rangle|$, we have $\xi_R^2 \geq \xi_S^2$. Therefore the definition by Wineland et al. is a more stringent condition on the spin squeezing. In the following, we study mainly the spin squeezing parameter by Kitagawa and Ueda, though the definition by Wineland et al. is more suitable to the atomic clock. Knowing ξ_S^2 and C, it is straight-froward to obtain ξ_R^2.

4.2 Numerical computation of squeezing parameters in the two-spin model

In this section, we compute the spin squeezing parameters by numerical simulations.

First, for the dephased regime ($J = 0.1\delta$, see Fig. 4.1), we can see from the numerical results that the spin squeezing has also multi-scale dynamics, with characteristic times scales identical to those of the contrast. Initially the spin squeezing parameter ξ_S^2 decreases and so does the contrast, and at one half of the fast oscillation time ($\tilde{t} = \tilde{t}_o/2$), the spin squeezing reaches its minimum. At longer times, the contrast is modulated by an envelope till the envelope time where it remains very small for a long time. The spin squeezing, on

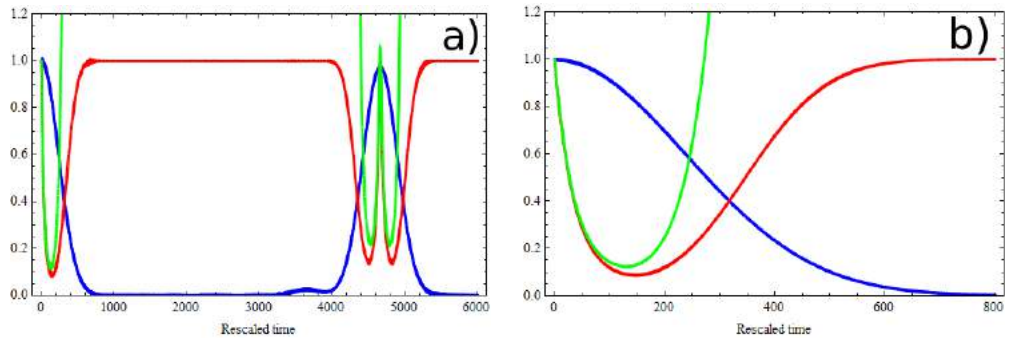

Figure 4.2: Numerical results of spin squeezing and contrast as a function of rescaled time (in units of $1/\delta$) for $S = 10$ and $J = 5\delta$. The unit of rescaled time is $1/\delta$. The blue line is the contrast, the red line the spin squeezing parameter ξ_S^2, and the green line ξ_R^2. a) shows the long time behavior till the approximate recurrence time $\tilde{t}_{ar}$ and b) the short time behavior till the envelope time $\tilde{t}_e$.

the other hand, begins increasing and goes to almost unity at the envelope time. And near the approximate recurrence time, the above process is first reversed ($\tilde{t} \sim \tilde{t}_{ar} - \tilde{t}_e$), and then happens again. ξ_R^2 changes more abruptly and diverges because of the zeros of the contrast.

For the synchronized regime ($J = 5\delta$, see Fig. 4.2), a similar behavior of the spin squeezing parameters is observed. Initially, there is a decrease of the spin squeezing parameter, indicating that the two spins are squeezed. But then ξ_S^2 increases to unity. ξ_R^2 is similar to ξ_S^2, but increases earlier and then diverges because the contrast goes towards zero. There is a time window during which $\xi_R^2 < 1$, and the experimental precision is better than that for independent atoms. Near the approximate recurrence time, the above process occurs in the reversed sense and then in the normal sense.

4.3 Effective models for the spin squeezing parameter

In the preceding section, we have computed the spin squeezing parameter by simulating exactly the temporal evolution of the two-spin system. Now we want to gain a more quantitative understanding of the system. The method to be used is the effective model developed in the previous chapter.

4.3.1 Weak interaction regime $J \ll \delta$

In the weak interaction regime, the effective Hamiltonian is

$$H_{eff} = \frac{\delta_S}{2}(S_1^z - S_2^z) + J_S S_1^z S_2^z,$$

with the eigenenergies and eigenvectors

$$E_i = \frac{\delta_S}{2}(m_1 - m_2) + J_S m_1 m_2, \quad |e_i\rangle = |m_1, m_2\rangle,$$

where $\{m_1, m_2\}$ are Fock states labeled by the z-axis quantum number of two spins. At time t, the state vector is

$$|\Psi(t)\rangle = \left(\frac{1}{2}\right)^{2S} \sum_{m_1,m_2=-S}^{S} \sqrt{\binom{2S}{S+m_1}\binom{2S}{S+m_2}} e^{-iE_i t}|m_1, m_2\rangle.$$

To get the spin squeezing parameter, we still need to compute the variance of the quantum operators such as $\langle (S_t^y)^2\rangle$, $\langle (S_t^z)^2\rangle$, $\langle S_t^y S_t^z\rangle$, and $\langle S_t^z S_t^y\rangle$ (see Eq. 4.9). The detailed calculation is given in appendix. Here we just list the results

$$\begin{aligned}
\langle (S_t^y)^2\rangle =& S^2[\cos(J_S t/2)]^{4S-2}[\cos(\delta_S t) - 1] + \frac{S}{2}(2S+1) \\
& - \frac{S}{2}(2S-1)\cos(\delta_S t)[\cos(J_S t)]^{2S}, \\
\langle (S_t^z)^2\rangle =& S, \\
\langle S_t^y S_t^z\rangle =& 2S^2 \cos(\delta_S t/2)\sin(J_S t/2)[\cos(J_S t/2)]^{2S-1} \\
& + iS\cos(\delta_S t/2)[\cos(J_S t/2)]^{2S}, \\
\langle S_t^z S_t^y\rangle =& 2S^2 \cos(\delta_S t/2)\sin(J_S t/2)[\cos(J_S t/2)]^{2S-1} \\
& - iS\cos(\delta_S t/2)[\cos(J_S t/2)]^{2S}.
\end{aligned} \tag{4.16}$$

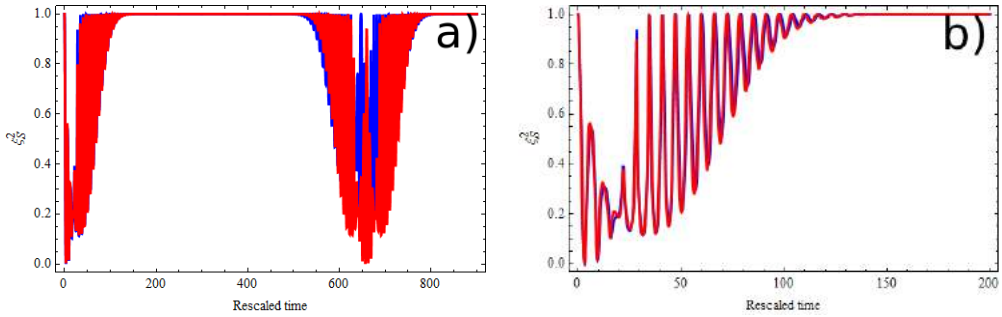

Figure 4.3: Comparison of numerical results of spin squeezing and those obtained from the effective model as a function of rescaled time (in units of $1/\delta$) for $S = 10$ and $J = 0.1\delta$. The unit of rescaled time is $1/\delta$. The blue line is the numerics and the red line the analytics from the effective model. a) shows the long time behavior till the approximate recurrence time $\tilde{t}_{ar}$ and b) the short time behavior till the envelope time $\tilde{t}_e$ discussed in the previous chapter.

Expressing them in rescaled quantities, we get

$$\begin{aligned}
\langle (S_t^y)^2 \rangle =& S^2[\cos(\frac{J\tilde{t}}{2\sqrt{S(S+1)}})]^{4S-2}[\cos(\delta\tilde{t})-1]+\frac{S}{2}(2S+1)\\
&-\frac{S}{2}(2S-1)\cos(\delta\tilde{t})[\cos(J\tilde{t}/\sqrt{S(S+1)})]^{2S},\\
\langle (S_t^z)^2 \rangle =& S,\\
\langle S_t^y S_t^z \rangle =& 2S^2\cos(\frac{\delta\tilde{t}}{2})\sin(\frac{J\tilde{t}}{2\sqrt{S(S+1)}})[\cos(\frac{J\tilde{t}}{2\sqrt{S(S+1)}})]^{2S-1}\\
&+iS\cos(\frac{\delta\tilde{t}}{2})[\cos(\frac{J\tilde{t}}{2})]^{2S},\\
\langle S_t^z S_t^y \rangle =& 2S^2\cos(\frac{\delta\tilde{t}}{2})\sin(\frac{J\tilde{t}}{2\sqrt{S(S+1)}})[\cos(\frac{J\tilde{t}}{2\sqrt{S(S+1)}})]^{2S-1}\\
&-iS\cos(\frac{\delta\tilde{t}}{2})[\cos(\frac{J\tilde{t}}{2})]^{2S},
\end{aligned} \tag{4.17}$$

From the comparison between the effective model and the numerics (see Fig. 4.3), we can see clearly that the effective model does not only describes correctly the contrast of the two-spin system, but also it gives very good agreement for the spin squeezing parameter. Since this regime is not particularly relevant to the experiments, we do not study ξ_R^2.

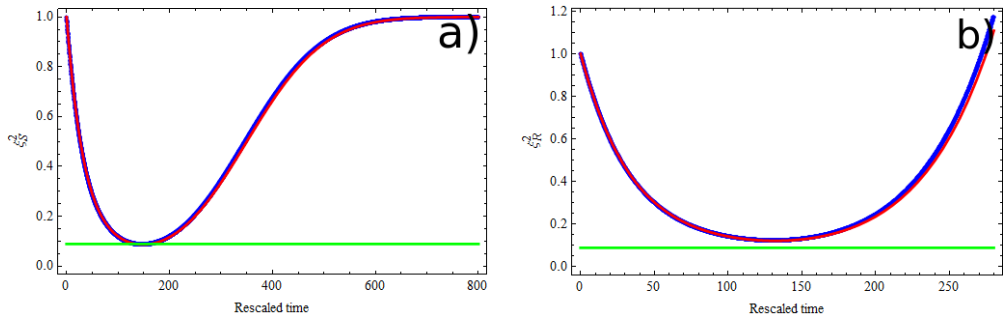

Figure 4.4: Comparison of numerical results of spin squeezing parameters as a function of time and those obtained from the effective model for $S = 10$ and $J = 5\delta$. The unit of rescaled time is $1/\delta$. The blue line is the numerics, the red line the result obtained from the effective model, and the green line is the lower bound in Eq. 4.21. a) The comparison for ξ_S^2. b) The comparison for ξ_R^2.

4.3.2 Strong interaction regime $J \gg \delta$

In this regime, we restrain ourselves to the largest Bloch sphere of the total spin. In this subspace, the effective Hamiltonian is (see Eq. 3.55)

$$H = -\chi (S_t^z)^2,$$

with the constant

$$\chi = \frac{\delta_S^2}{8S(4S-1)J_S}.$$

Then we can get

$$\begin{aligned}
\langle (S_t^y)^2 \rangle =& \frac{S}{2}\left[(4S+1) - (4S-1)\left(\cos\left(2\chi t\right)\right)^{4S-2}\right], \\
\langle (S_t^z)^2 \rangle =& S, \\
\langle S_t^y S_t^z \rangle =& \frac{1}{i}\left(-4S^2 e^{i\chi t} - S e^{-i\chi t}\right)\left(\cos\left(2\chi t\right)\right)^{4S-2}, \\
\langle S_t^z S_t^y \rangle =& \frac{1}{i}\left(4S^2 e^{-i\chi t} + S e^{i\chi t}\right)\left(\cos\left(2\chi t\right)\right)^{4S-2}.
\end{aligned} \tag{4.18}$$

We concentrate on the behavior of the spin squeezing before the envelope time, because this is experimentally relevant. First thing to note is that the agreement between the effective model and the numerics is very good. Second, this effective model in the strong interaction regime is equivalent to the

one-axis twisting scheme in [71], with a spin size $S_t = 2S$. Then our results can be obtained directly from theirs. The spin squeezing parameter ξ_S^2 reads

$$\xi_{S,min}^2 \approx \left(\frac{1}{(S_t\mu)^2} + \frac{1}{24}(S_t\mu^2)^2 \right), \tag{4.19}$$

with $\mu \equiv 2\chi t$. Then at

$$\mu_0 = \left(\frac{3}{4S^2 4} \right)^{1/6}, \tag{4.20}$$

the spin squeezing parameter reaches its minimum

$$\xi_{S,min}^2 = \frac{3}{4} \left(\frac{1}{6S^2} \right)^{1/3}. \tag{4.21}$$

The above result about μ_0 is different from that in [71], but agrees with that in [74]. And $\xi_{S,min}^2$ is also different from that in [71]. This difference is due to a minor computational error in [71]. For $S = 10$ system, this gives $\xi_{S,min}^2 \approx (3/4)(1/600)^{1/3}$. We can see that it agrees well with the numerics. In fact, for $S = 10$ and $J = 5$, we have

$$\begin{aligned} &t_{min} \approx 153/\delta, \\ &\xi_{S,min}^2 \approx 0.089. \end{aligned} \tag{4.22}$$

For ξ_R^2, the agreement is also very good. It scales similarly as

$$\xi_R^2 \propto S^{-3/2}. \tag{4.23}$$

It is thus advantageous to have larger spin size S to get a better experimental precision.

4.3.3 Husimi function of the effective model

In this subsection, we use the Husimi function to depict qualitatively the spin squeezing. We concentrate mainly on the strong interaction regime ($J \gg \delta/2$) since this is relevant for the experiments. We use the same effective model and consider the same subspace $S_t = 2S$ as used in the previous subsection. For $S = 10$, and $J = 5\delta$, the Husimi function $Q(\theta, \phi, \tilde{t}) = |\langle\theta, \phi|\psi(\tilde{t})\rangle|^2$ is presented on the Bloch spheres (see Fig. 4.5). The state $|\theta, \phi\rangle$ is the coherent state pointing in the direction $(\sin\theta\cos\phi, \sin\theta\sin\phi, \cos\theta)^T$ on the Bloch sphere $S_t = 2S$. This function is related to ξ_S^2 because the radius of the Bloch sphere is invariant, the same as the denominator in definition

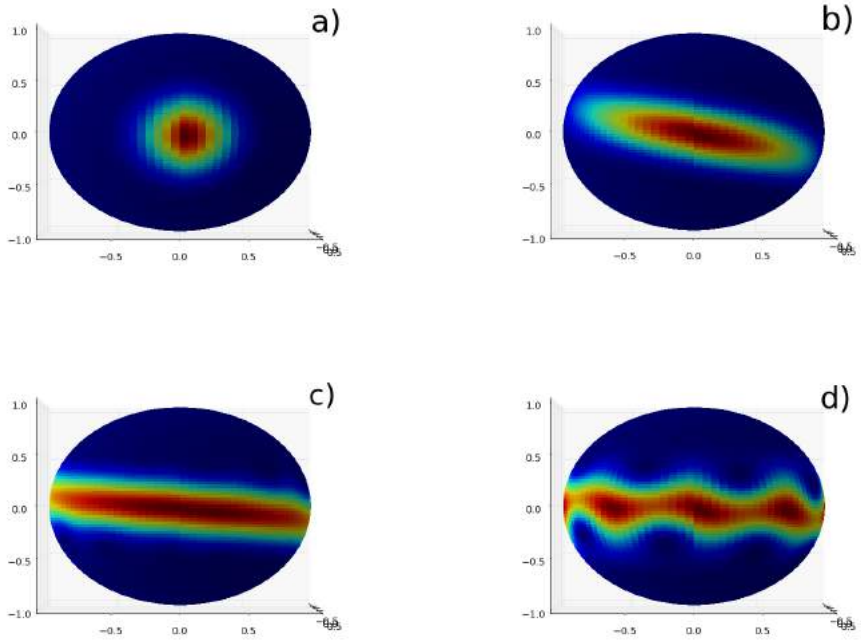

Figure 4.5: The Husimi function $Q(\theta, \phi, \tilde{t})$ represented on the Bloch sphere $S_t = 2S = 20$ for different times $\tilde{t}$ (in units of $1/\delta$) for $J = 5\delta$. The view point is the positive x-direction. In each plot, the Husimi function is rescaled by its maximum value $Q_{max}(\tilde{t})$. The color scale indicates the value of Q. The red is higher value and blue lower value. a) Initial state, $\tilde{t} = 0$, $Q_{max}(0) = 1$. b) Optimally squeezed state, $\tilde{t} = 153$, $Q_{max}(153) \approx 0.43$. c) Excessively twisted state, $\tilde{t} = 400$, $Q_{max}(400) \approx 0.18$. d) State at the envelope time, $\tilde{t} = 600$, $Q_{max}(600) \approx 0.14$.

ξ_S^2. So we speak of the optimally squeezed state and the excessively twisted state with respect to ξ_S^2.

From Fig. 4.5, it is clear that the state is first squeezed because of the nonlinear Hamiltonian, which deforms the Husimi function on the Bloch sphere, until it reaches the optimally squeezed state at $\tilde{t} \approx 153/\delta$. At this time, we obtain a minimum ξ_S^2. Then the Husimi function is further deformed but the spin squeezing parameter increases because of the excessive twisting. At about the envelope, the Husimi function spreads along the equator and some islands of high probability are about to form. Thus the spin squeezing is related to the spread of the wave packet in the phase space. (In this case, the reduced phase space is the single Bloch sphere $S_t = 20$.)

4.4 Summary and discussion

In this chapter, we have studied the spin squeezing phenomena in the two-spin system. We have seen that the spin squeezing is also multi-scaled and the characteristic time scales are identical to those of the contrast. Shortly after $t = 0$, the system is squeezed. But after a certain decrease in the spin squeezing parameter, the diffusion of the wave packet of the two-spin system dominates and the spin squeezing is less obvious. At the envelope time, the wave packet of the system is so diffused that the spins are not squeezed at all. The effective models developed in the previous chapter are also competent in describing the spin squeezing parameter till the approximate recurrence time, and thus provide us a more quantitative picture of the spin squeezing phenomena.

To conclude, we note that spin squeezing is related to other types of squeezing such as number squeezing in the bosonic Josephson junction [75], and other quantum effects such as correlation and entanglement [71, 76, 77, 78]. In addition, it can be used to detect the quantum phase transition and quantum chaos [79, 74]. These are promising domains and it would be interesting to apply these ideas to the two-spin model, which constitutes directions of future work.

4.5 Appendix: Details of calculation in effective models

In this section, we give the details omitted in the Sect. 4.3.

4.5.1 Weak interaction regime ($J \ll \delta/2$)

In this regime, the quantum expectation values of second order operators can be calculated as follows. For $(S_t^y)^2$, we have

$$\langle (S_t^y)^2 \rangle = -\frac{1}{4} \langle S_t^+ S_t^+ - S_t^+ S_t^- - S_t^- S_t^+ + S_t^- S_t^- \rangle. \tag{4.24}$$

Computation of the four terms on the right hand side of the equality yields

$$\begin{aligned}
\langle S_t^+ S_t^+ \rangle =& S(2S-1)\cos(\delta_S t)(\cos(J_S t))^{2S} + 2S^2\left(\cos(\frac{J_S t}{2})\right)^{4S-2}, \\
\langle S_t^+ S_t^- \rangle =& S(2S+1) + 2S^2\cos(\delta_S t)\left(\cos(\frac{J_S t}{2})\right)^{4S-2}, \\
\langle S_t^- S_t^+ \rangle =& S(2S+1) + 2S^2\cos(\delta_S t)\left(\cos(\frac{J_S t}{2})\right)^{4S-2}, \\
\langle S_t^- S_t^- \rangle =& S(2S-1)\cos(\delta_S t)(\cos(J_S t))^{2S} + 2S^2\left(\cos(\frac{J_S t}{2})\right)^{4S-2}.
\end{aligned} \tag{4.25}$$

Summing the above expressions, we get

$$\begin{aligned}
\langle (S_t^y)^2 \rangle =& S^2[\cos(J_S t/2)]^{4S-2}[\cos(\delta_S t) - 1] + \frac{S}{2}(2S+1) \\
& - \frac{S}{2}(2S-1)\cos(\delta_S t)[\cos(J_S t)]^{2S}.
\end{aligned} \tag{4.26}$$

$(S_t^z)^2$ is conserved and we have

$$\langle (S_t^z)^2 \rangle = S. \tag{4.27}$$

For $\langle S_t^y S_t^z \rangle$, we have

$$\langle S_t^y S_t^z \rangle = \frac{1}{2i}\langle S_t^+ S_t^z - S_t^- S_t^z \rangle. \tag{4.28}$$

For the above two terms, we have

$$\begin{aligned}
\langle S_t^+ S_t^z \rangle =& -S\cos(\delta_S t/2)[\cos(J_S t/2)]^{2S} \\
& + i2S^2\cos(\delta_S t/2)\sin(J_S t/2)[\cos(J_S t/2)]^{2S-1}, \\
\langle S_t^- S_t^z \rangle =& S\cos(\delta_S t/2)[\cos(J_S t/2)]^{2S} \\
& - 2iS^2\cos(\delta_S t/2)\sin(J_S t/2)[\cos(J_S t/2)]^{2S-1}.
\end{aligned} \tag{4.29}$$

Summing the two terms yields

$$\begin{aligned}
\langle S_t^y S_t^z \rangle =& 2S^2\cos(\delta_S t/2)\sin(J_S t/2)[\cos(J_S t/2)]^{2S-1} \\
& + iS\cos(\delta_S t/2)[\cos(J_S t/2)]^{2S}.
\end{aligned} \tag{4.30}$$

Taking the complex conjugate of the above expression, we get

$$\begin{aligned}
\langle S_t^y S_t^z \rangle =& 2S^2\cos(\delta_S t/2)\sin(J_S t/2)[\cos(J_S t/2)]^{2S-1} \\
& - iS\cos(\delta_S t/2)[\cos(J_S t/2)]^{2S}.
\end{aligned} \tag{4.31}$$

4.5.2 Strong interaction regime ($J \gg \delta/2$)

In this regime, the calculation is straight forward, and we do not list them.

Chapter 5

Conclusion and outlook

Now we are able to answer the questions asked in the introduction. Is there a synchronization transition? What is the difference between the classical and quantum dynamics? And what is the effect of spin size S on the synchronization?

There is a synchronization transition in the classical dynamics of the two-spin model when the interaction strength is superior to a critical value $J_{cri} = \delta/2$. This transition is due to a bifurcation in the reduced phase space of a single spin. The synchronization does not occur simultaneously with the bifurcation because of our choice of initial state. If we choose another initial state such as $\vec{n}_1 = (\sin\alpha, 0, \cos\alpha)^T$ and $\vec{n}_2 = (\sin\alpha, 0, -\cos\alpha)^T$ with $\alpha \approx 0$, the synchronization will happen immediately after the bifurcation at $J_{bif} = \delta/4$. Thus, by changing the initial state, we can have a synchronization transition with a weaker interaction. However, this may lead to a smaller signal. For example, for the initial state mentioned above, the maximum total spin is $2\sin\alpha$. So we need to find an optimal initial condition that makes a compromise between the need for a weaker interaction and a strong signal, which are pursued in the atomic clock experiments.

The synchronization transition is not present in the quantum dynamics, where the contrast will be lost eventually at an envelope time t_e. The quantum dynamics is different from classical dynamics in several aspects. First, whereas the spin size S plays a trivial role in the classical dynamics that can be eliminated by a rescaling, it is nontrivial in the quantum dynamics because the spin size S determines the dimension of Hilbert space in the quantum system. Therefore, the quantum dynamics depends on the spin size. Second, the cumulant expansion method reveals that once we take into account the quantum correlation effects (cumulant of second order operators), even partially, the synchronization is destroyed. The quantum correlations are thus

responsible for the loss of synchronization.

The classical limit is attained in the following way. In the quantum dynamics of two spins, there are many quantum time scales in addition to the two time scales equivalent to classical ones. The smallest one of these quantum time scales is the envelope time ($\tilde{t}_e$), which increases with the spin size S as $\tilde{t}_e \propto \sqrt{S}$ if the inhomogeneity of the external field and the interaction strength are kept constant. Therefore, in the semiclassical limit, this time scale is pushed to infinity and so are all the other quantum time scales. In this way we can observe only the classical dynamics, and we obtain the classical limit.

In addition, we also studied the spin squeezing in the two-spin model. The spin squeezing in the two-spin model can be used to improve the experimental precision of the measurements and we have shown that the spin squeezing is present in the two-spin model. The spins are squeezed when the dynamics takes place initially, as the contrast diminishes. After this initial squeezing, the spin squeezing phenomenon in the two-spin model reaches a maximum before the contrast vanishes. Then the system is less squeezed because of the excessive twisting mentioned in [71]. At the envelope time, where the contrast becomes zero, the system is not squeezed. So there is a time interval in which we can get higher measurement precision and a not so weak signal, which is advantageous. For $S = 10$ and $J = 5\delta$ system, this time interval is approximately $\tilde{t} \approx 260/\delta$, with a contrast C ≈ 0.6. The best squeezing in this system is about $\xi_R^2 \approx 0.1$.

Concerning the experiments on atomic clocks[24], we can make the following remarks. A first remark is that a higher density of atoms in the experiments is constructive for the fabrication of atomic clocks in that a higher density leads to a stronger interaction (larger J) and a larger number of atoms (larger S). The envelope time is therefore increased. At the same time, increasing the density means that lateral collisions become more frequent. To estimate the coherence time in the experiment, we make the correspondence between the parameters of the experiments and those of the two-spin model as follows. In the experiment, there are $N \sim 10^4$ atoms, so the spin size $S = N/4 \sim 10^4$. In the first experiment in [24], the inhomogeneity of the magnetic field in the two-spin model can be approximated as $\delta \sim 10^4 rad/s$, and the interaction strength is approximately $J/\delta \sim 100$. Then the envelope time is $t_e \approx \tilde{t}_e S \sim 10^4 - 10^5 s$. In the second experiment in [24], we have $\delta \sim 10^5 rad/s$, $J/\delta \sim 1 - 10$. Then the envelope time is $t_e \sim 10 - 100 s$. This envelope time might be accessible experimentally.

However, it may be rudimentary to describe real experiments by the two-spin. In the weak interaction regime ($J \ll \delta$), the two spin model assumes that the atoms in each group are aligned together. But this is not the case since

the inhomogeneity is large compared to the interaction. Therefore, the two-spin model does not describe properly the dynamics in this regime. In the strong interaction regime ($J \gg \delta$), the two-spin model is good because the strong interaction aligns all atoms together. Splitting them into two aligned groups is well justified.

In the two-spin model, we have used the rotating reference frame with an angular velocity equal to the rotation of the mean magnetic field, and thus are unable to study the central frequency of the system, which is a key ingredient in atomic clock experiments. To obtain this frequency, we could either average over the inhomogeneity of the effective field for each atom in the original experiment to get an estimation, or consider the full dynamics of the atoms and calculate the central frequency.

There are still many open questions left in this thesis. The first one is how to understand the dynamics near the critical point $J = \delta/2$. This special regime could be studied with the phase-space method sketched in chapter 3 with Husimi function. Since this method does not depend on the interaction strength, it may be useful in revealing the complex dynamics in this region. Another possible approach is to use the semiclassical quantization, which has been employed to treat the BHD model in [80, 81].

The cumulant expansion method does show that quantum corrections destroy the synchronization, but it diverges if we make the direct expansion to second order spin operators. After improving the expansion by imposing certain observations from numerical simulations about second order cumulants, the solution is convergent but in the synchronized regime deviates quickly from the exact quantum dynamics. A possible reason is that in the synchronized regime, there is a separatrix which separates the phase space into two regions with different dynamical behaviors. The cumulant expansion that works well in one region may not be applicable in the other. This has been observed by Garanin and Schilling in[42] in a biaxial model which is chaotic for a finite time interval. A remedy to this is to develop an expansion that is state dependent (see [82]).

A related question on the two-spin model is: what is the effect of dissipation or coupling to the environment in this model? In the context of cold atoms, the dissipation describes the loss of atoms, an unavoidable effect in cold atom experiments. In [83], it is shown that the dissipation can change the structure of the phase space by altering the position of the fixed points or changing the nature of the fixed points. Another article by Orth et al.[84] showed that the coupling to an harmonic bath can actually lead to synchronization in the dynamics of two Ising spins. It is thus interesting to see the effect of dissipation in the two-spin model.

Another direction is to consider a one-dimensional chain of N spins $1/2$

in an inhomogeneous external field instead of two macro-spins with spin size $S = N/4$. This approach is equivalent to considering the cold atoms in the energy space where the mean magnetic field is determined by their orbital movements[23]. However, in the energy space, the interaction between spins is long ranged. But a short range interaction on the spin chain simplifies greatly the treatment and, via Jordan-Wigner transformation, reduces the problem to the one of 1D spinless fermions (electrons) performing Bloch oscillations in a finite chain (some preliminary results are presented in chapter 6). In such a system, the exchange interaction can be mapped to a hopping term on the chain and the inhomogeneous magnetic field to an external electric field of constant strength. The problem of spin becomes the dynamics of Bloch oscillation. In Bloch oscillation, if the strength of the external electric field is inferior to a critical value, then the amplitude of the oscillation is so large that the electron can move in the entire system, characterizing a metal-insulator transition. This is similar to the synchronization transition in the spin models. It might be tempting to consider a finite chain with a short range interaction as a first step.

The experiments on atomic chips were performed at the temperature above the BEC. It is also interesting to consider a system already condensed, whose theoretical basis has been laid in [85]. Is there a synchronization in this system? If so, how does it happen? Can we find a simple model that captures the physics of the condensates? These are also directions for future work.

Chapter 6

Appendix: Dynamics on a spin chain

6.1 Statement of the problem

In this appendix we turn to a different model which is ongoing work. The model consists of a one-dimensional chain of spin $1/2$ particles in an inhomogeneous magnetic field with a linear gradient of δ. Each spin is fixed in real space and has index n to label its position. There are only interaction between nearest neigbors, and we assume an anisotropic interaction of the form $J_\perp(S_n^x S_{n+1}^x + S_i^y S_{n+1}^y) + J_z S_n^z S_{n+1}^z$ where $S_n^\alpha = \sigma_n^\alpha$, the Pauli matrix. The Hamiltonian is

$$H = \sum_{n=1}^{N} \frac{n}{N}\delta S_n^z + \sum_{n=1}^{N}\left[\frac{J_\perp}{2}(S_n^+ S_{n+1}^- + S_n^- S_{n+1}^+) + J_z S_n^z S_{n+1}^z\right]. \tag{6.1}$$

The different interaction strength in the xy-plane and the z-direction seems artificial, but later we will see that this leads to great simplification in the limit $J_z \to 0$. We take the periodic boudary condition

$$S_{N+1}^\alpha = S_1^\alpha. \tag{6.2}$$

Initially, all the spins are prepared in the x-dirction, perpendicular to the external magnetic field which reads

$$|\Psi(0)\rangle = \otimes_n \frac{1}{\sqrt{2}}\left(|\uparrow\rangle_n + |\downarrow\rangle_n\right) \tag{6.3}$$

So it will take all 2^N possible spin configurations.

The quantity of interest is the contrast defined as

$$\mathrm{C}(t) \equiv \frac{|\langle S_t^x(t)\rangle|}{|\langle S_t^x(0)\rangle|}, \tag{6.4}$$

with the total spin component operator

$$S_t^x \equiv \sum_{n=1}^{N} S_n^x. \tag{6.5}$$

6.2 A possible direction

In order to solve this problem, we carry out a Jordan-Wigner transformation

$$\begin{aligned} S_n^+ =& f_n^\dagger e^{i\pi \sum_{m<n} n_m}, \\ S_n^- =& e^{i\pi \sum_{m<n} n_m} f_n, \\ S_n^z =& f_n^\dagger f_n - 1/2, \end{aligned} \tag{6.6}$$

where $f_n^\dagger$ (f_n) is the creation (annihilation) operator of a fermion on the n-th site. The phase factor in the transformation is to ensure that $[S_m^\alpha, S_n^\beta] = 0$ for $m \neq n$. And for site n, the spin state can be described by the fermion state as

$$\begin{aligned} |\uparrow\rangle_n &= |1\rangle_n, \\ |\downarrow\rangle_n &= |0\rangle_n, \end{aligned} \tag{6.7}$$

where the fermion state $|1\rangle_n$ ($|0\rangle_n$) means there are 1 (0) fermion on the n-th site. Then the Hamiltonian takes the form

$$\begin{aligned} H =& \sum_n \frac{n}{2N}\delta + \sum_n \frac{n}{N}\delta f_n^\dagger f_n + \sum_n \left[\frac{J_\perp}{2}(f_n^\dagger f_{n+1} + f_{n+1}^\dagger f_n) \right. \\ & \left. + J_z(f_n^\dagger f_n f_{n+1}^\dagger f_{n+1} - f_n^\dagger f_n + \frac{1}{4}) \right]. \end{aligned} \tag{6.8}$$

The first term in the above Hamiltonian is a constant and can be neglected. The last term contains interaction between fermions on two nearby sites and is thus diffficult to treat. As a first step, we neglect this term, i.e. taking the limit $J_z \to 0$. And the resulting Hamiltonian reads

$$H = \sum_n \frac{n}{2N}\delta + \sum_n \frac{n}{N}\delta f_n^\dagger f_n + \sum_n \left[\frac{J_\perp}{2}(f_n^\dagger f_{n+1} + f_{n+1}^\dagger f_n) \right]. \tag{6.9}$$

The above Hamiltonian is a many-body version of the Bloch oscillation Hamiltonian which describes electrons in a one-dimensional lattice potential with an external electric field and cold atoms in a tilted lattice potential. For a finite lattice, a localization transition occurs if the external field strength is increased to a critical value. This is similar to our dephasing phenomenon in the two-spin model. In our two-spin system, if the inhomogeneity of the external field is strong enough, the two spins can not synchronized their movement. This is a motivation for this transformation.

However, the initial state is very complicated in this transformation

$$|\Psi(0)\rangle = \otimes_n \frac{1}{\sqrt{2}}(|1\rangle_n + |0\rangle_n), \tag{6.10}$$

corresponding to a state with $1/2$ fermion on each site.

6.3 Summary and discussion

The problem of a one-dimensional spin chain in an inhomogeneous magnetic field with anisotropic exchange interaction between nearest neighbors is considered in this chapter. Neglecting the interaction in the direction of the magnetic field and using the Jordan-Wigner transformation, we arrive at a tight-binding model with Bloch oscillation, whose eigenstates are known[86]. But the initial state in this transformation still takes a complicated form and an easy decomposition onto the eigenstates of the tight-binding model is not evident.

Bibliography

[1] B. I. HALPERIN and P. C. HOHENBERG, Hydrodynamic theory of spin waves, Phys. Rev. 188 (Dec, 1969) 898--918.

[2] P. M. Platzman and P. A. Wolff, Spin-wave excitation in nonferromagnetic metals, Phys. Rev. Lett. 18 (Feb, 1967) 280--283.

[3] S. Schultz and G. Dunifer, Observation of spin waves in sodium and potassium, Phys. Rev. Lett. 18 (Feb, 1967) 283--287.

[4] A. J. Leggett and M. J. Rice, Spin echoes in liquid he^3 and mixtures: A predicted new effect, Phys. Rev. Lett. 20 (Mar, 1968) 586--589.

[5] A. J. Leggett, Spin diffusion and spin echoes in liquid 3 he at low temperature, Journal of Physics C: Solid State Physics 3 no. 2, (1970) 448.

[6] E. Bashkin, Spin waves in polartized paramagnetic gases, JETP Lett. 33 (1981) 8.

[7] C. Lhuillier and F. Laloë, Transport properties in a spin polarized gas, i, Journal de Physique 43 no. 2, (1982) 197--224.

[8] C. Lhuillier and F. Laloë, Transport properties in a spin polarized gas, ii, Journal de Physique 43 no. 2, (1982) 225--241.

[9] P.-J. Nacher, G. Tastevin, M. Leduc, S. B. Crampton, and F. Laloë, Spin rotation effects and spin waves in gaseous 3he , Journal de Physique Lettres 45 no. 9, (1984) 441--448.

[10] W. J. Gully and W. J. Mullin, Observation of spin rotation effects in polarized ^{3}He-^{4}He mixtures, Phys. Rev. Lett. 52 (May, 1984) 1810--1813.

[11] G. Tastevin, P.-J. Nacher, M. Leduc, and F. Laloë, Direct detection of spin waves in gaseous 3he , Journal de Physique Lettres 46 no. 6, (1985) 249--254.

[12] M. H. Anderson, J. R. Ensher, M. R. Matthews, C. E. Wieman, and E. A. Cornell, Observation of bose-einstein condensation in a dilute atomic vapor, science 269 no. 5221, (1995) 198--201.

[13] K. B. Davis, M. O. Mewes, M. R. Andrews, N. J. van Druten, D. S. Durfee, D. M. Kurn, and W. Ketterle, Bose-einstein condensation in a gas of sodium atoms, Phys. Rev. Lett. 75 (Nov, 1995) 3969--3973.

[14] C. C. Bradley, C. A. Sackett, J. J. Tollett, and R. G. Hulet, Evidence of bose-einstein condensation in an atomic gas with attractive interactions, Phys. Rev. Lett. 75 (Aug, 1995) 1687--1690.

[15] C. C. Bradley, C. A. Sackett, and R. G. Hulet, Bose-einstein condensation of lithium: Observation of limited condensate number, Phys. Rev. Lett. 78 (Feb, 1997) 985--989.

[16] H. J. Lewandowski, D. M. Harber, D. L. Whitaker, and E. A. Cornell, Observation of anomalous spin-state segregation in a trapped ultracold vapor, Phys. Rev. Lett. 88 (Jan, 2002) 070403.

[17] M. O. Oktel and L. S. Levitov, Internal waves and synchronized precession in a cold vapor, Phys. Rev. Lett. 88 (May, 2002) 230403.

[18] J. N. Fuchs, D. M. Gangardt, and F. Laloë, Internal state conversion in ultracold gases, Phys. Rev. Lett. 88 (May, 2002) 230404.

[19] J. E. Williams, T. Nikuni, and C. W. Clark, Longitudinal spin waves in a dilute bose gas, Phys. Rev. Lett. 88 (May, 2002) 230405.

[20] X. Du, L. Luo, B. Clancy, and J. E. Thomas, Observation of anomalous spin segregation in a trapped fermi gas, Phys. Rev. Lett. 101 (Oct, 2008) 150401.

[21] S. S. Natu and E. J. Mueller, Anomalous spin segregation in a weakly interacting two-component fermi gas, Phys. Rev. A 79 (May, 2009) 051601.

[22] F. Piéchon, J. N. Fuchs, and F. Laloë, Cumulative identical spin rotation effects in collisionless trapped atomic gases, Phys. Rev. Lett. 102 (May, 2009) 215301.

[23] X. Du, Y. Zhang, J. Petricka, and J. E. Thomas, Controlling spin current in a trapped fermi gas, Phys. Rev. Lett. 103 (Jul, 2009) 010401.

[24] C. Deutsch, F. Ramirez-Martinez, C. Lacroûte, F. Reinhard, T. Schneider, J. N. Fuchs, F. Piéchon, F. Laloë, J. Reichel, and P. Rosenbusch, Spin self-rephasing and very long coherence times in a trapped atomic ensemble, Phys. Rev. Lett. 105 (Jul, 2010) 020401.

[25] C. Cohen-Tannoudji, B. Diu, and F. Laloë, Mécanique quantique Tome 1. Hermann, 1977.

[26] P. Rosenbusch, Magnetically trapped atoms for compact atomic clocks, Applied Physics B: Lasers and Optics 95 (May, 2009) 227--235.

[27] K. Gibble, Keeping atoms synchronized for better timekeeping, Physics 3 (Jul, 2010) 55.

[28] Y. Liu, F. Piéchon, and J. N. Fuchs, Quantum loss of synchronization in the dynamics of two spins, accepted for publication in Europhysics Letters .

[29] G. Burkard, D. Loss, and D. P. DiVincenzo, Coupled quantum dots as quantum gates, Phys. Rev. B 59 (Jan, 1999) 2070--2078.

[30] G. J. Milburn, R. Laflamme, B. C. Sanders, and E. Knill, Quantum dynamics of two coupled qubits, Phys. Rev. A 65 (Feb, 2002) 032316.

[31] B. Pigeau, C. Hahn, G. de Loubens, V. V. Naletov, O. Klein, K. Mitsuzuka, D. Lacour, M. Hehn, S. Andrieu, and F. Montaigne, Measurement of the dynamical dipolar coupling in a pair of magnetic nanodisks using a ferromagnetic resonance force microscope, Phys. Rev. Lett. 109 (Dec, 2012) 247602.

[32] L. Bogani and W. Wernsdorfer, Molecular spintronics using single-molecule magnets, Nature materials 7 no. 3, (2008) 179--186.

[33] H. Lipkin, N. Meshkov, and A. Glick, Validity of many-body approximation methods for a solvable model: (i). exact solutions and perturbation theory, Nuclear Physics 62 no. 2, (1965) 188 -- 198.

[34] G. J. Milburn, J. Corney, E. M. Wright, and D. F. Walls, Quantum dynamics of an atomic bose-einstein condensate in a double-well potential, Phys. Rev. A 55 (Jun, 1997) 4318--4324.

[35] A. Smerzi, S. Fantoni, S. Giovanazzi, and S. R. Shenoy, Quantum coherent atomic tunneling between two trapped Bose-Einstein condensates, Phys. Rev. Lett. 79 (Dec, 1997) 4950--4953.

[36] J. J. J. Sakurai and J. Napolitano, Modern quantum mechanics. ADDISON WESLEY Publishing Company Incorporated, 2011.

[37] M. Albiez, R. Gati, J. Fölling, S. Hunsmann, M. Cristiani, and M. K. Oberthaler, Direct observation of tunneling and nonlinear self-trapping in a single Bosonic Josephson junction, Phys. Rev. Lett. 95 (Jun, 2005) 010402.

[38] T. Zibold, E. Nicklas, C. Gross, and M. K. Oberthaler, Classical bifurcation at the transition from Rabi to Josephson dynamics, Phys. Rev. Lett. 105 (Nov, 2010) 204101.

[39] T. Zibold, Classical bifurcation and entanglement generation in an internal Bosonic Josephson junction. PhD thesis, Ruperto-Carola-University of Heidelberg, 2012.

[40] D. Garanin, Self-consistent Gaussian approximation for classical spin systems: Thermodynamics, Physical Review B 53 no. 17, (1996) 11593.

[41] K. Kladko, P. Fulde, and D. Garanin, Cumulant expansion for systems with large spins, EPL (Europhysics Letters) 46 no. 4, (1999) 425.

[42] D. A. Garanin and R. Schilling, Quantum nonlinear spin switching model, Phys. Rev. B 69 (Mar, 2004) 104412.

[43] W.-M. Zhang, D. H. Feng, and R. Gilmore, Coherent states: Theory and some applications, Rev. Mod. Phys. 62 (Oct, 1990) 867--927.

[44] J.-P. Gazeau, Coherent states in quantum physics. Wiley-VCH Berlin, 2009.

[45] C. Bloch and J. Horowitz, Sur la détermination des premiers états d'un système de fermions dans le cas dégénéré, Nuclear Physics 8 no. 0, (1958) 91 -- 105.

[46] P.-O. Löwdin, Studies in perturbation theory: Part VI. Contraction of secular equations, Journal of Molecular Spectroscopy 14 no. 1–4, (1964) 112 -- 118.

[47] D. Garanin, K. Kladko, and P. Fulde, Quasiclassical hamiltonians for large-spin systems, The European Physical Journal B-Condensed Matter and Complex Systems 14 no. 2, (2000) 293--300.

[48] L. M. Narducci, C. A. Coulter, and C. M. Bowden, Exact diffusion equation for a model for superradiant emission, Phys. Rev. A 9 (Feb, 1974) 829--845.

[49] R. Gilmore, C. M. Bowden, and L. M. Narducci, Classical-quantum correspondence for multilevel systems, Phys. Rev. A 12 (Sep, 1975) 1019--1031.

[50] K. E. Cahill and R. J. Glauber, Density operators and quasiprobability distributions, Phys. Rev. 177 (Jan, 1969) 1882--1902.

[51] C. Ferrie, Quasi-probability representations of quantum theory with applications to quantum information science, Reports on Progress in Physics 74 no. 11, (2011) 116001.

[52] E. Wigner, On the quantum correction for thermodynamic equilibrium, Phys. Rev. 40 (Jun, 1932) 749--759.

[53] G. S. Agarwal, Relation between atomic coherent-state representation, state multipoles, and generalized phase-space distributions, Phys. Rev. A 24 (Dec, 1981) 2889--2896.

[54] J. P. Dowling, G. S. Agarwal, and W. P. Schleich, Wigner distribution of a general angular-momentum state: Applications to a collection of two-level atoms, Phys. Rev. A 49 (May, 1994) 4101--4109.

[55] K. Husimi, Some formal properties of the density matrix, Proc. Phys.-Math. Soc. Japan 22 (1940) 264.

[56] E. C. G. Sudarshan, Equivalence of semiclassical and quantum mechanical descriptions of statistical light beams, Phys. Rev. Lett. 10 (Apr, 1963) 277--279.

[57] R. J. Glauber, Coherent and incoherent states of the radiation field, Phys. Rev. 131 (Sep, 1963) 2766--2788.

[58] C. Brif and A. Mann, Phase-space formulation of quantum mechanics and quantum-state reconstruction for physical systems with Lie-group symmetries, Phys. Rev. A 59 (Feb, 1999) 971--987.

[59] F. Trimborn, D. Witthaut, and H. J. Korsch, Exact number-conserving phase-space dynamics of the m-site Bose-Hubbard model, Phys. Rev. A 77 (Apr, 2008) 043631.

[60] F. Trimborn, D. Witthaut, and H. J. Korsch, Beyond mean-field dynamics of small Bose-Hubbard systems based on the number-conserving phase-space approach, Phys. Rev. A 79 (Jan, 2009) 013608.

[61] A. Altland and F. Haake, Quantum chaos and effective thermalization, Phys. Rev. Lett. 108 (Feb, 2012) 073601.

[62] A. Altland and F. Haake, Equilibration and macroscopic quantum fluctuations in the dicke model, New Journal of Physics 14 no. 7, (2012) 073011.

[63] C. W. Gardiner et al., Handbook of stochastic methods, vol. 3. Springer Berlin, 1985.

[64] H. P. Breuer and F. Petruccione, The theory of open quantum systems. Oxford University Press, 2002.

[65] G. P. Berman, E. N. Bulgakov, and D. D. Holm, Quantum chaos of atoms in a resonator driven by an external resonant field, Phys. Rev. A 49 (Jun, 1994) 4943--4956.

[66] K. W. Mahmud, H. Perry, and W. P. Reinhardt, Quantum phase-space picture of bose-einstein condensates in a double well, Phys. Rev. A 71 (Feb, 2005) 023615.

[67] W.-M. Zhang, Microscopic study of fermionic collective motion: (i). functional representation of collective motion, Nuclear Physics A 467 no. 3, (1987) 422 -- 436.

[68] H. P. Yuen, Two-photon coherent states of the radiation field, Phys. Rev. A 13 (Jun, 1976) 2226--2243.

[69] V. V. Dodonov, `nonclassical' states in quantum optics: a `squeezed' review of the first 75 years, Journal of Optics B: Quantum and Semiclassical Optics 4 no. 1, (2002) R1.

[70] D. J. Wineland, J. J. Bollinger, W. M. Itano, F. L. Moore, and D. J. Heinzen, Spin squeezing and reduced quantum noise in spectroscopy, Phys. Rev. A 46 (Dec, 1992) R6797--R6800.

[71] M. Kitagawa and M. Ueda, Squeezed spin states, Phys. Rev. A 47 (Jun, 1993) 5138--5143.

[72] D. J. Wineland, J. J. Bollinger, W. M. Itano, and D. J. Heinzen, Squeezed atomic states and projection noise in spectroscopy, Phys. Rev. A 50 (Jul, 1994) 67--88.

[73] J. Ma, X. Wang, C. Sun, and F. Nori, Quantum spin squeezing, Physics Reports 509 no. 2, (2011) 89--165.

[74] J. Ma and X. Wang, Fisher information and spin squeezing in the lipkin-meshkov-glick model, Phys. Rev. A 80 (Jul, 2009) 012318.

[75] G. Ferrini, A. Minguzzi, and F. W. J. Hekking, Number squeezing, quantum fluctuations, and oscillations in mesoscopic Bose Josephson junctions, Phys. Rev. A 78 (Aug, 2008) 023606.

[76] D. Ulam-Orgikh and M. Kitagawa, Spin squeezing and decoherence limit in ramsey spectroscopy, Phys. Rev. A 64 (Oct, 2001) 052106.

[77] J. K. Korbicz, J. I. Cirac, and M. Lewenstein, Spin squeezing inequalities and entanglement of n qubit states, Phys. Rev. Lett. 95 (Sep, 2005) 120502.

[78] J. K. Korbicz, O. Gühne, M. Lewenstein, H. Häffner, C. F. Roos, and R. Blatt, Generalized spin-squeezing inequalities in n-qubit systems: Theory and experiment, Phys. Rev. A 74 (Nov, 2006) 052319.

[79] J. Vidal, Concurrence in collective models, Phys. Rev. A 73 (Jun, 2006) 062318.

[80] E. Boukobza, M. Chuchem, D. Cohen, and A. Vardi, Phase-diffusion dynamics in weakly coupled bose-einstein condensates, Phys. Rev. Lett. 102 (May, 2009) 180403.

[81] K. Smith-Mannschott, M. Chuchem, M. Hiller, T. Kottos, and D. Cohen, Occupation statistics of a bose-einstein condensate for a driven landau-zener crossing, Phys. Rev. Lett. 102 (Jun, 2009) 230401.

[82] J. R. Anglin and A. Vardi, Dynamics of a two-mode bose-einstein condensate beyond mean-field theory, Phys. Rev. A 64 (May, 2001) 013605.

[83] F. Trimborn, D. Witthaut, and S. Wimberger, Mean-field dynamics of a two-mode bose–einstein condensate subject to noise and dissipation, Journal of Physics B: Atomic, Molecular and Optical Physics 41 no. 17, (2008) 171001.

[84] P. P. Orth, D. Roosen, W. Hofstetter, and K. Le Hur, Dynamics, synchronization, and quantum phase transitions of two dissipative spins, Phys. Rev. B 82 (Oct, 2010) 144423.

[85] T. Nikuni and J. Williams, Kinetic theory of a spin-1/2 bose-condensed gas, Journal of Low Temperature Physics 133 no. 5-6, (2003) 323--375.

[86] T. Hartmann, F. Keck, H. J. Korsch, and S. Mossmann, Dynamics of bloch oscillations, New Journal of Physics 6 no. 1, (2004) 2.